TÉCNICO LISBOA

Spontaneous Scalarization of Charged Black Holes

Pedro Gonçalo da Silva Fernandes

Thesis to obtain the Master of Science Degree in

Engineering Physics

Supervisors: Prof. Dr. Carlos Alberto Ruivo Herdeiro
Dr. Eugen Radu

Examination Committee

Chairperson: Prof. Dr. José Pizarro de Sande e Lemos
Supervisor: Prof. Dr. Carlos Alberto Ruivo Herdeiro
Member of the Committee: Dr. Masato Minamitsuji

July 2019

Ao meu avô,
que sempre me escreveu
palavras e poemas
em situações importantes.
Agora que cá não está
escrevo eu para continuar
a história e o legado
dos Pedro Fernandes

Acknowledgments

First, I would like to express my gratitude towards my supervisor, Carlos Herdeiro, for, without knowing me at all, accepting to work with me, for all his guidance and support. I have learnt a lot working with you, not only about black holes, but about physics in general and about the scientific research world. Next, I want to thank my co-supervisor, Eugen Radu, for his guidance, infinite patience and availability to explain me everything. I would also like to thank Alexandre Pombo, that was like a third supervisor for me. For all you three, a major thanks for everything you did for me, for receiving and reading the 10^{2864} emails I sent you during this work, for all the times I was annoying. It was truly a pleasure working with you, and an experience I won't ever forget.

Next, I want to thank my university colleagues, (i) from mechanical engineering: the one year I spent in mechanical engineering was amazing thanks to you; (ii) from physics, that made the next four years great; namely André Weigel, Nuno Miguel Guerreiro, Bruno Abrantes, Fernando Lima, Júlia Silva, Ricardo Barrué, João Melo, Tiago França, Nelson Eiró.

I would also like to thank my friends without whom... I would probably have finished this thesis earlier. I honestly do not know how I was able to make it to this point with all the nights out with you along these five years. You have made my university years the best of my life. Thank you for all your support, for all the crazy nights, for all the afternoons, for all the holidays... It was truly gratifying to grow up by your side, and to watch you grow up. This acknowledgement is for you Gonçalo Nogueira, Luís Judícibus, Francisco Dias Pereira, Simão Escudeiro, Bernardo Sá, Diogo Sá, Daniel Alves, Gonçalo Figueiredo, Hugo Luzio, João Tomázio, Vítor Silva. I also want to thank Carolina Liquito, Marisa Frade, Pedro Didelet Alves, Teresa Bonito, Daniela Miranda, Cláudia Pinto, André Rijo and everyone from the group of the cards.

Final acknowledgments go to my family, namely to my mother, father, sister and niece. Thank you for always being there for me, for doing everything for me, for having the patience to put up with me. Living with me is most certainly not an easy task. I love you all! Next, I want to thank Bruno Valeixo Bento, for (i) reading every page of this thesis - your corrections made this a significantly better work; (ii) truly being the friend everyone would love to have - your friendship is the most important thing I take from university. Lastly, this acknowledgement is for you, Sofia Pinto. You are the most amazing person I have ever known. No words can express how I feel about you. I want to thank you for every Planck time we share together, for your endless fountain of support, for being able to amaze me each and every day, for teaching me about life in a way that I understand, for showing me that us sharing life together as one is the most amazing experience I have ever had... Thank you for always being my home. I love you.

To the brightest person I have ever known, my grandfather Pedro Correia Fernandes, that passed away before I could finish this journey - this work is yours.

Resumo

Neste trabalho o fenómeno de *escalarização espontânea* de buracos negros com carga é estudado no contexto de modelos Einstein-Maxwell scalar (EMS). Este fenómeno ocorre devido a um acoplamento não-mínimo entre os campos escalar e de Maxwell, e não requer acoplamentos do campo escalar a invariantes de curvatura, pelo que apresenta uma simplificação técnica em relação à escalarização que se conjectura em modelos extended-Scalar-Tensor-Gauss-Bonnett (eSTGB). Primeiro, estudamos a escalarização espontânea no contexto de buracos negros puramente eléctricos, e observamos que diferenças aparecem quando mudamos o acoplamento não-mínimo. De seguida, um estudo similar é efectuado para buracos negros diónicos, onde existem soluções extremas, e fazemos uma comparação com o caso do buraco negro dilatónico. Por fim, generalizamos os modelos EMS para incluír um acoplamento do tipo axiónico e mostramos que escalarização espontânea é possível a partir deste tipo de acoplamento. Também é feito um estudo de buracos negros com cabelo axiónico. Em todos os casos, estudamos os perfis radiais, a estabilidade perturbativa e o domínio de existência de buracos negros fundamentais esfericamente simétricos e obtemos, em particular, a sua entropia, que mostra que os buracos negros escalarizados são sempre entropicamente preferidos em relação ao buraco negro de Reissner-Nordström com o mesmo rácio de carga sobre massa. São também apresentados resultados de simulações dinâmicas, que mostram que os buracos negros escalarizados se formam dinamicamente. Alguns dos resultados obtidos nesta tese aparecem nas refs. [1, 2].

Palavras-chave: Buracos negros com carga; Escalarização espontânea; Campo escalar; Einstein-Maxwell scalar; Cabelo escalar; Axião.

Abstract

In this work the phenomenon of *spontaneous scalarization* of charged black holes (BHs) is studied in the framework of Einstein-Maxwell scalar (EMS) models. This phenomenon is allowed by a non-minimal coupling between the scalar and the Maxwell fields, and does not require non-minimal couplings of the scalar field to curvature invariants, which presents a technical simplification over the BH scalarization that has been conjectured to occur in extended Scalar-Tensor Gauss-Bonnet (eSTGB) models. First we study spontaneous scalarization in the context of purely electric BHs and verify what differences emerge when the non-minimal coupling is changed. Next, a similar study is performed in the context of dyonic BHs where extremal solutions emerge and a comparison with the dilatonic BH case is done. Finally a generalisation of EMS models to include an axionic-like coupling is done. It is shown that spontaneous scalarization through an axionic-like coupling can occur and a study of BHs with axionic hair is done. In all cases we obtain and study the radial profiles, the perturbative stability, and the domain of existence of fundamental, spherically symmetric, scalarized BHs and compute, in particular, their entropy. The latter shows that scalarized EMS BHs are always entropically preferred over the Reissner-Nordström BHs with the same total charge to mass ratio. Furthermore, results of fully non-linear dynamical evolutions are also presented, showing that scalarized BHs do form dynamically. Part of the results obtained for this thesis appear in refs. [1, 2].

Keywords: Charged black holes; Spontaneous scalarization; Scalar fields; Einstein-Maxwell scalar; Scalar hair; Axion.

Contents

Acknowledgments v
Resumo vii
Abstract ix
List of Tables xv
List of Figures xvii
Nomenclature xxi

1 Introduction **1**
1.1 General Relativity 1
1.2 General Relativity via a Variational Principle 2
1.2.1 Lagrangian Mechanics 2
1.2.2 Classical Field Theory 2
1.2.3 General Relativity as a Field Theory 2
1.3 Black Holes 3
1.3.1 Observation and Astrophysical Formation of Black Holes 5
1.3.2 No-Hair Theorems 5
1.4 Spontaneous scalarization 7
1.4.1 A toy model: spontaneous scalarization of a charged sphere 7
1.4.2 Spontaneous scalarization of black holes 9
1.5 Computational shooting method: an introduction 10
1.6 Thesis outline 11

2 EMS models: introduction and spontaneous scalarization of purely electric black holes **13**
2.1 The EMS model 14
2.2 Physical relations 15
2.2.1 Smarr law 16
2.2.2 Virial relation 16
2.3 Conditions for the occurrence of spontaneous scalarization 17
2.3.1 The coupling functions 18
2.4 Bifurcating points from the RN BH - The existence line for scalarized solutions 19

2.5 Results . . . 20
2.5.1 Solutions of the radial profiles . . . 20
2.5.2 Domain of Existence . . . 21
2.5.3 Perturbative stability . . . 23
2.5.4 Entropic preference . . . 26

3 Spontaneous scalarization of dyonic black holes 27
3.1 The EMS model for dyonic BHs . . . 28
3.1.1 Physical relations and perturbative stability . . . 30
3.1.2 Perturbative stability . . . 31
3.2 The coupling functions, spontaneous scalarization and the existence line . . . 32
3.2.1 Dilatonic class . . . 32
3.2.2 Spontaneously scalarized class . . . 32
3.2.3 The existence line . . . 32
3.3 Results . . . 33
3.3.1 The purely electric BHs . . . 33
3.3.2 Dyonic BHs . . . 35

4 Spontaneous scalarization of charged black holes from axion-like coupling and study of black holes with axion-hair 39
4.1 The model . . . 40
4.2 Conditions for the occurrence of spontaneous scalarization . . . 42
4.3 Bifurcating points from the scalar free solution - The existence line . . . 43
4.4 Physical relations and tests to the code . . . 44
4.4.1 Smarr law . . . 44
4.4.2 Virial relation . . . 45
4.5 Perturbative stability analysis . . . 45
4.6 Particular cases of the model - results . . . 47
4.6.1 A Toy Model . . . 47
4.6.2 The axionic case . . . 48
4.6.3 Spontaneous scalarization: power law coupling . . . 51

5 Conclusions and Future Work 57

Bibliography 59

A Dynamical preference in the EMS model 65
A.1 Dynamical preference for Chapter 2 BHs (purely electric case) . . . 65
A.2 Dynamical preference for Chapter 4 BHs (axionic case) . . . 67

B Exact solutions with a dilatonic coupling **69**

B.1 Purely electric BHs 69

B.2 Dyonic BHs 70

List of Tables

2.1 Minimum value of $|\alpha|$ for scalarization of a RN BH with charge to mass ratio q. 19
2.2 Characteristic quantities for scalarized BH solutions with four choices of couplings, $\alpha = -10$ and $q = 0.66$. 21

4.1 Minimum value of α for bifurcation from a dyonic RN BH for several values of $\mathcal{Q}$. 43
4.2 Characteristic quantities for scalarized BH solutions for $\alpha = 15$ and $\alpha = 35$ for several values of P/Q and $r_H = 0.29736$. 48
4.3 Characteristic quantities for scalarized BH solutions for $\alpha = 20$ and $\alpha = 35$, with $Q = 0.12$, $P = 0.06$ and $r_H = 0.44604$. 53

List of Figures

1.1 Penrose diagram for the Schwarzschild BH with the future (and past) EH and the future (and past) null infinity represented. Source: [10] 3

1.2 First image of a BH shadow (center of the M87 galaxy). Source: [15] 5

2.1 Left: Asymptotic value U_∞ of the $l = 0$ amplitude U for $\alpha = -38$ as a function of q. Right: Existence lines for the $n = 0$ mode, *i.e.*, the bifurcating points from the RN BH, and for the $n = 1$ mode. 20

2.2 Scalarized BH radial functions for $\alpha = -10$ and $q = 0.66$. (Left panel) f_E; (Middle panel) f_P; (Right panel) f_F. Source: [1]. 21

2.3 A typical scalarized BH in an EMS model with the coupling function f_F, which possesses a region with negative energy density, $\rho < 0$. Left: Profiles of the metric and matter functions; Right: the energy density (zoom in presented in the inset), the Ricci and Kretschmann scalars and the inverse of the coupling function $f_F(\phi)$ which changes sign at some finite r. This plot manifests that solutions with $\rho < 0$ are smooth. Source: [1]. . . . 22

2.4 Domain of existence of scalarized BHs in EMS models (shaded blue regions). Left: $f_E(\phi)$, $f_C(\phi)$ and $f_P(\phi)$ couplings. Right: $f_F(\phi)$ coupling. Here we only exhibit the physical region, which is delimited by the existence line and the line at which the coupling function diverges at the horizon. The latter is the boundary of the physical region; above it, solutions have a negative energy density in the vicinity of the horizon. Source: [1]. 22

2.5 Characteristic quantities at the horizon for f_E and $\alpha = -10$. Left panel: Horizon area A_H. Right panel: Kretschmann scalar at the horizon $K(r_H)$. One can observe a divergence of $K(r_H)$, and that A_H vanishes at the critical line. 23

2.6 Perturbative potential, U_Ω, for a sequence of solutions. Left panel: exponential coupling, $\alpha = -10$ and $Q = 0.12$. The solutions have $r_H = 0.324$ ($q = 0.651$) – lowest curve – up to $r_H = 0.297$ ($q = 0.695$) – top curve. Right panel: fractional coupling. The sequence is plotted for the same sequence of q values. The inset plot in black corresponds to the smallest value of q considered. One observes that after a determined value of q the potential diverges at some range of the radial coordinate r for which $\phi(r) = 1/\sqrt{|\alpha|}$, and has both negative and positive regions. 25

2.7 Perturbative potential, U_Ω, for the exponential coupling for several values of α and n. One observes that the overtone solutions have a region where $U_\Omega < 0$. 25

2.8 Reduced area a_H *vs.* q for: (top, left panel) $f_E(\phi)$; (top, right panel) $f_C(\phi)$; (bottom left panel) $f_P(\phi)$; (bottom right panel) $f_F(\phi)$. The blue lines are the sequence of non-scalarized RN BHs. The red lines are sequences of (numerical data points representing) scalarized BHs for a given α. Different sequences are presented, for a range of values of α. The solid black line shows the sequence of solutions along the boundary of the physical region for the f_F model. Source: [1]. 26

3.1 Existence line for several values of P/Q. 33

3.2 Reduced area a_H (top panels) and reduced temperature t_H (bottom panels) *vs.* reduced charge q for dilatonic (left panels) and scalarized solutions (right panels). All solutions have $P = 0$. The blue lines are the set of RN BHs ($\phi = 0$). The red lines are sequences of BHs with a nontrivial scalar field for a given α. Different sequences are presented, for a range of values of α. The black dots indicate the RN solutions from which the scalarized BHs bifurcate. Source: [47]. 34

3.3 Illustrative radial profiles for the dilatonic and scalarized models for $Q = 0.12$, $r_H = 0.2676$, $\alpha = 5$. Left panel: Dilatonic radial profiles. Right panel: Scalarized radial profiles. 35

3.4 Sequence of perturbative potentials, U_Ω, for the purely electric dilaton case with $\alpha = 5$. The bottom curve has $q = 0.687$, while the top one has $q = 0.735$. The perturbative potentials are always positive definite. 35

3.5 Illustrative radial profiles for the dilatonic and scalarized models for $Q = 0.12$, $\alpha = 5$ and several values of P. Top left panel: dilatonic radial profiles for $P/Q = 0.1$ and $r_H = 0.565$. Top right panel: dilatonic radial profiles for $P/Q = 0.25$ and $r_H = 0.565$. Bottom left panel: scalarized radial profiles for $P/Q = 0.1$ and $r_H = 0.297$. Bottom right panel: scalarized radial profiles for $P/Q = 0.25$ and $r_H = 0.297$. 36

3.6 Reduced area a_H (top panels) and reduced temperature t_H (bottom panels) *vs.* reduced charge q for dilatonic (left panels) and scalarized solutions (right panels). All solutions have $P/Q = 0.1$. The blue lines are the set of RN BHs ($\phi = 0$). The red lines are sequences of BHs with a non-trivial scalar field for a given α. Different sequences are presented, for a range of values of α. The black dots indicate the RN solutions from which the scalarized BHs bifurcate. The dashed black lines represent the extremal BHs. Source: [47]. 37

3.7 Sequence of perturbative potentials, U_Ω, for the dyonic dilaton and scalarized cases with $\alpha = 5$. The potentials are always positive definite for the dilatonic case, whereas for small enough q for a certain P/Q, the scalarized case yields a potential with a negative region. . 37

3.8 Domain of existence of dilatonic BHs (left panel) and scalarized BHs (right panel) for several values of P/Q. The existence line of the right panel is referent to the purely electrical case. Source: [47]. 38

4.1 Left: U_∞ as a function of q for two values of P/Q and $\alpha = 40$. An infinite set of configurations with $U_\infty = 0$ exist, labelled by n, the number of nodes of $U(r)$. The first configuration for which $U_\infty = 0$ is labelled by $n = 0$ and so on. Right: Existence line for several values of $\mathcal{Q}$. 44

4.2 Scalarized BH radial functions for $\alpha = 15$ and $\alpha = 35$, with $Q = 0.12$, $P = 0.012$ and $r_H = 0.29736$. 49

4.3 Comparison between the analytical approximations and the numerical results. Top left: $\alpha = 0.3$, $Q = 0.12$, $P = 0.012$, $r_H = 0.282474$, approximation for small α. Top right: $\alpha = 100$, $Q = 0.12$, $P = 0.012$, $r_H = 0.529659$, approximation for big α. Bottom left: $\alpha = 10$, $Q = 0.12$, $P = 0.012$, $r_H = 0.33453$. Bottom right: $\alpha = 30$, $Q = 0.12$, $P = 0.012$, $r_H = 0.33453$. The approximations hold really well for the appropriate cases. The intermediate cases show a clear deviance between the numerical solution and the analytical approximations. 49

4.4 Zoomed plots for the scalar field radial profiles, in order to make a comparison between the new and first analytical approximations and the numerical results. Left: $\alpha = 0.3$, $Q = 0.12$, $P = 0.012$, $r_H = 0.282474$. Right: $\alpha = 100$, $Q = 0.12$, $P = 0.012$, $r_H = 0.529659$. 50

4.5 Left: Domain of existence of scalarized solutions in the (α, q) plane, in the shadowed region. The domain is bounded by a critical line at which solutions are singular, for each presented P/Q value. Right: t_H as a function of q for $P/Q = 0.1$. One observes that for small α, solutions approximate an extremal RN BH. 51

4.6 Perturbative potential, U_Ω, for $r_H = 0.1204$, $Q = 0.12$ and several values of P/Q. Left panel: $\alpha = 5$. Right panel: $\alpha = 10$. One observes that the potential is always positive until a critical P/Q value is reached, and afterwards it always has a negative region. . . . 52

4.7 Top: scalarized BH radial functions for $\alpha = 20$ (left) and $\alpha = 35$ (right), with $Q = 0.12$, $P = 0.06$ and $r_H = 0.44604$. Bottom left: Overtone solution $n = 1$ with $\alpha = 10$, $Q = 0.12$, $P = 0.06$ and $r_H = 0.171279$. Bottom right: Overtone solution $n = 2$ with $\alpha = 10$, $Q = 0.12$, $P = 0.06$ and $r_H = 0.142733$. 52

4.8 Comparison between the analytical approximations and the numerical results. Top left: $\alpha = 1$, $Q = 0.12$, $P = 0.06$, $r_H = 0.142733$, approximation for small α. Top right: $\alpha = 100$, $Q = 0.12$, $P = 0.06$, $r_H = 0.683928$, approximation for big α. 54

4.9 Domain of existence of scalarized solutions in the (α, q) plane. The domain is bounded by an extremal line (solid lines) at which solutions are extremal BHs and by an existence line (dashed), for each presented P/Q value. 55

4.10 Left: Zoomed domain of existence for $P/Q = 0.2$ and $P/Q = 0.4$. One observes that there is a region at which the bigger value of P/Q allows greater overcharging. Right: $(P/Q, q)$ plane. The solid lines correspond to the extremal solution for each P/Q value, for a constant α. The black curve is the curve that interpolates the optimum values of P/Q. 55

4.11 Sequence of perturbative potentials, U_Ω, for $\alpha = 10$, $P/Q = 0.4$ (left) and $P/Q = 0.5$ (right). The deeper potentials at each figure, occur for higher values of q. There is always a region where the potential is negative. Left panel: bottom curve has $q = 0.785$ and top curve has $q = 0.736$. Right panel: bottom curve has $q = 0.746$ and top curve has $q = 0.701$. 56

4.12 a_H vs q for $P/Q = 0.5$ and $P/Q = 0.6$. The blue lines are the sequence of non-scalarized BHs, while the red lines are sequences of (numerical data points representing) scalarized BHs for a given α. The black line represents the entropy of the extremal BH solutions for the different α values. 56

A.1 Four snapshots of the time evolution of the scalar field around an unstable RN BH with $q = 0.2$ in the EMS model, with the exponential coupling and $\alpha = -400.979$. 65

A.2 (Left panel) Scalar field value at the horizon for $q = 0.2$ and a range of couplings α, for the exponential and power-law coupling. The solid line is obtained from the static solutions. The crosses are the dynamically obtained value from the numerical simulations after saturation and equilibrium has been reached. The agreement is notorious. (Right panel) A similar study, for the exponential coupling, but for various values of q. The agreement between the points and the lines with the same q is restricted to $q \lesssim 0.4$. For larger q, the evolution points match static solution lines with a smaller q. 66

A.3 Twelve snapshots in the $x - z$ ($y = 0$) plane of the time evolution of an unstable RN BH with $q = 0.2$ in the EMS system, with the exponential coupling and $\alpha = -1200$ and an $\ell = 2$, $m = 0$ perturbation. The snapshots correspond to t between 0 and 140.8. The data for negatives values of x and z are mirrored by the corresponding positive values, due to equatorial symmetry. 67

A.4 Scalar field value at the horizon obtained via the dynamical simulations and the static solutions for different values of Q and P. 68

Nomenclature

Acronyms

BH	Black Hole
EFE	Einstein Field Equations
EH	Event Horizon
EM	Einstein-Maxwell
EMFE	Einstein-Maxwell Field Equations
EMS	Einstein-Maxwell Scalar
eSTGB	Extended Scalar-Tensor Gauss-Bonnet
GB	Gauss-Bonnet
GR	General Relativity
ODE	Ordinary Differential Equation
QM	Quantum Mechanics
RN	Reissner-Nordström

Chapter 1

Introduction

1.1 General Relativity

Upon the beginning of the XXth century it was clear, from observational and theoretical evidence, that the Newtonian theory of gravity was not the ultimate theory of gravitation [3]. For instance, Newtonian gravity could not explain the observed anomalous perihelion advance of Mercury and was not compatible with special relativity [4].

In 1915, Albert Einstein published the final form of his field equations in a theory that became known as *General Relativity* (GR). GR provided an explanation for gravity as the curvature of *spacetime*, caused by the presence of matter [3] (eq. 1.1)

$$G_{\mu\nu} \equiv R_{\mu\nu} - \frac{1}{2} g_{\mu\nu} R = \kappa T_{\mu\nu}, \tag{1.1}$$

where $R_{\mu\nu}$ and R are respectively the Ricci tensor and the Ricci scalar (that are purely geometric quantities that depend solely on the metric $g_{\mu\nu}$), $\kappa = \frac{8\pi G}{c^4}$ the coupling constant (with G the Newtonian gravitational constant and c the speed of light in a vacuum), and $T_{\mu\nu}$ the *energy-momentum* tensor that describes the presence of matter. Apart from equation 1.1, geometric units ($4\pi G = c = 1$) will be adopted throughout this work, as well as the metric signature $(-,+,+,+)$.

GR could explain the anomalous perihelion advance of Mercury, and predicted phenomena such as the bending of light by massive objects, the gravitational redshift of light, which turned out to be true with observational evidence agreeing with the theory [4]. GR also predicts the existence of *black holes*, which are strongly supported by experimental evidence.

Nowadays it is clear that GR is not the ultimate theory of gravitation. GR and quantum mechanics (QM) are incompatible and in a regime where both are relevant we are unable to make predictions. Moreover, GR predicts the existence of singularities that in no sensible way can be considered physical, while it is also unable of explaining dark matter and dark energy on its own. It is widely believed that a theory of quantum gravity is needed.

1.2 General Relativity via a Variational Principle

1.2.1 Lagrangian Mechanics

Obtaining the equations of motion of a system is a central task when studying physical theories. Such equations of motion may elegantly be determined via a variational principle.

To describe a classical system with a discrete number of components, one may use *Lagrangian mechanics* instead of the Newtonian approach [5]. Lagrangian mechanics is based on a variational principle, the principle of least action, that may be mathematically represented by the simple equation

$$\delta S = 0, \tag{1.2}$$

where S is the action that describes the system, which is defined as

$$S = \int L \, dt, \tag{1.3}$$

with $L \equiv L(q, \dot{q})$ the lagrangian of the system, which is a function of the generalized coordinates q and respective derivatives. In classical mechanics, L is simply given by the kinetic energy minus the potential energy of the system. Using the principle of least action, one can obtain the *Euler-Lagrange equations*

$$\frac{d}{dt}\left(\frac{\partial L}{\partial \dot{q}}\right) - \frac{\partial L}{\partial q} = 0. \tag{1.4}$$

When applied to a physical system, the Euler-Lagrange equations become the equations of motion of that system, describing its physical configurations.

1.2.2 Classical Field Theory

Lagrangian mechanics is used for a system with a discrete number of components, each with a finite number of degrees of freedom. If the system to be studied is a continuum/field with an infinite number of degrees of freedom, classical field theory must be used. Instead of a lagrangian L, in classical field theory a *lagrangian density* $\mathcal{L} \equiv \mathcal{L}(\phi_i, \partial\phi_i)$ is used, and this lagrangian density depends on the fields $\phi_i \equiv \phi_i(x^\mu)$ and its derivatives [5], which depend on the spacetime point. The action and Euler-Lagrange equations may be written as

$$S = \int d^4x \, \sqrt{-g} \, \mathcal{L}, \tag{1.5}$$

$$\frac{\partial \mathcal{L}}{\partial \phi_i} = \partial_\mu \left(\frac{\partial \mathcal{L}}{\partial \left(\partial_\mu \phi_i\right)} \right). \tag{1.6}$$

1.2.3 General Relativity as a Field Theory

The EFEs can be obtained via a variational principle, as the equations of motion of a theory described by the *Einstein-Hilbert* action [3, 6]

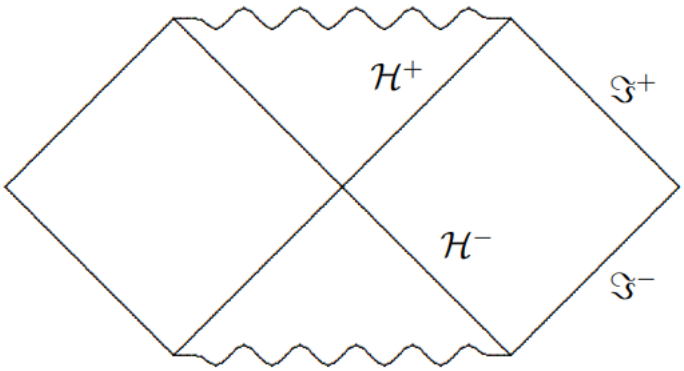

Figure 1.1: Penrose diagram for the Schwarzschild BH with the future (and past) EH and the future (and past) null infinity represented. Source: [10]

$$S = \int d^4x\sqrt{-g}\left(\frac{1}{2\kappa}R + \mathcal{L}_M\right), \tag{1.7}$$

by performing the variations with respect to the metric. The term $\mathcal{L}_M$ is a matter term that defines the energy momentum tensor $T_{\mu\nu}$ by

$$T_{\mu\nu} = -\frac{2}{\sqrt{-g}}\frac{\delta S_M}{\delta g^{\mu\nu}} = -2\frac{\delta \mathcal{L}_M}{\delta g^{\mu\nu}} + \mathcal{L}_M g_{\mu\nu}. \tag{1.8}$$

1.3 Black Holes

In 1784, using Newtonian mechanics, John Mitchel and Pierre-Simon Laplace [7] calculated that there could exist sufficiently massive and compact objects such that the respective escape velocity would exceed the speed of light. Such objects were named *"dark stars"*.

In 1916, Karl Schwarzschild discovered the first non-trivial vacuum solution of the EFEs, that also describes a *black hole* (BH), known as the *Schwarzschild metric*. BHs emerge as a prediction of GR and are objects so compact that are characterised by a hypersurface known as *event horizon* (EH). The region of spacetime enclosed by the EH is causally disconnected from the exterior Universe and constitutes the BH [6, 8, 9].

Definition 1.3.1 ([10])**.** *Event Horizon: Let M be an asymptotically flat spacetime. We define $J^-(U)$ to be the causal past of points $U \subset M$ and $\overline{J}^-(U)$ to be the topological closure of $J^-(U)$ (i.e., including limit points). Define the boundary of $\overline{J}^-(U)$ to be $\dot{J}^-(U) = \overline{J}^-(U) - J^-(U)$. The future EH of M is then*

$$\mathcal{H}^+ = \dot{J}^-\left(\Im^+\right), \tag{1.9}$$

with $\Im^+$ the future null infinity, i.e., the future EH is the boundary of the closure of the causal past of $\Im^+$.

The Schwarzschild metric, that describes the simplest known BH, is given in Schwarzschild coordinates

(t, r, θ, ϕ) by [9, 10]

$$\mathrm{d}s^2 = -\left(1 - \frac{2M}{r}\right)\mathrm{d}t^2 + \left(1 - \frac{2M}{r}\right)^{-1}\mathrm{d}r^2 + r^2\left(\mathrm{d}\theta^2 + \sin^2\theta\mathrm{d}\phi^2\right), \tag{1.10}$$

where M is interpreted as the ADM mass of the BH. The metric has two singularities, where the coefficients g_{tt} and g_{rr} diverge, being the hypersurfaces $r = 0$ and $r = 2M$. The singularity $r = 2M$ is just a consequence of a deficiency of the used coordinate system and it can be removed by an appropriate change of coordinates (being called *removable singularity* for this reason), while the $r = 0$ singularity is *irremovable*. In fact, it can be proved that the Kretschmann scalar $R^{\alpha\beta\mu\nu}R_{\alpha\beta\mu\nu}$ diverges at $r = 0$ [10]. It can also be proved [9, 10] that the hypersurface $r = 2M \equiv r_S$ is the EH of the Schwarzschild BH, with r_S being called the *Schwarzchild radius*.

If an electromagnetic field is considered in the theory, *i.e.*, $\mathcal{L}_M = -\frac{1}{4}F_{\mu\nu}F^{\mu\nu}$ in equation 1.7, with $F_{\mu\nu} = \partial_\mu A_\nu - \partial_\nu A_\mu$ the usual Maxwell tensor (and A_μ the electromagnetic 4-potential) [9], one obtains an energy-momentum tensor given by

$$T^{EM}_{\mu\nu} = F_{\mu\alpha}F_{\mu}{}^{\alpha} - \frac{1}{4}g_{\mu\nu}F_{\alpha\beta}F^{\alpha\beta}, \tag{1.11}$$

and so, the source-free Einstein-Maxwell Field Equations (EMFE) are [10]

$$G_{\mu\nu} = 2T^{EM}_{\mu\nu}, \tag{1.12}$$

$$\nabla_\mu F^{\mu\nu} = 0. \tag{1.13}$$

The EMFEs have the spherically-symmetric Reissner-Nordström (RN) solution [10]

$$ds^2 = -\left(1 - \frac{2M}{r} + \frac{Q^2}{r^2}\right)dt^2 + \frac{dr^2}{\left(1 - \frac{2M}{r} + \frac{Q^2}{r^2}\right)} + r^2\left(\mathrm{d}\theta^2 + \sin^2\theta\mathrm{d}\phi^2\right), \tag{1.14}$$

$$A = \frac{Q}{r}dt, \tag{1.15}$$

that describes an electrically charged BH with mass M and electric charge Q.

The most general solution of the EMFEs is known as the *Kerr-Newman metric*, that describes a rotating BH with mass M, angular momentum J, electric charge Q and magnetic charge P and is given in Boyer-Lindquist coordinates (t, r, θ, ϕ) by [11]

$$\mathrm{d}s^2 = -\frac{\Delta}{\Sigma}\left[\mathrm{d}t - a\sin^2\theta\mathrm{d}\phi\right]^2 + \frac{\sin^2\theta}{\Sigma}\left[\left(r^2 + a^2\right)\mathrm{d}\phi - a\mathrm{d}t\right]^2 + \frac{\Sigma}{\Delta}\mathrm{d}r^2 + \Sigma\mathrm{d}\theta^2, \tag{1.16}$$

$$A = -\left[Q\frac{r}{\Sigma} + P\frac{a\cos\theta}{\Sigma}\right]dt + \left[Q\frac{ar\sin^2\theta}{\Sigma} + P\left(\pm 1 - \cos\theta\frac{r^2 + a^2}{\Sigma}\right)\right]d\phi, \tag{1.17}$$

where $\Sigma = r^2 + a^2\cos^2\theta$, $\Delta = r^2 - 2Mr + a^2 + Q^2 + P^2$ and $a = \frac{J}{M}$. The Schwarzschild and RN solutions can be obtained from the Kerr-Newman metric in the appropriate limits. A particularly important case occurs in the limit where there is neither electric nor magnetic charge, for which the *Kerr metric* is

Figure 1.2: First image of a BH shadow (center of the M87 galaxy). Source: [15]

obtained [12].

1.3.1 Observation and Astrophysical Formation of Black Holes

Although predicted by GR, it is legitimate to ask whether BHs actually do exist in Nature. One can argue that, even though observations support the existence of BHs [13], their existence is not proved, and so, only BH candidates could be listed (objects that resemble BHs but are not proved as so). However, in the last years a diversity of observational data has been delivering information with unprecedented accuracy on the strong gravity region around these objects including, for instance, the gravitational waves events that have been observed as a result of BH binaries inspiral and merger (see a catalogue of gravitational wave events, as of February 2019 in [14]). Another direct observational evidence for the existence of BHs comes from the first image of a BH shadow from the center of the M87 galaxy (fig. 1.2) by the Event Horizon Telescope Collaboration [15] (see *e.g.* [16] for a review on BH shadows).

It is believed that BHs are the endpoints of stellar evolution. Nuclear fusion occurs in stars, and the released energy is able to balance the stars' gravity. However, once the nuclear reactions in the star start to fuse iron, the energy that balances the stars' gravity ceases to exist, and the star undergoes gravitational collapse. The gravitational collapse can lead into one of three (known) possible states, that are mainly determined by the stars' mass M: a white dwarf, a neutron star or a BH [9, 17].

1. If $M \lesssim 1.4M_\odot$, with $M_\odot$ the mass of the sun, then the endpoint is a white dwarf. This result is known as the Chandrasekhar limit [18].

2. If $1.4M_\odot \lesssim M \lesssim 3M_\odot$, the endpoint is a neutron star [9].

3. If $M \gtrsim 3M_\odot$, then a BH is the endpoint of stellar evolution. This result is known as the Tolman–Oppenheimer–Volkoff (TOV) limit [19, 20].

1.3.2 No-Hair Theorems

The Kerr metric is widely considered as the astrophysical relevant BH solution of the EFEs and it is thought to describe astrophysical BHs. This led to a paradigm which is commonly referred to as the *"Kerr hypothesis"*, that states that the Kerr metric provides an exact representation of all the BHs in

the Universe. In the words of Subramanian Chandrasekhar [21]: *"In my entire scientific life, extending over forty-five years, the most shattering experience has been the realization that an exact solution of Einstein's field equations of general relativity, discovered by the New Zealand mathematician, Roy Kerr, provides the absolutely exact representation of untold numbers of massive black holes that populate the Universe."*. The Kerr hypothesis relies on two main steps:

1. In the late 1960s and the early 1970s a set of mathematical results known as the *"uniqueness theorems"* (see [22, 23] for reviews on the uniqueness theorems) established that the most general physical BH solution in (electro-)vacuum is represented by the Kerr(-Newman) solution.

2. Inspired by the uniqueness theorems, a much more ambitious idea known as the *no-hair conjecture*, put forward by John Wheeler and Remo Ruffini [24] that generalizes the uniqueness theorems to non-(electro-)vaccum. The no-hair conjecture states that, regardless of the type of matter/energy one starts with, gravitational collapse leads to BHs that are totally described by their mass, angular momentum (and electric charge), all of which are asymptotically measured quantities subject to a Gauss law, and have no other defining quantities referred to as *hair*. In other words, the no-hair conjecture states that the only type of BHs that can emerge dynamically are Kerr BHs (it is thought that electric charge is not relevant in astrophysical BHs). Two BHs with the same mass and angular momentum will be exactly equal, making BHs remarkably different of any other macroscopic object. For instance, two stars may have equal masses and angular momenta, but these may be distributed in different ways across the stars, a difference which will be manifest in the higher multipole moments of the gravitational field. For two BHs with equal masses and angular momenta, all higher multipole moments of the gravitational field will coincide, although they are non-trivial [25].

However the no-hair conjecture is not a proved fact, and there must be some skepticism and questions should be asked about whether may be other good alternative BH models. Three broad criteria for a good BH model are:

1. Appear as a solution of a well motivated and consistent physical model.

2. Has a dynamical formation mechanism.

3. Is sufficiently stable.

One of the most widely studied types of hairy BHs are BHs with scalar hair. These BHs assume the existence of a scalar field in the theory that is intimately connected with the BH. There are a set of well established no-hair theorems for scalar fields, but these may be evaded by relaxing some of their assumptions in a smart way. A review on the no-scalar-hair theorems, as well as on the known regular (on and outside the EH) asymptotically flat BH solutions with scalar hair, can be found in [26].

But why is scalar hair so widely studied? Asking "why scalar hair?" is tantamount equivalent to asking "why scalar fields?". Scalar fields were proved to exist in Nature with the discovery of the Higgs boson [27, 28] and constitute a proxy to describe different types of realistic matter. Scalar fields also

appear in several models, from cosmology (for the evolution of the Universe *e.g.* the "inflaton" and as candidates for dark matter [29]) to extensions of the standard model (*e.g.* the axion, to solve the strong CP problem [30]). Thus, scalar fields are both motivated by fundamental theories and a useful phenomenological tool.

1.4 Spontaneous scalarization

A dynamical mechanism that could lead to the formation of BHs that differ from the standard GR (electro-)vacuum BHs is ***spontaneous scalarization***. Spontaneous scalarization is a phenomenon through which an unstable object becomes immersed in a non-trivial, asymptotically vanishing scalar-field configuration (similar to spontaneous magnetization in ferromagnetic materials [31]). It was first proposed by Damour and Esposito-Farèse in the context of neutron stars [32–34]. Remarkably, spontaneous scalarization is not exclusive of neutron stars as it is conjectured to occur in other objects like BHs (which result in hairy BHs with scalar hair), as pointed out in the original works [35–37], nor it is not exclusive of gravitational theories! As an introduction, a toy model from [38] shall be followed.

1.4.1 A toy model: spontaneous scalarization of a charged sphere

Consider the following scalar field action on a non-trivial background (electromagnetic field) in flat (Minkowski) spacetime

$$S_\phi = -\int d^4x\sqrt{-g}\left[2\partial_\mu\phi\partial^\mu\phi + f(\phi)\mathcal{I}\right], \tag{1.18}$$

with $\mathcal{I} = F_{\mu\nu}F^{\mu\nu}$, $F_{\mu\nu}$ the usual Maxwell tensor, ϕ the scalar field and $f(\phi)$ the coupling function. For spontaneous scalarization to occur three conditions are required:

1. Maxwell's theory must be recovered near infinity (since the scalar field is asymptotically vanishing).
2. The system must allow the existence of a scalar free solution (so that a scalar field may spontaneously emerge).
3. The system must undergo an instability (in this case, it must be unstable against scalar perturbations $\delta\phi$).

From the Euler-Lagrange equations, the scalar field equation of motion may be obtained:

$$\Box\phi = \frac{\dot{f}(\phi)\mathcal{I}}{4}, \tag{1.19}$$

with $\Box \equiv \partial_\mu\partial^\mu$, the dot denotes differentiation with respect to the scalar field. Equation 1.19 may be linearized around a scalar free solution for scalar perturbations

$$\left(\Box - \mu_{eff}^2\right)\delta\phi = 0, \tag{1.20}$$

with $\mu_{eff}^2 = \ddot{f}(0)\mathcal{I}/4$ acting as an "effective mass". From equations 1.19 and 1.20, the restrictions on

the form of the coupling function may be extrapolated, in order for spontaneous scalarization to occur. From the previous three conditions:

1. $f(\phi(\infty)) = f(0) = 1$, in order to recover Maxwell's theory near infinity.
2. $\dot{f}(0) = 0$, from equation 1.19 to allow the existence of a scalar free solution.
3. $\ddot{f}(0) > 0$, from equation 1.20, in order to have $\mu^2_{eff} < 0$, so that a *tachyonic instability* can settle in the system (for a purely electrical field $\mathcal{I} < 0$).

The system allows a scalar free solution given by

$$\phi = 0, \qquad A = \frac{Q}{r} dt, \tag{1.21}$$

which is the Coulomb solution. Consider also, in appropriate units the following coupling function that satisfies the previous conditions

$$f(\phi) = \frac{1}{1 - \phi^2}, \tag{1.22}$$

and so, the scalar free solution is unstable against scalar perturbations. The model then admits the spherically symmetric scalarized solution given by

$$\phi = \zeta \sin\left(\frac{Q}{r}\right), \qquad A = \left[\left(1 - \frac{\zeta^2}{2}\right)\frac{Q}{r} + \frac{\zeta^2}{4}\sin\left(\frac{2Q}{r}\right)\right] dt, \tag{1.23}$$

where ζ is an integration constant. Defining the energy density as $\rho = -T^t_t$, then the total energy is given by

$$E = 4\pi \int_{r_0}^{\infty} r^2 \rho \, dr. \tag{1.24}$$

Consider now a conducting sphere at $r = r_0$, and defining the energies of the scalar free and scalarized solutions as $E^{(\phi=0)}$ and $E^{(\phi\neq 0)}$ respectively one obtains

$$E^{(\phi\neq 0)} - E^{(\phi=0)} = 4\pi\zeta^2 Q \sin\left(\frac{2Q}{r_0}\right), \tag{1.25}$$

which implies that the scalarized solution is energetically favoured in a set of bands

$$\frac{Q}{r_0} \in]n\pi + \frac{\pi}{2}, n\pi + \pi[, \tag{1.26}$$

with $n \in \mathbb{N}_0$ an integer that labels the bands and defines the number of nodes of the scalar field radial profile. Within these bands the unstable scalar free system is likely to evolve into the more stable scalarized system. A few conclusions may be taken from this example:

1. We emphasise again that spontaneous scalarization is not exclusive of gravitational theories.
2. It sometimes leads to more stable configurations.
3. It can occur through non-minimal couplings of the scalar field to a source term (like the electromagnetic field).

4. The coupling function must obey some specific conditions in order for spontaneous scalarization to occur.

1.4.2 Spontaneous scalarization of black holes

Spontaneous scalarization is conjectured to occur in BHs. This area of research was triggered by the works [35–37], where spontaneous scalarization occurs through non-minimal couplings of the scalar field to higher order curvature terms, namely the Gauss-Bonnet (GB) term $\mathcal{G}$.

1.4.2.1 The Gauss-Bonnet term and Lovelock gravity

A possible generalisation of GR includes adding higher order curvature correction terms to the action, but these will usually include third-order equations of motion which yield additional dynamical degrees of freedom and other pathologies. There is however one exception that generalises GR to an arbitrary number of dimensions while maintaining the equations of motion to second order. This exception is called *Lovelock Gravity* [39] and is a generalisation of the Einstein-Hilbert lagrangian to an arbitrary number of dimensions

$$\mathcal{L} = \sum_{n=0}^{p} \alpha_n \mathcal{R}^n, \quad \mathcal{R}^n = \frac{1}{2^n} \delta^{\mu_1\nu_1\ldots\mu_n\nu_n}_{\alpha_1\beta_1\ldots\alpha_n\beta_n} \prod_{r=1}^{n} R^{\alpha_r\beta_r}{}_{\mu_r\nu_r}, \tag{1.27}$$

where $\mathcal{R}^n$ is the n^{th} Euler density (which is a topological invariant in $D = 2n$ dimensions), δ is the generalized Kronecker delta, $D = 2p + 2$ for an even number of dimensions and $D = 2p + 1$ for an odd number, where p is an integer. Expanding the above expression for five dimensions yields

$$\mathcal{L} = \alpha_0 + \alpha_1 R + \alpha_2 \mathcal{G}, \tag{1.28}$$

where $\mathcal{R}^2 = \mathcal{G}$ is the *Gauss-Bonnet* (GB) term:

$$\mathcal{G} = R^2 - 4R_{\mu\nu}R^{\mu\nu} + R_{\mu\nu\alpha\beta}R^{\mu\nu\alpha\beta}. \tag{1.29}$$

The Einstein-Hilbert lagrangian plus a constant that plays the role of a cosmological constant is recovered in four dimensions. In this four-dimensional case, if one insists to add the GB term to the action, the integral over the GB term is a topological invariant, so it cannot contribute to the dynamics, hence GR is recovered. In higher dimensions this term becomes dynamically non-trivial.

In the context of scalar-tensor theories of gravity, the addition of the GB term to the theory, non-minimally coupled to a scalar field, constructs the class known as ***extended Scalar-Tensor Gauss-Bonnet models*** (eSTGB). Moreover, despite being quadratic in the Riemann and Ricci tensors, terms containing more than two partial derivatives of the metric cancel out, making the Euler-Lagrange equations second order partial differential equations for any coupling of the scalar field to the GB term. A recent work [40] in the context of eSTGB showed that spontaneous scalarization can occur for Kerr BHs, and that for some values of the spin parameter, these scalarized Kerr BHs are compatible with the observed M87 BH shadow.

1.4.2.2 Einstein-Maxwell Scalar models

The main focus of this thesis will be the study of ***Einstein-Maxwell Scalar*** (EMS) models, first studied in the context of spontaneous scalarization in [38]. A simple and natural generalisation of the Einstein-Maxwell theory, *i.e.* electrovacuum, is to consider an additional dynamical real scalar field, forming the EMS models. A variety of such models is possible depending on the way the scalar-field couples to the Maxwell field.[1] If the scalar-field is minimally coupled to the Maxwell field, no new BH solutions beyond the RN BH arise, hence no hairy BHs exist. However new hairy BH solutions appear once non-minimal couplings are considered. The first such non-minimally coupled EMS model emerged in the pioneering unification theory of Kaluza [41] and Klein [42].

In what concerns BH spontaneous scalarization, eSTGB models belong to a wider universality class that also contains the EMS models. EMS models allow the occurrence of spontaneous scalarization through certain non-minimal couplings of the scalar field to the electromagnetic field. In this type of models, no higher curvature terms are required in order for spontaneous scalarization to occur, which results in a computationally less demanding problem, that also allows an indirect study of the involved dynamical phenomena and processes. Since ref. [38] was published, EMS models have been further studied in this spontaneous scalarization context [1, 43–47].

1.5 Computational shooting method: an introduction

A standard numerical technique used throughout this dissertation is the *shooting method*. To better understand a shooting problem it is helpful to think of the well studied "particle in a 1D infinite potential well with length L" problem [48], for a particle with mass m. It consists in solving the time-independent Schrödinger equation for the wavefunction $\psi(x)$

$$-\frac{\hbar^2}{2m}\frac{d^2}{dx^2}\psi(x)+V(x)\psi(x)=E\psi(x), \tag{1.30}$$

for the potential

$$V(x)=\begin{cases} 0, & 0<x<L, \\ \infty, & \text{otherwise}, \end{cases} \tag{1.31}$$

which is an eigenvalue problem. The suitable boundary conditions for the problem are $\psi(0)=\psi(L)=0$, but not all values of the energy E can solve the problem - only discrete values for the energy given by

$$E_n=\frac{n^2\pi^2\hbar^2}{2mL^2}, \tag{1.32}$$

with n an integer that also labels the state of the particle, are the eigenvalues of the problem. This problem has an analytical solution, but when dealing with more complicated systems solutions must be obtained via a numerical procedure. To numerically solve this problem, using a shooting method, the following algorithm is used: (i) decompose the Schrödinger equation into two coupled first order ordinary

[1] Herein we shall always consider that the scalar field is minimally coupled to gravity.

differential equations (ODEs):

$$\begin{cases} \frac{d\psi}{dx} &= z, \\ \frac{dz}{dx} &= -\frac{2m}{\hbar^2}\left(E - V(x)\right)\psi, \end{cases} \tag{1.33}$$

but these require two initial conditions, instead of two boundary conditions, so a shooting method to "transform" this initial value problem into a boundary value problem is required; (ii) give a known boundary condition $\psi(0) = 0$, a guess for the initial value of z and two initial guesses for the energy; (iii) solve the system for the two values of the energy using an ODE integrator and check if the wavefunction, at the other boundary, is within an acceptable tolerance of the expected value; (iv) if it is not, using the secant method, obtain the next iterative value for the energy

$$E[i+1] = E[i] + \frac{\psi_{BC}(L) - \psi(L)[i]}{\psi(L)[i] - \psi(L)[i-1]}(E[i] - E[i-1]), \tag{1.34}$$

and solve the system, with i denoting the iteration variable and $\psi_{BC}(L) = 0$; (v) repeat until the wavefunction value at the boundary is within an acceptable tolerance of the expected value.

This algorithm will be used when studying EMS models, where systems of coupled ODEs have to be solved, and a shooting must be done on some essential parameters in order to fulfil the boundary conditions.

1.6 Thesis outline

In Chapter 2 we introduce the EMS models and study spontaneous scalarization of purely electric BHs for four different types of non-minimal couplings, namely the domain of existence, perturbative stability and entropic preference of the scalarized solutions. In Chapter 3, EMS models and spontaneous scalarization are studied within the framework of dyonic BHs (BHs with both electric and magnetic charge). Next, in Chapter 4 we generalise EMS models to include an axionic-like coupling and show that spontaneous scalarization is possible in this new model with a new source term. We study the new features that arise and perform a study of BHs with axionic hair. Finally, Chapter 5 features the final conclusions, as we examine the achievements of the work developed in the scope of this thesis, and we explore further avenues of future research.

Chapter 2

EMS models: introduction and spontaneous scalarization of purely electric black holes

In the present chapter a study of spontaneous scalarization of purely electric BHs in EMS models is done. In Section 2.1 the basics of EMS models are presented. Following, in Section 2.2 some physical relations, which include a Virial relation and a Smarr law are deduced. In Section 2.3 a discussion on the necessary conditions for the occurrence of spontaneous scalarization is done, and the therein studied coupling functions are presented. The bifurcating solutions from the scalar free RN BH are discussed in Section 2.4. Finally, in Section 2.5 the results are presented. In particular the numerical static solutions are obtained and the domain of existence discussed, it is shown that for all examples of couplings considered the scalarized BHs are thermodynamically preferred over the electro-vacuum solutions - the RN BHs with comparable global charges, and a perturbative stability analysis is done. In Appendix A we address the time evolution problem (whose details are beyond the scope of this thesis) and show that scalarized BHs do form dynamically, and we also consider the time evolution of unstable RN BHs under non-spherical perturbations to show that, in all cases, the end point is a spherically symmetric scalarized BH. In this Chapter, refs. [1, 38] will be followed. For an aesthetic purpose that will become clearer throughout this thesis, the Maxwell equations will be written

$$\begin{cases} \nabla \cdot \mathbf{E} & = 4\pi\rho_{\mathrm{e}}, \\ \nabla \cdot \mathbf{B} & = 0, \\ \nabla \times \mathbf{E} & = -\frac{1}{c}\frac{\partial \mathbf{B}}{\partial t}, \\ \nabla \times \mathbf{B} & = \frac{1}{c}\left(4\pi\mathbf{j}_{\mathrm{e}} + \frac{\partial \mathbf{E}}{\partial t}\right), \end{cases} \tag{2.1}$$

2.1 The EMS model

The EMS model describes a real scalar field ϕ non-minimally coupled to Maxwell's electromagnetism through a function $f_i(\phi)$ and minimally coupled to Einstein's gravity, and is described by the action

$$\mathcal{S} = \int d^4x\sqrt{-g}\Big(R - 2\partial_\mu\phi\partial^\mu\phi - f_i(\phi)\mathcal{I}(\psi, g)\Big), \tag{2.2}$$

where $\mathcal{I}$ is a source term which generically depends on matter field(s), ψ, and the metric tensor $g_{\mu\nu}$. In EMS models the source term is $\mathcal{I} = F_{\mu\nu}F^{\mu\nu}$, with $F_{\mu\nu}$ the usual Maxwell tensor, whereas in eSTGB models $\mathcal{I} = \mathcal{G}$, and thus both belong to a wider universality class of models. The subscript of the coupling function $f_i(\phi)$ will denote the several coupling choices as it will later be specified. Notice that the toy model considered in subsection 1.4.1 is the EMS action without Einstein's gravity. The generic, spherically symmetric, line element which can be used to describe both a scalar-free and a scalarized BH solution is

$$ds^2 = -N(r)e^{-2\delta(r)}dt^2 + \frac{dr^2}{N(r)} + r^2\left(d\theta^2 + \sin^2\theta d\varphi^2\right), \tag{2.3}$$

(since any spherically symmetric metric can be brought to this form [49]), where $N(r) = 1 - \frac{2m(r)}{r}$, with $m(r)$ the Misner-Sharp mass function [50]. Spherical symmetry, in the absence of a magnetic charge, imposes an electrostatic 4−vector potential given by

$$A(r) = V(r)\,dt, \tag{2.4}$$

and a scalar field that is purely radial dependent $\phi(r)$. Integrating the trivial angular dependence allows to define (up to an overall constant that does not affect the equations of motion) an effective lagrangian

$$\mathcal{L}_{eff} = e^{-\delta}m' - \frac{1}{2}e^{-\delta}r^2N\phi'^2 + \frac{1}{2}e^{\delta}f_i(\phi)r^2V'^2\ . \tag{2.5}$$

Recall that the functions m, δ, ϕ and V are solely radial dependent, and such dependence shall be omitted for notation simplicity. The prime denotes a radial derivative. The equations of motion may be derived from the Euler-Lagrange equations and are presented as follows

$$m' = \frac{1}{2}r^2N\phi'^2 + \frac{1}{2}e^{2\delta}f_i(\phi)r^2V'^2\ , \tag{2.6}$$

$$\delta' = -r\phi'^2\ , \tag{2.7}$$

$$\left(e^{\delta}f_i(\phi)r^2V'\right)' = 0\ , \tag{2.8}$$

$$\left(e^{-\delta}r^2N\phi'\right)' = -\frac{1}{2}\dot{f}_i(\phi)\,e^{\delta}\,r^2V'^2\ , \tag{2.9}$$

where we denote $\dot{f}_i = df_i/d\phi$ (also $\ddot{f}_i = d^2f_i/d\phi^2$). The equations simplify as we notice the existence of a first integral

$$V' = -e^{-\delta}\frac{Q}{r^2f_i(\phi)}, \tag{2.10}$$

with Q an integration constant interpreted as the electric charge. To solve the set of ordinary differential equations (ODEs) 2.6-2.9 suitable boundary conditions are implemented for the functions m, δ, ϕ and V. Assuming the existence of an event horizon located at $r = r_H > 0$, in its vicinity one finds the following approximate solution to the field equations

$$\begin{aligned} m(r) &= \frac{r_H}{2} + m_1 (r - r_H) + \dots , \qquad \delta(r) = \delta_0 + \delta_1 (r - r_H) + \dots , \\ \phi(r) &= \phi_0 + \phi_1 (r - r_H) + \dots , \qquad V(r) = v_1 (r - r_H) + \dots , \end{aligned} \tag{2.11}$$

where

$$\begin{aligned} m_1 &= \frac{Q^2}{2 f_i(\phi_0) r_H^2} , \qquad \phi_1 = \frac{\dot{f}_i(\phi_0)}{2 r_H f_i(\phi_0)} \left(\frac{Q^2}{Q^2 - r_H^2 f_i(\phi_0)} \right) , \\ \delta_1 &= -\phi_1^2 r_H , \qquad v_1 = -\frac{e^{-\delta_0} Q}{r_H^2 f_i(\phi_0)} . \end{aligned} \tag{2.12}$$

This approximation of the field equations contains only two essential parameters ϕ_0 and δ_0 that are found, through a standard shooting method, by matching the above expansion with the following asymptotics in the far field

$$m(r) = M - \frac{Q^2 + Q_s^2}{2r} + \dots , \qquad \phi(r) = \frac{Q_s}{r} + \frac{Q_s M}{r^2} + \dots , \qquad \delta(r) = \frac{Q_s^2}{2r^2} + \dots , \qquad V(r) = \Phi + \frac{Q}{r} + \dots , \tag{2.13}$$

with Q_s the "scalar charge", Φ the electrostatic potential difference between the EH and infinity and M the ADM mass. The following results and definitions for the EMS model will be useful later

$$F_{\mu\nu} F^{\mu\nu} = -\frac{2Q^2}{r^4 f_i(\phi)^2} \tag{2.14}$$

$$K(r_H) = \frac{4}{r_H^4} \left[3 - \frac{6Q^2}{r_H^2 f_i(\phi_0)} + \frac{5Q^4}{r_H^4 f_i^2(\phi_0)} \right] , \quad \rho(r_H) = \frac{2Q^2}{r_H^4 f_i(\phi_0)} , \tag{2.15}$$

$$q = \frac{Q}{M}, \qquad a_H = \frac{A_H}{16\pi M^2}, \qquad A_H = 4\pi r_H^2, \qquad t_H = 8\pi M T_H, \qquad T_H = \frac{1}{4\pi} N'(r_H) e^{-\delta_0} \tag{2.16}$$

with $K(r_H)$ the Kretschmann scalar at the EH, $\rho(r_H)$ the energy density at the horizon, q the reduced charge, a_H the reduced EH area, A_H being the EH area, t_H the reduced horizon temperature and T_H the horizon temperature. The reduced quantities are convenient because they are invariant under the scaling symmetry

$$r \to \lambda r, \qquad \xi \to \lambda \xi, \tag{2.17}$$

with ξ representing any quantity of the model, while $f_i(\phi)$ remains unchanged.

2.2 Physical relations

It is of uttermost importance to verify that the scalarized solutions obtained when numerically solving the coupled ODE system are indeed physical. Two relations are used to test the code: a Smarr law and a Virial relation.

2.2.1 Smarr law

The Smarr law [51, 52] provides a relation between the total mass of the spacetime and other measurable quantities (like the horizon temperature, area...), hence being a physical energetic balance equation, which is independent of the equations of motion, making it ideal to test whether the obtained solutions are physical, or not. The Smarr law can be obtained via the integral mass formula, that for our model reads

$$M = \frac{1}{2}T_H A_H - \frac{1}{16\pi}\int_V (2T^b_a - T\delta^b_a)K^a d\Sigma_b, \tag{2.18}$$

where K^a is the timelike translational killing vector, and T the trace of the energy-momentum tensor. The energy-momentum tensor is

$$T_{\mu\nu} = 4\left[f_i(\phi)\left(F_{\mu\alpha}F^{\alpha}_{\nu} - \frac{1}{4}g_{\mu\nu}F_{\alpha\beta}F^{\alpha\beta}\right) + \partial_\mu\phi\partial_\nu\phi - \frac{1}{2}g_{\mu\nu}\partial_\alpha\phi\partial^\alpha\phi\right]. \tag{2.19}$$

One can thus arrive at the Smarr law

$$M = \frac{1}{2}T_H A_H + \Phi Q, \tag{2.20}$$

with

$$\Phi = \int_{r_H}^{\infty} dr\left(\frac{Q}{r^2 f_i(\phi)}e^{-\delta}\right) \equiv -\int_{r_H}^{\infty} dr V', \tag{2.21}$$

the electrostatic potential difference. The Smarr law turns out to have no explicit imprint of the scalar hair. The solutions also satisfy a *non-linear Smarr law* [38] given by

$$M^2 + Q_s^2 = \frac{1}{4}T_H^2 A_H^2 + Q^2 \tag{2.22}$$

2.2.2 Virial relation

Derrick type arguments [53] can be used to establish no-hair theorems in BH physics [26], as well as to provide a physical relation that must be obeyed and that is independent of the equations of motion, hence providing useful insights about whether a solution is physical or not. Consider the effective action

$$\mathcal{S}_{eff} = \int_{r_H}^{\infty} dr\mathcal{L}_{eff}, \tag{2.23}$$

and assume that hairy BH solutions exist such that they are described by the functions $\phi(r), \delta(r), V(r), m(r)$ with suitable boundary conditions at the event horizon and at infinity. Next consider the 1-parameter family of configurations described by the scaled functions

$$F_\lambda(r) \equiv F(r_H + \lambda(r - r_H)), \tag{2.24}$$

with $F \in \{\phi, \delta, V, m\}$. If the initial configuration was indeed a solution, then there must be a critical point at $\lambda = 1$ such that the effective action is extremized: $\left(\frac{dS^\lambda_{eff}}{d\lambda}\right)_{\lambda=1} = 0$. It is then straightforward

to obtain a Virial relation given by

$$\int_{r_H}^{\infty} dr \left\{ e^{-\delta} r^2 \phi'^2 \left[1 - \frac{2r_H}{r} \left(1 - \frac{m}{r} \right) \right] \right\} = \left(\Phi + \int_{r_H}^{\infty} dr \left\{ \frac{2r_H}{r} V' \right\} \right) Q. \tag{2.25}$$

One can show that the left hand side integrand is strictly positive. Thus, the virial identity shows that a nontrivial scalar field requires a nonzero electric charge so that the right hand side is nonzero.

2.3 Conditions for the occurrence of spontaneous scalarization

As discussed in the toy model of section 1.4.1, in order for spontaneous scalarization to occur in a model, the coupling function (and respective derivatives) must satisfy a set of conditions. These conditions emerge as a consequence of **i)** the far field equations of motion; **ii)** allowing the existence of a scalar free solution; **iii)** imposing a tachyonic instability in the system. The coupling functions are then restrained in the following way

1. Maxwell's theory must be recovered near infinity, hence, for an asymptotically vanishing scalar field profile

$$f_i(0) = 1. \tag{2.26}$$

2. The system must accommodate a scalar free solution. The Klein-Gordon equation of motion is

$$\Box\phi = \frac{\dot{f}_i(\phi) F_{\mu\nu} F^{\mu\nu}}{4}, \tag{2.27}$$

with $\Box \equiv \nabla_\mu \nabla^\mu$, from which, in order for a non-scalarized solution to exist, follows that

$$\dot{f}_i(0) = 0. \tag{2.28}$$

3. Spontaneous scalarization occurs if the system is unstable against scalar perturbations $\delta\phi$. These obey (neglecting second order terms)

$$(\Box - \mu_{eff}^2)\delta\phi = 0, \tag{2.29}$$

with $\mu_{eff}^2 < 0$ given by

$$\mu_{eff}^2 = \frac{\ddot{f}_i(0) F_{\mu\nu} F^{\mu\nu}|_{\phi=0}}{4} = -\ddot{f}_i(0) \frac{Q^2}{2r^4}, \tag{2.30}$$

from which $\ddot{f}_i(0) > 0$.

In fact two Bekenstein type identities [54] can be derived, in a similar way as in [37, 47], which set constraints on the coupling $f_i(\phi)$. A first identity can be obtained by multiplying eq. 2.27 by $\dot{f}_i(\phi)$ and integrating over a spacetime volume. Then after integrating by parts and discarding the boundary terms

by virtue of the horizon properties and asymptotic flatness, one obtains

$$\int d^4x\sqrt{-g}\left(\ddot{f}_i(\phi)\partial_\mu\phi\partial^\mu\phi+\frac{\dot{f}_i(\phi)^2}{4}F_{\mu\nu}F^{\mu\nu}\right)=0. \tag{2.31}$$

For a purely electrical potential $F_{\mu\nu}F^{\mu\nu}<0$, which implies

$$\ddot{f}_i(\phi)>0, \tag{2.32}$$

must hold for some range of the radial coordinate r, otherwise the two terms of the integrand will always have the same sign (since with our metric signature $\partial_\mu\phi\partial^\mu\phi>0$ in the BH exterior), in which case the identity can only be respected for $\phi=0$. The second identity can be found in a similar way, but by multiplying eq. 2.27 by ϕ

$$\int d^4x\sqrt{-g}\left(\partial_\mu\phi\partial^\mu\phi+\frac{\phi\dot{f}_i(\phi)}{4}F_{\mu\nu}F^{\mu\nu}\right)=0, \tag{2.33}$$

that, once again, for a purely electrical potential implies

$$\phi\dot{f}_i(\phi)>0, \tag{2.34}$$

for some range of r.

2.3.1 The coupling functions

Hereby we shall consider four forms of coupling functions compatible with the above presented constraints for spontaneous scalarization

i) an exponential coupling, $f_E(\phi)=e^{-\alpha\phi^2}$, first used in this context in [38];

ii) a hyperbolic cosine coupling, $f_C(\phi)=\cosh(\sqrt{2|\alpha|}\phi)$;

iii) a power coupling, $f_P(\phi)=1-\alpha\phi^2$, already discussed in this context for eSTGB models in [55];

iv) a fractional coupling, $f_F(\phi)=\frac{1}{1+\alpha\phi^2}$.

The coupling constant α is a dimensionless constant in all cases, and, except for the hyperbolic function, the conditions on f_i imply that $\alpha<0$ for a purely electric field. The f_i candidates shall be specified by the subscript $i\in\{E,\ C,\ P,\ F\}$, respectively. For $|\alpha|\phi^2\ll 1$ (and $\alpha<0$), f_E, f_C and f_F possess the same Taylor expansion to first order which coincides with the (exact) form of f_P:

$$f_F(\phi)\approx f_C(\phi)\approx f_E(\phi)\approx 1+|\alpha|\,\phi^2+\mathcal{O}(\phi^4)\ . \tag{2.35}$$

2.4 Bifurcating points from the RN BH - The existence line for scalarized solutions

Scalar perturbations obey eq. 2.29. Due to the spherical symmetry, performing a spherical harmonic decomposition of the scalar field

$$\delta\phi(r,\theta,\varphi)=\sum_{\ell,\mathbf{m}}Y_{\ell\mathbf{m}}(\theta,\varphi)U_\ell(r), \tag{2.36}$$

the scalar field equation of motion 2.27 simplifies to

$$\frac{e^\delta}{r^2}\left(\frac{r^2N}{e^\delta}U_\ell'\right)'-\left[\frac{\ell(\ell+1)}{r^2}+\mu_{\rm eff}^2\right]U_\ell=0\ , \tag{2.37}$$

while $\mu_{eff}^2=-|\alpha|Q^2/r^4<0$ for all previous choices of couplings. This is an eigenvalue problem: fixing the coupling α, for a given ℓ, requiring an asymptotically vanishing, smooth scalar field, a discrete set of BHs solutions are selected, *i.e.* RN solutions with a certain charge to mass ratio q. These are the bifurcation points from the scalar-free solution. They are labelled by an integer $n\in\mathbb{N}_0$ (that also represents the number of nodes in the scalar field profile); $n=0$ is the fundamental mode, whereas $n>1$ are excited states (overtones). One expects only the fundamental solutions to be stable [43]. Clearly, for any $f_i(\phi)$, setting $\delta=0$ and $N(r)=1-2M/r+Q^2/r^2$ in 2.37 allows us to recover the usual RN metric. Then, a scalarized solution can be dynamically induced by a scalar perturbation of the background, as long as the scalar-free RN solution is in the unstable regime. As pointed out in [1, 38], for $\ell=0$, one finds the following exact solution[1]

$$U(r)=LP_u\left[1+\frac{2Q^2(r-r_H)}{r\,(r_H^2-Q^2)}\right]\ ,\qquad\text{where}\qquad u\equiv\frac{1}{2}(\sqrt{4\alpha+1}-1)\ , \tag{2.38}$$

and LP_u being a Legendre function. The function $U(r)$ approaches a constant non-zero value as $r\to\infty$,

$$U(r)\to U_\infty={}_2F_1\left[\frac{1}{2}(1-\sqrt{4\alpha+1}),\frac{1}{2}(1+\sqrt{4\alpha+1}),1;\frac{q^2}{2\left(q^2-1-\sqrt{1-q^2}\right)}\right]+\mathcal{O}\left(\frac{1}{r}\right)\ , \tag{2.39}$$

thus finding the $\ell=0$ unstable mode of the RN BH reduces to a study of the zeros of the hypergeometric function ${}_2F_1$. A plot of U_∞ as a function of q is given in Fig. 2.1 (left panel) for an illustrative value of α. Some values of the minimum value of $|\alpha|$ for scalarization of a RN BH with charge to mass ratio q can be found in Table. 2.1. In Fig. 2.1 (right panel) the existence lines for the $n=0$ and $n=1$ mode are presented.

q	1.0	0.9	0.8	0.7	0.6	0.5	0.4	0.3	0.2	0.1
$\lvert\alpha\rvert$	0.25	2.995	5.121	8.019	12.37	19.50	32.56	60.72	141.0	574.9

Table 2.1: Minimum value of $|\alpha|$ for scalarization of a RN BH with charge to mass ratio q.

[1] No exact solution appears to exist for $\ell\geqslant 1$, and equation (2.37) is solved numerically. These modes, nonetheless, also possess non-linear continuations leading to static, non-spherically symmetric scalarized BHs [1, 38]

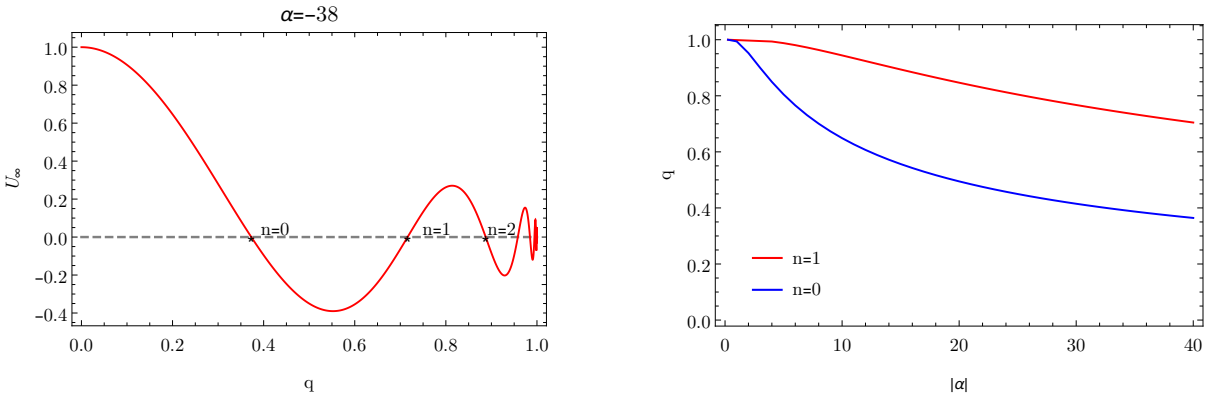

Figure 2.1: Left: Asymptotic value U_∞ of the $l = 0$ amplitude U for $\alpha = -38$ as a function of q. Right: Existence lines for the $n = 0$ mode, *i.e.*, the bifurcating points from the RN BH, and for the $n = 1$ mode.

2.5 Results

The set of four ODEs 2.6-2.9 can be numerically solved through a Runge-Kutta strategy, given the aforementioned boundary conditions. Our numerical method implements a six(five) Runge-Kutta integration algorithm (RK65) with an adaptative step size and a shooting method. The latter is implemented in the unknown parameters and ensures the fulfilment of the boundary conditions. This code is written in C. It was originally developed by Alexandre Pombo [1], who provided me the code that I later improved and adapted.

2.5.1 Solutions of the radial profiles

Let us start by exhibiting some typical solutions obtained from the numerical integration. In Fig. 2.2 the various radial functions defining the scalarized BHs are represented for an illustrative coupling of $\alpha = -10$, charge to mass ratio $q \equiv Q/M = 0.66$ and for three different choices of coupling. A universal feature of those nodeless solutions is that the scalar field is a monotonically decreasing function of the radius. Thus the scalar field value at the horizon, ϕ_0, is always the maximum of the scalar field. The scalar field vanishes asymptotically. In fact, at far enough radius, all defining functions of the scalarized BHs converge to the ones of a comparable (*i.e.* with the same global charges) RN BH. Another typical feature illustrated by the figure is that the differences between the exponential and power-law couplings are small (the same would apply to the cosh coupling, thus not shown) – see Table 2.2, and more pronounced for the fractional coupling. Yet, for the same values of α and q the scalarization with the exponential coupling is stronger than the one with the power law (and intermediate in the cosh one); this is visible in the value of the scalar field at the horizon on the two top panels of the figure. We remark that these data are well within the numerical errors: our tests have exhibited a relative difference of 10^{-8} for the Virial relation and 10^{-7} for the Smarr relation.

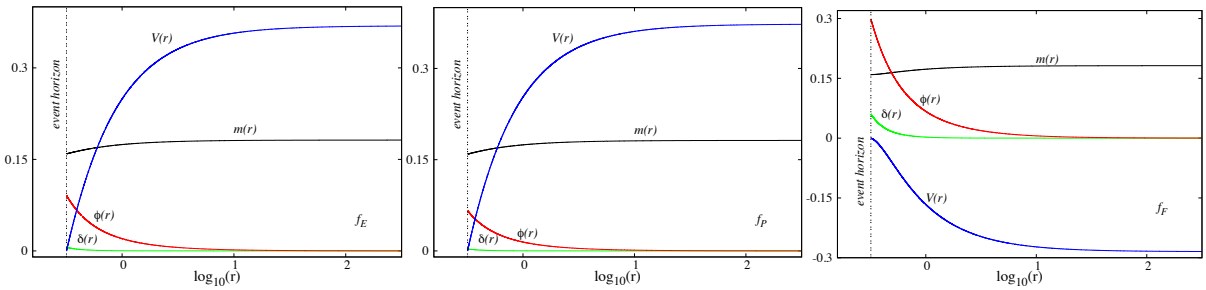

Figure 2.2: Scalarized BH radial functions for $\alpha = -10$ and $q = 0.66$. (Left panel) f_E; (Middle panel) f_P; (Right panel) f_F. Source: [1].

$f_i(\phi)$	r_H	M	Q_s	Φ	a_H	T_H
f_E	0.3180	0.1816	0.0167	0.3689	0.7663	0.2162
f_C	0.3180	0.1816	0.0132	0.3720	0.7663	0.2156
f_P	0.3180	0.1816	0.0122	0.3729	0.7663	0.2154
f_F	0.3186	0.1818	0.0561	0.2848	0.7680	0.2314

Table 2.2: Characteristic quantities for scalarized BH solutions with four choices of couplings, $\alpha = -10$ and $q = 0.66$.

For the particular case of the fractional coupling, however, a different type of solutions, that we call *exotic* is possible. If $1+\alpha\phi_0^2 < 0$, then the corresponding solutions have a region of negative energy density in the vicinity of the horizon, *cf.* eq. 2.15 and Fig. 2.3 (right panel). Moving away from the horizon, as the value of the scalar field decreases monotonically, *cf.* Fig. 2.3 (left panel), it passes through the point at which the coupling diverges. This divergence is, however, benign and the geometry is smooth therein. This can be understood from the equations of motion, which contain $1/f_F$ terms but no divergencies. Moreover, beyond a certain radius the energy density becomes positive - Fig. 2.3 (right panel inset). The negative energy region in the vicinity of the horizon leads to a decrease in the mass function profile - see Fig. 2.3 (left panel).

2.5.2 Domain of Existence

The solution of eq. 2.37 yields a RN BH surrounded by a vanishingly small scalar field. As discussed before, the full set of such configurations makes up the *existence line* which is *common* for all specific coupling functions discussed herein, as they are identical for small ϕ. The differences in the domain of existence of the four couplings emerge for larger values of ϕ, wherein non-linearities become important. The domains of existence for the scalarized BHs with the f_E, f_C, f_P couplings are exhibited in Fig. 2.4 (left panel). They are delimited by the *existence line* – (dashed blue) on which the RN BHs that support the zero mode exist – and a *critical line* – (solid red) which corresponds to a *singular* scalarized BH configuration that will be adressed later. In between (shaded blue regions: dark for f_P, dark+medium for f_C, dark+medium+light for f_E), scalarized BHs exist. In particular, for $q \leqslant 1$ the usual RN BH and

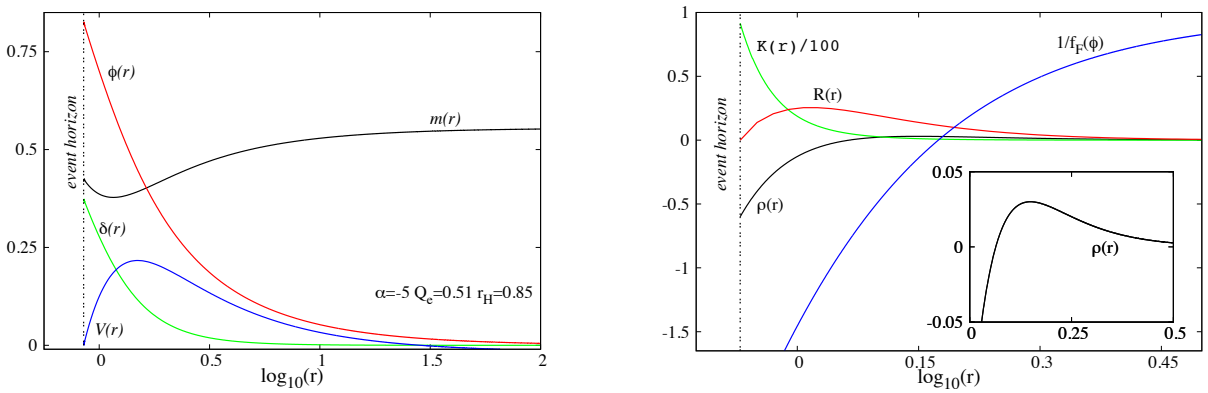

Figure 2.3: A typical scalarized BH in an EMS model with the coupling function f_F, which possesses a region with negative energy density, $\rho < 0$. Left: Profiles of the metric and matter functions; Right: the energy density (zoom in presented in the inset), the Ricci and Kretschmann scalars and the inverse of the coupling function $f_F(\phi)$ which changes sign at some finite r. This plot manifests that solutions with $\rho < 0$ are smooth. Source: [1].

the scalarized solutions co-exist with the same global charges. In this region there is non-uniqueness. At

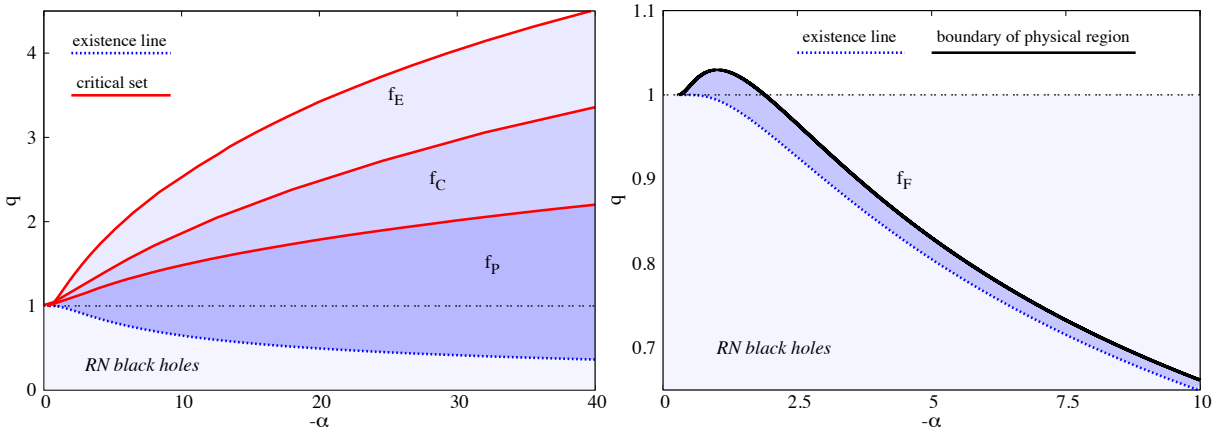

Figure 2.4: Domain of existence of scalarized BHs in EMS models (shaded blue regions). Left: $f_E(\phi)$, $f_C(\phi)$ and $f_P(\phi)$ couplings. Right: $f_F(\phi)$ coupling. Here we only exhibit the physical region, which is delimited by the existence line and the line at which the coupling function diverges at the horizon. The latter is the boundary of the physical region; above it, solutions have a negative energy density in the vicinity of the horizon. Source: [1].

the critical line, numerics suggest $K, T_H \to \infty$, $A_H \to 0$, while M, Q_s remain finite as seen in Fig. 2.5 for an illustrative coupling $\alpha = -10$ for f_E. As another feature, along $\alpha = constant$ branches, q increases beyond unity: therefore, scalarized BHs can be overcharged. Comparing the domain of existence of the exponential, cosh and power-law couplings (Fig. 2.4, left panel) we see that they are qualitatively similar. The critical set for the same α, however, occurs at the smallest value of q for the power law coupling, an intermediate value for the hyperbolic coupling and the largest value of q for the exponential coupling. So, the exponential coupling maximises the possibility of overcharging the BH and, in this sense, maximises the differences with the RN BH case. Moreover, as seen before (*cf.* Fig. 2.2), scalarization is "stronger" for the f_E coupling than for f_P (with an intermediate value for f_C). We also remark that for a given α, as q increases, so does the scalar field's initial amplitude ϕ_0. As already mentioned, the scalar field

profile is always such that the scalar field is monotonically decreasing. Thus, the global maximum of the scalar field occurs at the BH horizon and, for fixed α, it increases with q, meaning one can take ϕ_0 as a measure of q and vice-versa.

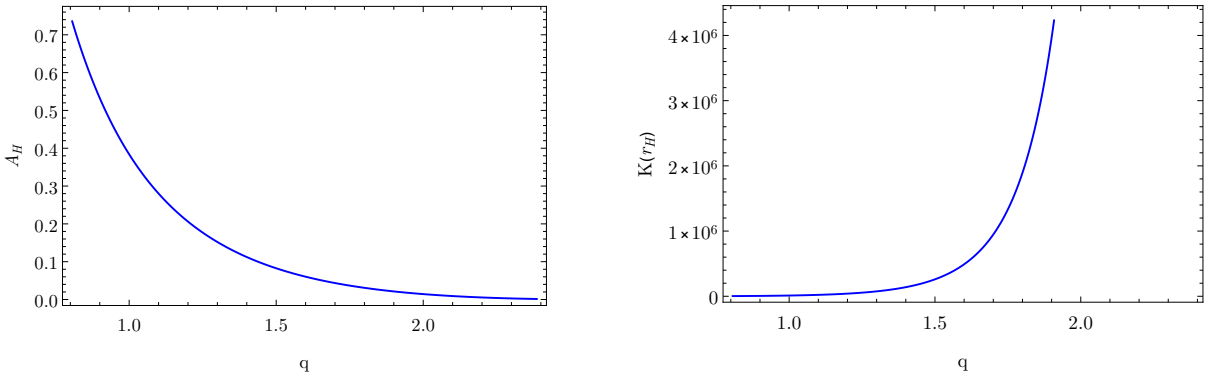

Figure 2.5: Characteristic quantities at the horizon for f_E and $\alpha = -10$. Left panel: Horizon area A_H. Right panel: Kretschmann scalar at the horizon $K(r_H)$. One can observe a divergence of $K(r_H)$, and that A_H vanishes at the critical line.

The domain of existence of the f_F coupling function (Fig. 2.4 - right panel) can be divided into two parts. For $\alpha = constant$, ϕ_0 grows (with q) from the existence line until it reaches $\phi_0^2 = 1/|\alpha|$ at the *divergence line*, corresponding to the pole of the coupling. These solutions span the physical region wherein solutions have a positive energy density. Beyond the divergence line solutions have $\phi_0^2 > 1/|\alpha|$, resulting in a negative energy density region near the horizon which extends up to a certain radius at which $\rho = 0$, and after that point $\rho > 0$ - see Fig. 2.3. Beyond this the divergence line the solutions are not physical ("*exotic*"). Solutions in the exotic region appear to be smooth exhibiting no other obvious pathologies apart from the negative energy density. The physical region of the domain of existence will tend to thin down to zero, as $|\alpha|$ increases. Unlike the other studied couplings, for a model with f_F, the scalarized BH can only be overcharged and in the physical region if the coupling constant is in a compact interval: $-\alpha \in [1/4, 1.89074]$, with a maximum of $q = 1.02971$ for $\alpha = -1.0115$ - *cf.* Fig. 2.4 - right panel.

2.5.3 Perturbative stability

Following a standard technique for studying perturbative stability against radial perturbations [1], we consider spherically symmetric, linear perturbations of our equilibrium solutions, keeping the metric ansatz (2.3), but allowing the functions N, δ, ϕ, V to depend on t as well as on r:

$$ds^2 = -\tilde{N}(r,t)e^{-2\tilde{\delta}(r,t)}dt^2 + \frac{dr^2}{\tilde{N}(r,t)} + r^2(d\theta^2 + \sin^2\theta d\varphi^2) \ , \qquad A = \tilde{V}(r,t)dt \ , \qquad \phi = \tilde{\phi}(r,t) \ . \tag{2.40}$$

The time dependence enters as a periodic perturbation with frequency Ω, for each of these functions:

$$\begin{aligned} \tilde{N}(r,t) &= N(r) + \epsilon N_1(r)e^{-i\Omega t} \ , \qquad \tilde{\delta}(r,t) = \delta(r) + \epsilon\delta_1(r)e^{-i\Omega t} \ , \\ \tilde{\phi}(r,t) &= \phi(r) + \epsilon\phi_1(r)e^{-i\Omega t} \ , \qquad \tilde{V}(r,t) = V(r) + \epsilon V_1(r)e^{-i\Omega t} \ . \end{aligned} \tag{2.41}$$

From the linearised field equations around the background solution, the metric perturbations and $V_1(r)$ can be expressed in terms of the scalar field perturbation,

$$N_1 = -2rN\phi'\phi_1 \ , \qquad \delta_1' = -2r\phi'\phi_1' \ , \qquad V_1' = -\left(\delta_1 + \frac{\dot{f}_i(\phi)}{f_i(\phi)}\phi_1\right) V' \ , \tag{2.42}$$

thus yielding a single perturbation equation for ϕ_1. Introducing a new variable $\Psi(r) = r\phi_1$, the scalar-field equation of motion 2.27 may be written as

$$\left(Ne^{-\delta}\right)^2 \Psi'' + Ne^{-\delta}\left(Ne^{-\delta}\right)' \Psi' + \left(\Omega^2 - U_\Omega\right)\Psi = 0, \tag{2.43}$$

which, by introducing the 'tortoise' coordinate x [56] as

$$\frac{dx}{dr} = \frac{1}{e^{-\delta}N}, \tag{2.44}$$

can be written in the the standard Schrödinger-like form:

$$-\frac{d^2}{dx^2}\Psi + U_\Omega \Psi = \Omega^2 \Psi \ . \tag{2.45}$$

The perturbation potential U_Ω is defined as:

$$U_\Omega = \frac{e^{-2\delta}N}{r^2}\left\{1 - N - 2r^2\phi'^2 - \frac{Q^2}{r^2 f(\phi)}\left[1 - 2r^2\phi'^2 + \frac{\ddot{f}(\phi)}{2f(\phi)} + 2r\phi'\frac{\dot{f}(\phi)}{f(\phi)} - \left(\frac{\dot{f}(\phi)}{f(\phi)}\right)^2\right]\right\} \tag{2.46}$$

The potential U_Ω is not positive definite, but is regular in the entire range $-\infty < x < \infty$. Also, it vanishes at the BH event horizon and at infinity. It follows from a standard result in quantum mechanics (see *e.g.* [57]) that eq. (2.45) has no bound states if U_Ω is everywhere larger than the lowest of its two asymptotic values, *i.e.*, if it is positive. [2]

For all couplings analysed, for solutions with a q close to the RN BH, the potential has a region where it is negative. However for the case of the exponential, cosh and power-law coupling, for larger q, the potential is, generically, everywhere positive for the vast majority of the solutions analysed, which are therefore free of instabilities - see the related analysis in [38, 43] and as an illustration, in Fig. 2.6 the potential is plotted for a sequence of solutions for the exponential coupling (left). One can see that the potential is smaller than zero in a small q-region close to the RN limit – the RN BH has the zero mode at $q = 0.649$ ($\alpha = -10$). Then the potential becomes positive and remains so for arbitrary large q along the remaining α branch. For the fractional coupling, on the other hand, there can be negative regions in

[2] A simple proof is as follows. Write Eq. (2.45) in the equivalent form

$$\frac{d}{dx}\left(\Psi\frac{d\Psi}{dx}\right) = \left(\frac{d\Psi}{dx}\right)^2 + (U_\Omega - \Omega^2)\Psi^2 \ . \tag{2.47}$$

After integrating from the horizon to infinity it follows that

$$\int_{-\infty}^{\infty} dx\left[\left(\frac{d\Psi}{dx}\right)^2 + U_\Omega\Psi^2\right] = \Omega^2\int_{-\infty}^{\infty} dx\Psi^2 \tag{2.48}$$

which for $U_\Omega > 0$ implies $\Omega^2 > 0$.

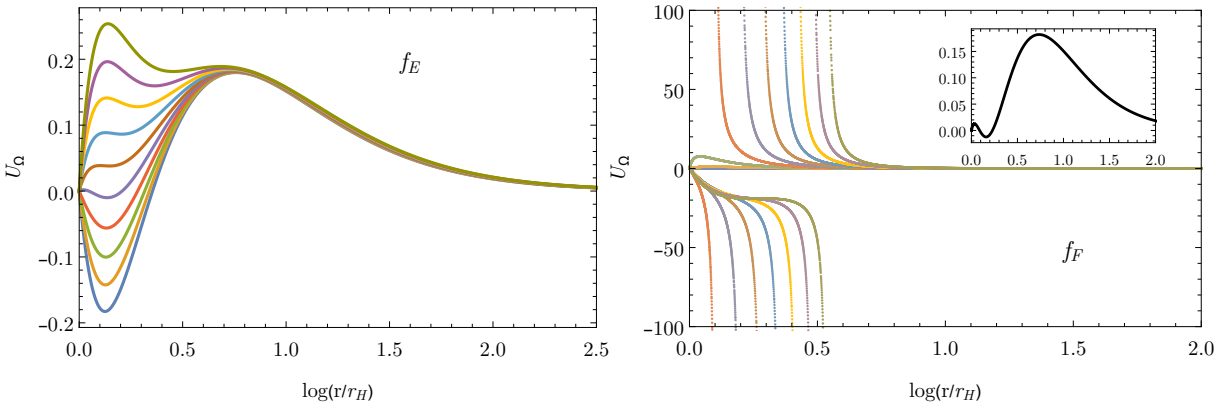

Figure 2.6: Perturbative potential, U_Ω, for a sequence of solutions. Left panel: exponential coupling, $\alpha = -10$ and $Q = 0.12$. The solutions have $r_H = 0.324$ ($q = 0.651$) – lowest curve – up to $r_H = 0.297$ ($q = 0.695$) – top curve. Right panel: fractional coupling. The sequence is plotted for the same sequence of q values. The inset plot in black corresponds to the smallest value of q considered. One observes that after a determined value of q the potential diverges at some range of the radial coordinate r for which $\phi(r) = 1/\sqrt{|\alpha|}$, and has both negative and positive regions.

the potential both for physical and exotic solutions (*c.f.* right panel Fig. 2.6). As discussed in [43], the $n \geqslant 1$ solutions are not stable, and the negative potential region (see Fig. 2.7) does, in fact, correspond to an instability, which is not true for the $n = 0$ solutions. We emphasise that the existence of a negative potential region is a necessary, but not sufficient, condition for instability.

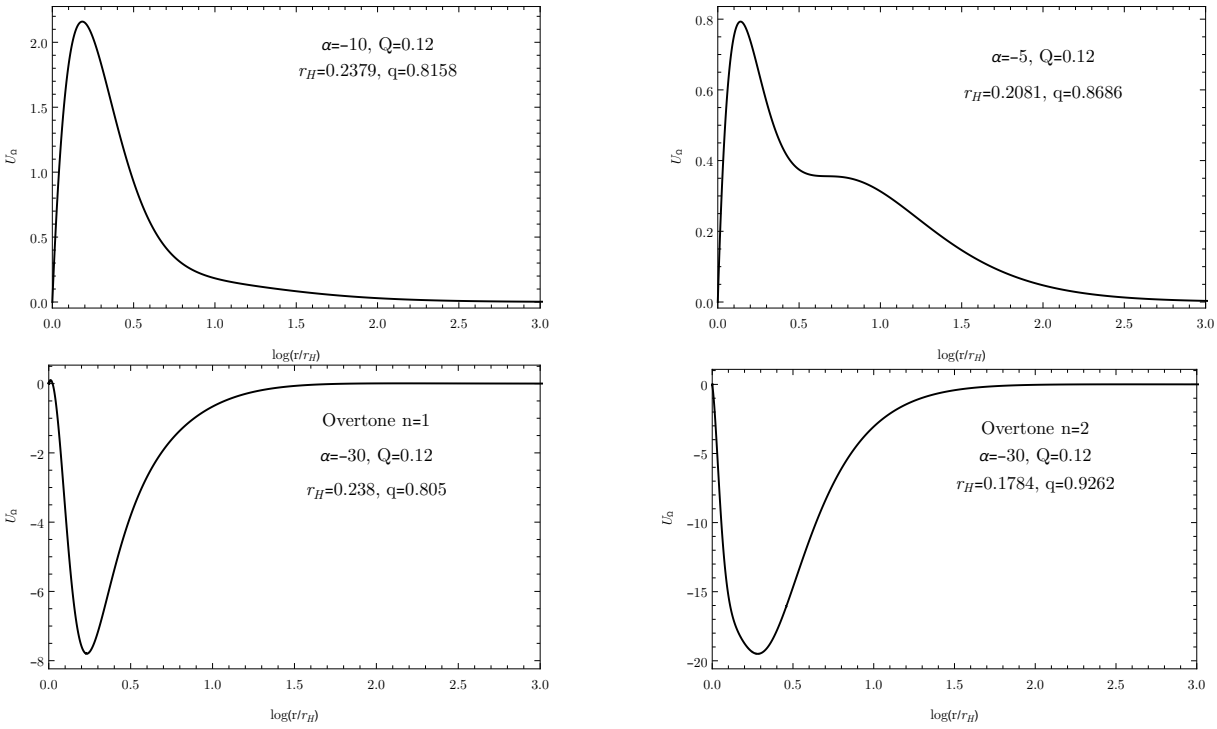

Figure 2.7: Perturbative potential, U_Ω, for the exponential coupling for several values of α and n. One observes that the overtone solutions have a region where $U_\Omega < 0$.

2.5.4 Entropic preference

In the EMS model, the Bekenstein-Hawking BH entropy formula holds. Thus, the entropy analysis reduces to the analysis of the horizon area. It is convenient to use the already introduced reduced event horizon area a_H. Then, in the region where the RN BH and scalarized BHs co-exist – the non-uniqueness region – and for the same q, the scalarized solutions are always *entropically preferred*. This is shown in Fig. 2.8 for all four coupling functions studied herein. One also observes that, for the same q, a_H increases with the growth of $|\alpha|$. For the same power-law coupling here considered, eSTGB BHs are not entropically favoured and the scalarized spherically symmetric, fundamental BH solutions are not necessarily perturbatively stable, which creates a difference between the two models [55]. Such entropic considerations are not, however, sufficient to establish if the endpoint of the instability of the RN BH is the corresponding hairy BH with the same q. In [38], fully non-linear dynamical evolutions were performed that established that for f_E, and sufficiently small q, this is indeed the case. The endpoint of the instability, however, can only be established once fully non-linear numerical evolutions are studied. Such evolutions, whose details are beyond the scope of this work, are addressed in Appendix A.

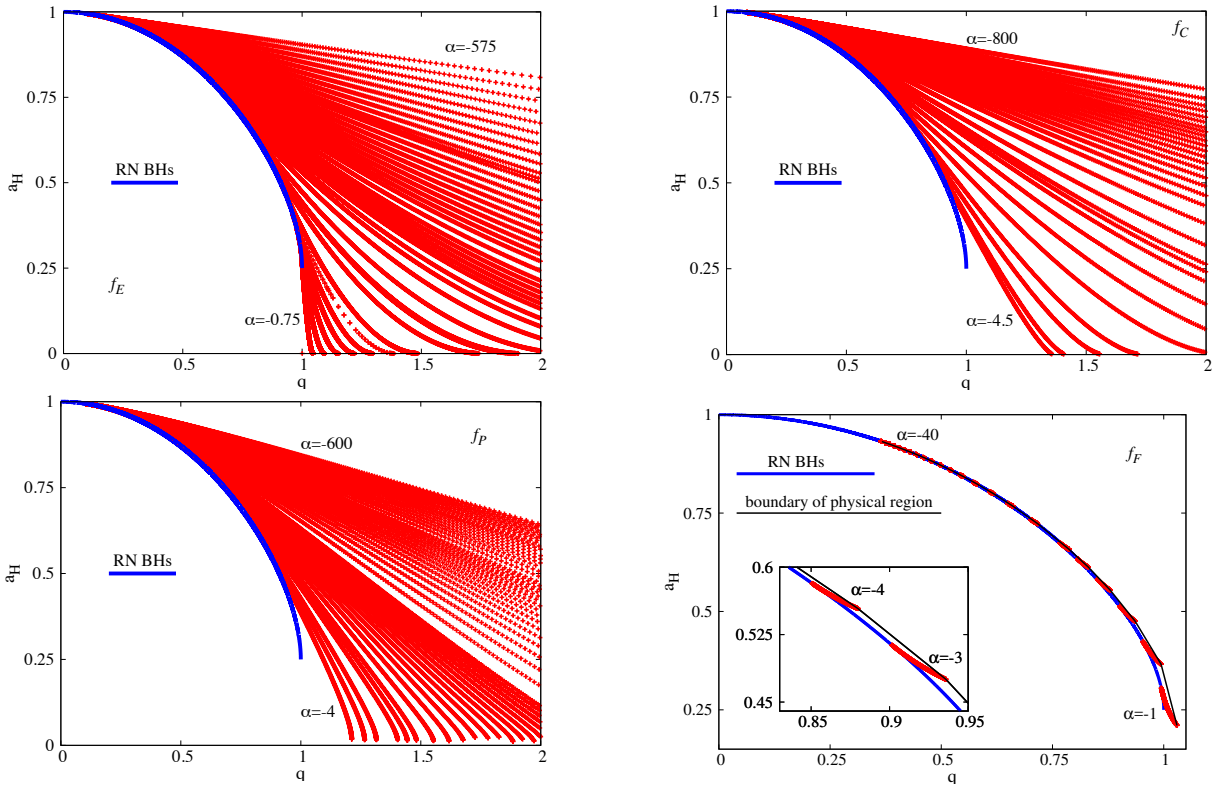

Figure 2.8: Reduced area a_H *vs.* q for: (top, left panel) $f_E(\phi)$; (top, right panel) $f_C(\phi)$; (bottom left panel) $f_P(\phi)$; (bottom right panel) $f_F(\phi)$. The blue lines are the sequence of non-scalarized RN BHs. The red lines are sequences of (numerical data points representing) scalarized BHs for a given α. Different sequences are presented, for a range of values of α. The solid black line shows the sequence of solutions along the boundary of the physical region for the f_F model. Source: [1].

Chapter 3

Spontaneous scalarization of dyonic black holes

There is an asymmetry between the electric and magnetic fields, visible in Maxwell's equations. Maxwell himself pointed out that it would be necessary to assert that there are no magnetically charged bodies and no magnetic currents, *i.e.*, magnetic monopoles [58]. If one were to assume the existence of a magnetic charge density ρ_m and a magnetic current density $\mathbf{j}_{\rm m}$ the Maxwell equations would be written [59]

$$\begin{cases} \nabla\cdot\mathbf{E} & = 4\pi\rho_{\rm e}, \\ \nabla\cdot\mathbf{B} & = 4\pi\rho_{\rm m}, \\ \nabla\times\mathbf{E} & = -\frac{1}{c}\left(4\pi\mathbf{j}_{\rm m}+\frac{\partial\mathbf{B}}{\partial t}\right), \\ \nabla\times\mathbf{B} & = \frac{1}{c}\left(4\pi\mathbf{j}_{\rm e}+\frac{\partial\mathbf{E}}{\partial t}\right), \end{cases} \tag{3.1}$$

which are symmetric under the transformation

$$\begin{aligned} \mathbf{E}\to\mathbf{B}, \qquad \rho_e\to\rho_m, \qquad \mathbf{j}_{\rm e}\to\mathbf{j}_{\rm m}, \\ \mathbf{B}\to-\mathbf{E}, \qquad \rho_m\to-\rho_e, \qquad \mathbf{j}_{\rm m}\to-\mathbf{j}_{\rm e}. \end{aligned} \tag{3.2}$$

Dyons, first proposed by Julian Schwinger in 1969 [60], are hypothetical particles with both an electric and a magnetic charge. A dyon with a zero electric charge is usually referred to as a magnetic monopole. The addition of a magnetic charge to a BH gives rise to a class of systems dubbed *dyonic* BHs. An example includes the 3-parameter electro-vacuum dyonic RN BH (which is a particular limit of the Kerr-Newman metric)

$$ds^2=-\left(1-\frac{2M}{r}+\frac{Q^2+P^2}{r^2}\right)dt^2+\frac{dr^2}{\left(1-\frac{2M}{r}+\frac{Q^2+P^2}{r^2}\right)}+r^2d\Omega_2,$$

that describes BH with both electric charge Q and magnetic charge P. For a given M, these BHs can only sustain charges if $M\geq\sqrt{Q^2+P^2}$. When the equality holds, the extremality limit is attained, yielding extremal BHs. These extremal solutions are non-singular spacetimes on and outside a degenerate and smooth event horizon that, amongst other properties [10]: i) has a vanishing Hawking temperature, ii)

has a near-horizon geometry given by the Robinson-Bertotti metric, which is a kind of Kaluza-Klein vacuum in which two directions are compactified and the effective spacetime is the two-dimensional AdS spacetime of negative curvature, iii) allows a multi-BH generalisation. Until now, in this work, only purely electric BHs have been considered.

A class of well studied BHs in the EMS model are dubbed *dilatonic*. The coupling function of the dilatonic class prevents EM theory to be a consistent truncation of this class of EM-dilaton models. In particular, the RN solution of EM theory does not solve these EM-dilaton models. Instead, new charged BHs with a non-trivial scalar field profile exist [61, 62], which are known in closed analytic form and that present RN-unlike features. As an example, the charge to mass ratio can exceed unity and there are no extremal BHs for purely electric (or magnetic) solutions. However, the introduction of an additional magnetic charge leads to dyonic BHs with an extremal limit, which have been constructed for specific couplings (see *e.g* [63]).

As seen in chapter 2, purely electrical EMS spontaneously scalarized BHs possess no extremal limits, but critical limits (with singular solutions) instead. Given the importance of extremal solutions, it is interesting to inquire which are the properties of the family of dyonic spontaneously scalarized BHs and, in particular, of their extremal limit, in case it exists (as suggested by the dilatonic case). The next natural generalisation of EMS models, and the aim of the present chapter, is then to include a magnetic charge and observe what new features arise. All the notations from the last chapter are adopted here. This chapter will be based on the work done in ref. [47].

3.1 The EMS model for dyonic BHs

We start by considering once again the EMS action

$$\mathcal{S} = \int d^4x\sqrt{-g}\Big(R - 2\partial_\mu\phi\partial^\mu\phi - f(\phi)F_{\mu\nu}F^{\mu\nu}\Big), \tag{3.3}$$

in the previously presented metric ansatz

$$ds^2 = -N(r)e^{-2\delta(r)}dt^2 + \frac{dr^2}{N(r)} + r^2\left(d\theta^2 + \sin^2\theta d\varphi^2\right), \tag{3.4}$$

with $N(r) = 1 - 2m(r)/r$. To include a magnetic charge in the model, however, we consider the gauge 4-potential (compatible with the symmetries of eq. 3.4) given by

$$A = V(r)dt - P\cos\theta d\varphi, \tag{3.5}$$

with P the magnetic charge. Integrating the trivial angular dependence allows to define an effective lagrangian

$$\mathcal{L}_{eff} = -\frac{e^{-\delta}P^2 f(\phi)}{2r^2} + \frac{1}{2}e^{\delta}r^2 f(\phi)V'^2 + \frac{1}{2}e^{-\delta}\left(1 - N - rN' - r^2N\phi'^2\right), \tag{3.6}$$

from which the equations of motion can be derived. Noticing the existence of a first integral

$$V' = -\frac{Q}{r^2 f(\phi)} e^{-\delta}, \tag{3.7}$$

with Q the electric charge, the equations of motion are

$$\delta' = -r\phi'^2, \tag{3.8}$$

$$\left(e^{-\delta} r^2 N \phi'\right)' = -\frac{1}{2} e^{\delta} r^2 \dot{f}(\phi) V'^2 + \frac{e^{-\delta} P^2 \dot{f}(\phi)}{2r^2}, \tag{3.9}$$

$$N' = -\frac{Q^2 + P^2 f(\phi)^2 + f(\phi) r^2 \left(r^2 N \phi'^2 + N - 1\right)}{f(\phi) r^3}. \tag{3.10}$$

To solve the equations of motion we have to implement suitable boundary conditions for the desired functions and corresponding derivatives. We assume the existence of an event horizon in $r = r_H > 0$ and that the solution possesses a power series expansion in $(r - r_H)$

$$\begin{aligned} N(r) &= N_1 (r - r_H) + \dots, \qquad \delta(r) = \delta_0 + \delta_1 (r - r_H) + \dots, \\ \phi(r) &= \phi_0 + \phi_1 (r - r_H) + \dots, \qquad V(r) = v_1 (r - r_H) + \dots, \end{aligned} \tag{3.11}$$

with the lower order coefficients being

$$\begin{aligned} N_1 = -\frac{Q^2 + P^2 f(\phi_0)^2 - r_H^2 f(\phi_0)}{r_H^3 f(\phi_0)}\ , \qquad \delta_1 = -\phi_1^2 r_H, \qquad v_1 = -\frac{Q}{r_H^2 f(\phi_0)} e^{-\delta_0}\ , \\ \phi_1 = \frac{\dot{f}(\phi_0)\left(Q^2 - P^2 f(\phi_0)^2\right)}{2 r_H f(\phi_0)\left[Q^2 - r_H^2 f(\phi_0) + P^2 f(\phi_0)^2\right]}\ , \end{aligned} \tag{3.12}$$

which are fully determined via the two essential parameters ϕ_0 and δ_0. Also, of interest at the horizon we have the Hawking temperature T_H, horizon area A_H, the energy density $\rho(r_H)$ and the Kretschmann scalar $K(r_H)$ given respectively by

$$\begin{aligned} T_H = \frac{1}{4\pi} N_1 e^{-\delta_0}\ , \qquad A_H = 4\pi r_H^2\ , \qquad \rho(r_H) = \frac{2\left(P^2 f(\phi_0)^2 + Q^2\right)}{r_H^4 f(\phi_0)}\ , \\ K(r_H) = \frac{12}{r_H^4}\left\{1 - \frac{2}{r_H^2}\left[\frac{Q^2}{f(\phi)} + f(\phi) P^2\right] + \frac{5}{3 r_H^4}\left[\frac{Q^2}{f(\phi)} + f(\phi) P^2\right]^2\right\}. \end{aligned} \tag{3.13}$$

An asymptotic approximation of the solution in the far field takes the form

$$N(r) = 1 - \frac{2M}{r} + \frac{Q^2 + P^2 + Q_s^2}{r^2} + \dots\ , \qquad \phi(r) = \frac{Q_s}{r} + \dots\ , \qquad \delta(r) = \frac{Q_s^2}{2r^2} + \dots\ , \qquad V(r) = \Phi_e + \frac{Q}{r} + \dots\ , \tag{3.14}$$

with Q_s the scalar charge, Φ_e the electrostatic potential difference between the EH and infinity and M the ADM mass. The following results and reduced quantities will be useful later

$$F_{\mu\nu} F^{\mu\nu} = \frac{2\left[P^2 f(\phi)^2 - Q^2\right]}{r^4 f(\phi)^2}, \tag{3.15}$$

$$q = \frac{\sqrt{Q^2 + P^2}}{M}, \qquad a_H = \frac{A_H}{16\pi M^2}, \qquad t_H = 8\pi M T_H \tag{3.16}$$

q is defined as the reduced dyonic charge, a_H is the reduced event horizon area and t_H the reduced horizon temperature.

3.1.1 Physical relations and perturbative stability

Following a similar procedure as in the last chapter, a Virial relation and a Smarr law are derived for the EMS model in the presence of a magnetic charge. This relations will later be used as tests to the code used to obtain the solutions.

3.1.1.1 Smarr law

The integral mass formula and energy-momentum tensor presented in Chapter 2 hold in this generalisation, taking into account the new form of $F_{\mu\nu}F^{\mu\nu}$. One can then arrive at a Smarr law given by

$$M = \frac{1}{2} T_H A_H + \Phi_e Q + \Phi_m P, \tag{3.17}$$

with

$$\Phi_e = \int_{r_H}^{\infty} dr \left(\frac{Q}{r^2 f(\phi)} e^{-\delta} \right) \equiv - \int_{r_H}^{\infty} dr V', \qquad \Phi_m = \int_{r_H}^{\infty} dr \left(e^{-\delta} f(\phi) \frac{P}{r^2} \right) \equiv - \int_{r_H}^{\infty} dr V'_m, \tag{3.18}$$

the electrostatic and magnetostatic potential differences respectively. A non-linear Smarr relation can also be established for this family of models

$$M^2 + Q_s^2 = \frac{1}{4} A_H^2 T_H^2 + Q^2 + P^2. \tag{3.19}$$

3.1.1.2 Virial relation

Similarly to what was done in Chapter 2, consider the effective action

$$\mathcal{S}_{eff} = \int_{r_H}^{\infty} dr \mathcal{L}_{eff}, \tag{3.20}$$

and assume that hairy BH solutions exist such that they are described by the functions $\phi(r), \delta(r), V(r), N(r)$ with suitable boundary conditions at the event horizon and at infinity. Next consider the 1-parameter family of configurations described by the scaled functions

$$F_\lambda(r) \equiv F(r_H + \lambda(r - r_H)), \tag{3.21}$$

with $F \in \{\phi, \delta, V, N\}$. If the initial configuration was indeed a solution, then there must be a critical point at $\lambda = 1$ such that the effective action is extremized: $\left(\frac{dS^\lambda_{eff}}{d\lambda} \right)_{\lambda=1} = 0$. It is then straightforward

to obtain a Virial relation given by

$$\int_{r_H}^{\infty} dr \left\{ e^{-\delta} r^2 \phi'^2 \left[1 - \frac{r_H}{r} (1+N) \right] \right\} = \Phi_e Q + \Phi_m P + \int_{r_H}^{\infty} dr \left\{ \frac{2 r_H}{r} \left[V' Q + V'_m P \right] \right\} . \tag{3.22}$$

One can show that the left hand side integrand is strictly positive. Thus, the virial identity shows that a nontrivial scalar field requires a nonzero electric/magnetic charge so that the right hand side is nonzero.

3.1.2 Perturbative stability

Following a procedure similar to the one done in Chapter 2 for studying perturbative stability against radial perturbations, we consider spherically symmetric, linear perturbations of our equilibrium solutions, keeping the metric ansatz, but allowing the functions N, δ and ϕ, V to depend on t as well as on r:

$$ds^2 = -\tilde{N}(r,t) e^{-2\tilde{\delta}(r,t)} dt^2 + \frac{dr^2}{\tilde{N}(r,t)} + r^2 (d\theta^2 + \sin^2\theta d\varphi^2) , \qquad A = \tilde{V}(r,t) dt - P \cos\theta d\varphi^2 , \qquad \phi = \tilde{\phi}(r,t) . \tag{3.23}$$

The time dependence enters as a periodic perturbation with frequency Ω, for each of these functions:

$$\begin{aligned} \tilde{N}(r,t) &= N(r) + \epsilon N_1(r) e^{-i\Omega t} , \qquad \tilde{\delta}(r,t) = \delta(r) + \epsilon \delta_1(r) e^{-i\Omega t} , \\ \tilde{\phi}(r,t) &= \phi(r) + \epsilon \phi_1(r) e^{-i\Omega t} , \qquad \tilde{V}(r,t) = V(r) + \epsilon V_1(r) e^{-i\Omega t} . \end{aligned} \tag{3.24}$$

From the linearised field equations around the background solution, the metric perturbations and $V_1(r)$ can be expressed in terms of the scalar field perturbation,

$$N_1 = -2rN\phi'\phi_1 , \qquad \delta'_1 = -2r\phi'\phi'_1 , \qquad V'_1 = -V' \left(\delta_1 + \frac{\dot{f}(\phi)}{f(\phi)} \phi_1 \right) , \tag{3.25}$$

thus yielding a single perturbation equation for ϕ_1. Introducing a new variable $\Psi(r) = r\phi_1$, the scalar-field equation of motion may be written as

$$\left(N e^{-\delta} \right)^2 \Psi'' + N e^{-\delta} \left(N e^{-\delta} \right)' \Psi' + \left(\Omega^2 - U_\Omega \right) \Psi = 0, \tag{3.26}$$

which, by introducing the 'tortoise' coordinate x [56] as

$$\frac{dx}{dr} = \frac{1}{e^{-\delta} N}, \tag{3.27}$$

can be written in the the standard Schrödinger-like form:

$$-\frac{d^2}{dx^2} \Psi + U_\Omega \Psi = \Omega^2 \Psi . \tag{3.28}$$

The perturbation potential U_Ω is defined as:

$$U_\Omega = U_0 + P^2 U_2, \tag{3.29}$$

with

$$
\begin{aligned}
U_0 &= \frac{e^{-2\delta}N}{r^2}\left\{1-N-2r^2\phi'^2-\frac{Q^2}{r^2 f(\phi)}\left(1-2r^2\phi'^2+\frac{\ddot{f}(\phi)}{2f(\phi)}+2r\phi'\frac{\dot{f}(\phi)}{f(\phi)}-\frac{\dot{f}(\phi)^2}{f(\phi)^2}\right)\right\},\\
U_2 &= \frac{e^{-2\delta}N}{r^4}\left\{\frac{\ddot{f}(\phi)}{2}+2r\phi'\dot{f}(\phi)-f(\phi)\left(1-2r^2\phi'^2\right)\right\}.
\end{aligned}
\tag{3.30}
$$

3.2 The coupling functions, spontaneous scalarization and the existence line

Two classes of coupling functions will be considered, one for which spontaneous scalarization does not occur – dilatonic –, and one for which it does – spontaneously scalarized (or simply, scalarized).

3.2.1 Dilatonic class

The dilatonic class is characterised by a set of field equations that do not allow a scalar-free solution (*i.e.* the RN BH). Hence, from the scalar field equation of motion $\dot{f}(0) \neq 0$. A well motivated coupling of such type is the standard dilationic coupling

$$f(\phi) = e^{2\alpha\phi}, \tag{3.31}$$

in which case we refer to ϕ as the dilaton field. This coupling appears naturally in Kaluza-Klein models and supergravity/low-energy string theory models. Three reference values for the coupling constant α are

$$\alpha = 0 \text{ (EM theory)} \qquad \alpha = 1 \text{ (low-energy strings)} \qquad \alpha = \sqrt{3} \text{ (KK theory)}. \tag{3.32}$$

For this type of coupling some exact BH solutions are known (see *e.g.* [47]).

3.2.2 Spontaneously scalarized class

The scalarized class was already discussed in the last chapter, and we shall here adopt the same exponential coupling as before (that is in some way, a natural generalisation of the dilationic model for a spontaneous scalarization model)

$$f(\phi) = e^{2\alpha\phi^2}. \tag{3.33}$$

where $\alpha > 0$ is the coupling constant. The previous coupling function was extensively studied in the last chapter for the purely electrical case. Here we shall dissect it in detail in the presence of a magnetic charge.

3.2.3 The existence line

For the scalarized class there will be a set of bifurcating solutions from the RN BH. This set of bifurcating solutions form the existence line. By linearising the scalar field equation of motion and performing a

spherical harmonic decomposition one can arrive at

$$\frac{e^{\delta}}{r^2}\left(\frac{r^2 N}{e^{\delta}}U_{\ell}'\right)' - \left[\frac{\ell(\ell+1)}{r^2} + \mu_{\text{eff}}^2\right]U_{\ell} = 0\ , \tag{3.34}$$

with $\mu_{eff}^2 = \alpha(P^2 - Q^2)/r^4 < 0$. One can observe that for spontaneously scalarized solutions, with a positive coupling constant, $|Q| > |P|$. In the spherically symmetric case ($\ell = 0$), eq. 3.34 possesses and exact solution given by

$$U(r) = LP_u\left(1 + \frac{2\left(Q^2 - P^2\right)(r - r_H)}{r\left(r_H^2 + P^2 - Q^2\right)}\right), \quad \text{where } u = \frac{1}{2}\left(\sqrt{1 - 8\alpha} - 1\right), \tag{3.35}$$

where LP_u is a Legendre function. $U(r)$ approaches a constant non-zero value U_{∞} as $r \to \infty$

$$U(r) \to U_{\infty} = {}_2F_1\left[\frac{1 - \sqrt{1 - 8\alpha}}{2}, \frac{1 + \sqrt{1 - 8\alpha}}{2}, 1; \frac{q^2(1 - \mathcal{Q}^2)}{2(q^2 - (1 + \sqrt{1 - q^2})(1 + \mathcal{Q}^2))}\right] + \mathcal{O}\left(\frac{1}{r}\right), \tag{3.36}$$

with $\mathcal{Q} = P/Q$. Thus finding the $\ell = 0$ unstable mode of a RN BH with a given $\mathcal{Q}$ reduces to studying the zeros of the hypergeometric function ${}_2F_1$, so that $U_{\infty} = 0$. The set of bifurcating points from the RN BH form the existence line, that can be seen in Fig. 3.1 for several values of P/Q. As one can observe, higher values of P/Q lead to a higher q_{min} for scalarization to occur.

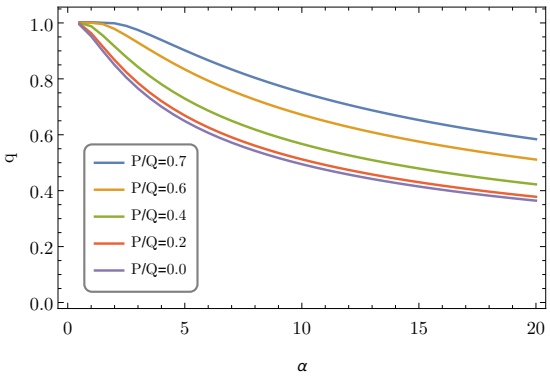

Figure 3.1: Existence line for several values of P/Q.

3.3 Results

3.3.1 The purely electric BHs

Before jumping into the dyonic case, a study of the purely electrical BHs will be done. Such study was already done for the scalarized case in Chapter 2, contrarily to the dilatonic one, that will now be studied. The behaviour of the dilatonic BHs with any $\alpha > 0$ is rather similar, albeit $\alpha = 1$ is a somewhat special point that separates the family into two subsets with respect to the behaviour of some physical quantities. This can be seen from the study of the exact solutions in Appendix B. For any given α, the branch of dilatonic BHs bifurcates from the Schwarzschild BH ($q = 0$), rather than RN BHs, and ends in a critical

solution which is approached for a certain maximal q

$$q_{\rm max}^{\rm (D)} = \sqrt{1+\alpha^2}\ , \tag{3.37}$$

where the superscript 'D' refers to dilatonic. The critical solution has, for any $\alpha > 0$, a singular horizon, as one can see by evaluating the Kretschmann scalar at the horizon. The reduced temperature t_H, on the other hand, goes to zero for $\alpha < 1$ and diverges for $\alpha > 1$. The solutions with $\alpha = 1$ have $t_H = 1$. These features can be seen in Fig. 3.2 (left panels), where the behaviour of a_H, t_H *vs.* q are illustrated for several values of α. Illustrative radial profiles of the solutions can be seen in Fig. 3.3.

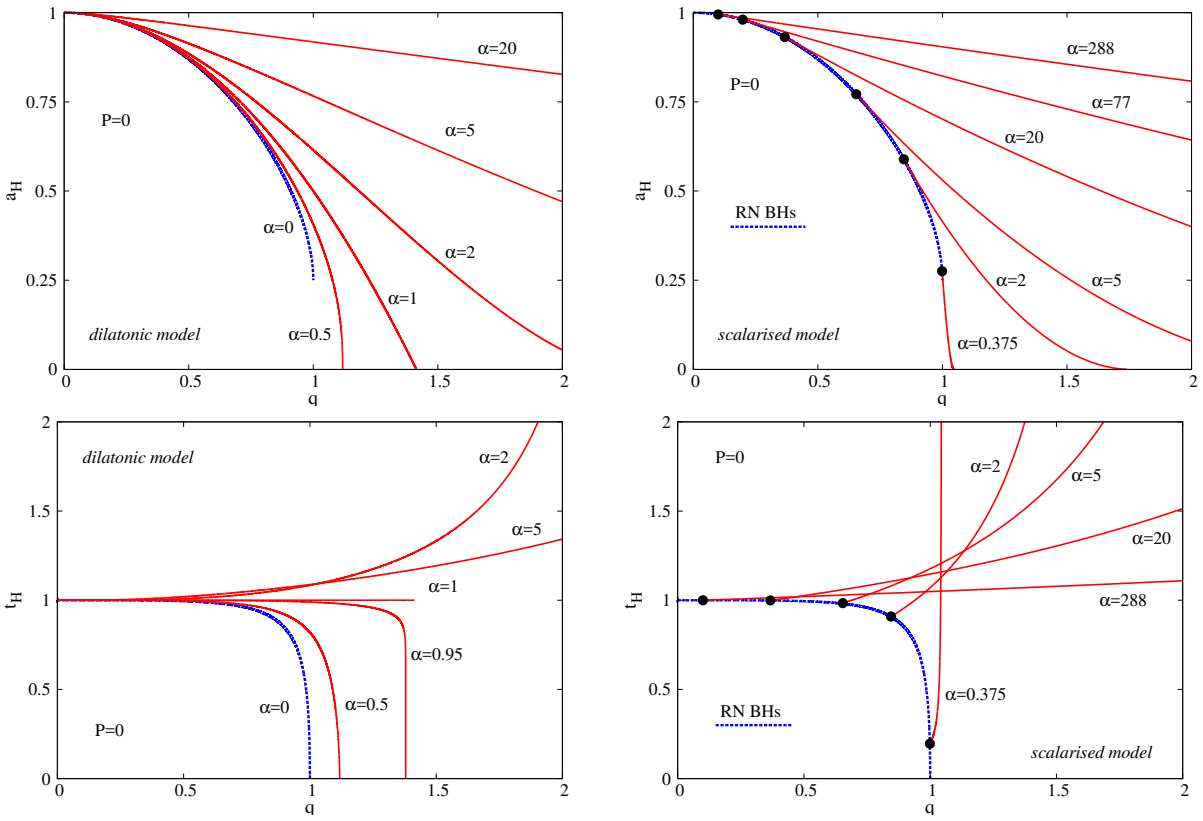

Figure 3.2: Reduced area a_H (top panels) and reduced temperature t_H (bottom panels) *vs.* reduced charge q for dilatonic (left panels) and scalarized solutions (right panels). All solutions have $P = 0$. The blue lines are the set of RN BHs ($\phi = 0$). The red lines are sequences of BHs with a nontrivial scalar field for a given α. Different sequences are presented, for a range of values of α. The black dots indicate the RN solutions from which the scalarized BHs bifurcate. Source: [47].

In what concerns perturbative stability, the results for the scalarized case can be seen in Chapter 2, Section 2.5.3. For the dilatonic case, an illustrative plot for the perturbative potential U_Ω is found in Fig. 3.4. The potential is positive definite and regular in the entire range $-\infty < x < \infty$. Also, the potential vanishes at the BH event horizon and at infinity. It follows that, as previously discussed, the BH solutions are perturbatively stable.

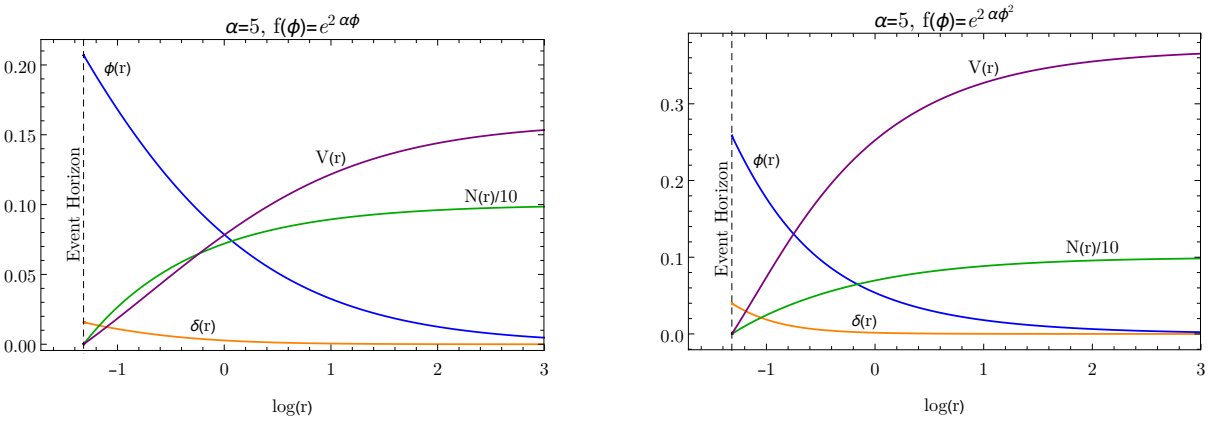

Figure 3.3: Illustrative radial profiles for the dilatonic and scalarized models for $Q = 0.12$, $r_H = 0.2676$, $\alpha = 5$. Left panel: Dilatonic radial profiles. Right panel: Scalarized radial profiles.

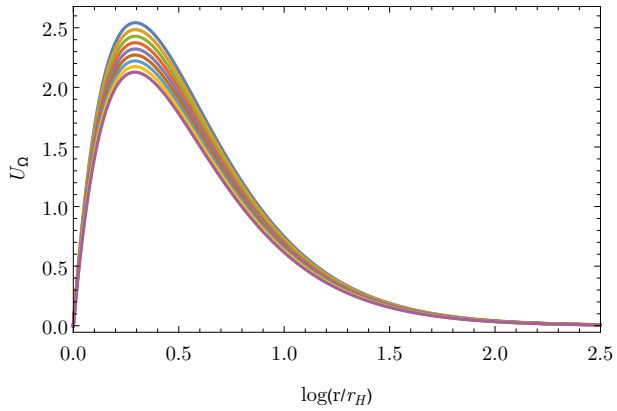

Figure 3.4: Sequence of perturbative potentials, U_Ω, for the purely electric dilaton case with $\alpha = 5$. The bottom curve has $q = 0.687$, while the top one has $q = 0.735$. The perturbative potentials are always positive definite.

3.3.2 Dyonic BHs

Here we address the generalisation of the EMS model with a non-zero magnetic charge. The profile functions of illustrative dyonic BHs are shown in Fig. 3.5, for both the dilatonic and scalarized cases. Dyonic BHs preserve some, but not all, of the qualitative characteristics of the purely electric solutions. In the dilatonic case, the branch of solutions with a given α starts again from the Schwarzschild limiting solution (which has $a_H = 1$, $t_H = 1$ and $q = 0$) and ends in a limiting configuration with $a_H > 0$, $t_H = 0$ and $q = q_{\rm max} > 0$ - Fig. 3.6 (left panels). This limiting solution, however, is now an extremal BH (rather than a singular critical solution) as will be discussed next. Unlike the dilatonic solutions, which exist for arbitrarily small q for any α, scalarized BHs with a given α exist for $q > q_{min}$ only. They bifurcate from a RN BH (with $q > 0$) and form a branch ending again on an extremal solution with vanishing horizon temperature and nonzero horizon area - Fig. 3.6 (right panels). As in the case of purely electric solutions, for the same global quantities M, P, Q, the dyonic scalarized solutions are always entropically preferred over the corresponding RN solution.

Dilatonic dyon BHs were found to be perturbatively stable, similarly to the purely electric situation, yielding a perturbative potential that is everywhere regular and positive, for all values of P/Q and q – *c.f.*

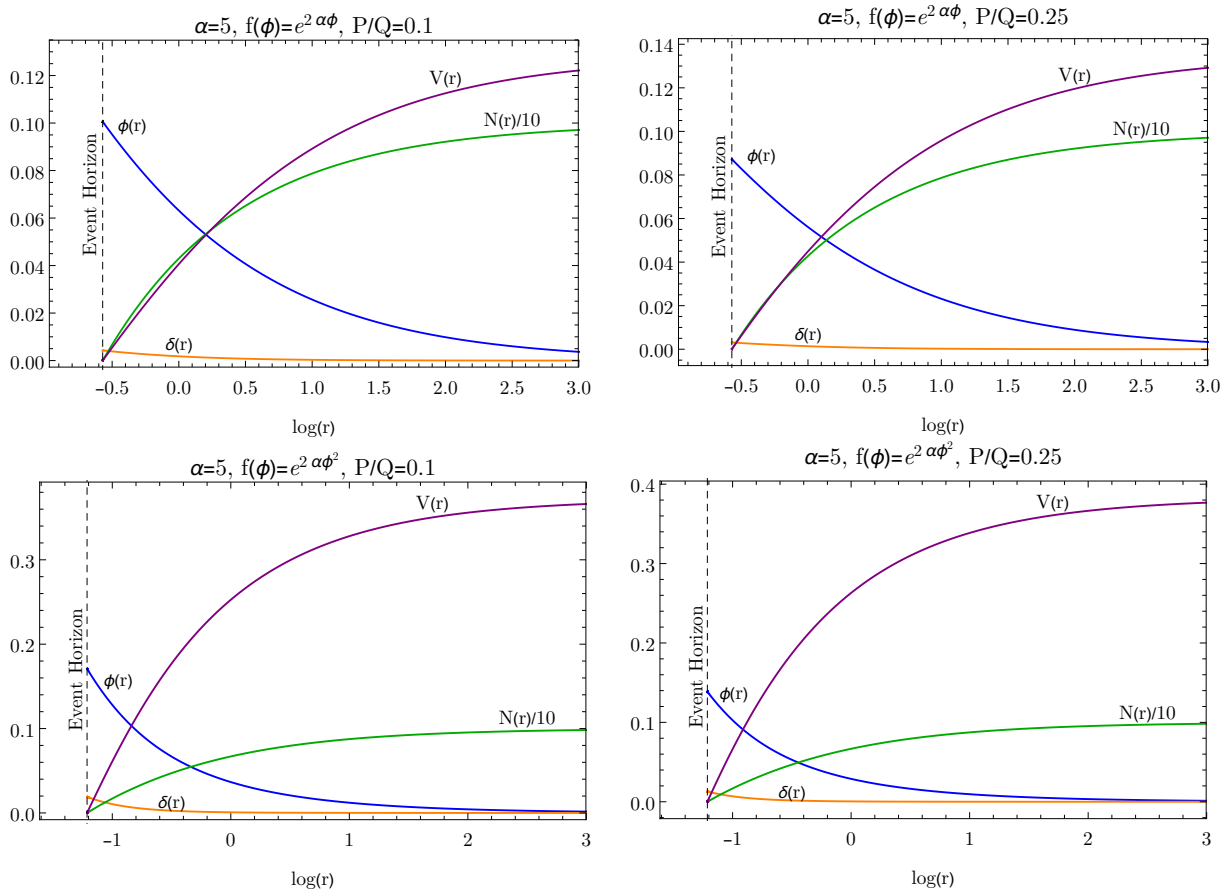

Figure 3.5: Illustrative radial profiles for the dilatonic and scalarized models for $Q = 0.12$, $\alpha = 5$ and several values of P. Top left panel: dilatonic radial profiles for $P/Q = 0.1$ and $r_H = 0.565$. Top right panel: dilatonic radial profiles for $P/Q = 0.25$ and $r_H = 0.565$. Bottom left panel: scalarized radial profiles for $P/Q = 0.1$ and $r_H = 0.297$. Bottom right panel: scalarized radial profiles for $P/Q = 0.25$ and $r_H = 0.297$.

Fig. 3.7 (left panel). On the other hand, as expected, the scalarized dyon BHs (right panel of Fig. 3.7) have a negative potential region (which does not imply instability) for solutions close to the bifurcating points (this is, for small values of q, near the existence line for a certain P/Q ratio).

3.3.2.1 Extremal solutions and the domain of existence

To address extremal BHs one needs to impose a different near-horizon expansion which accounts for the degenerate horizon [64, 65]. The leading order terms of the appropriate expansion are:

$$N(r) = N_2(r - r_H)^2 + \dots\ , \qquad \phi(r) = \phi_0 + \phi_c(r - r_H)^k + \dots\ ,$$
$$\delta(r) = \delta_0 + \delta_1(r - r_H)^{2k-1} + \dots\ , \qquad V(r) = v_1(r - r_H) + \dots\ . \tag{3.38}$$

It is convenient to take r_H and ϕ_0 as essential parameters. Then the field equations imply

$$Q = \frac{r_H\sqrt{f\left(\phi_0\right)}}{\sqrt{2}}, \qquad P = \frac{r_H}{\sqrt{2f\left(\phi_0\right)}}, \qquad N_2 = \frac{1}{r_H^2}. \tag{3.39}$$

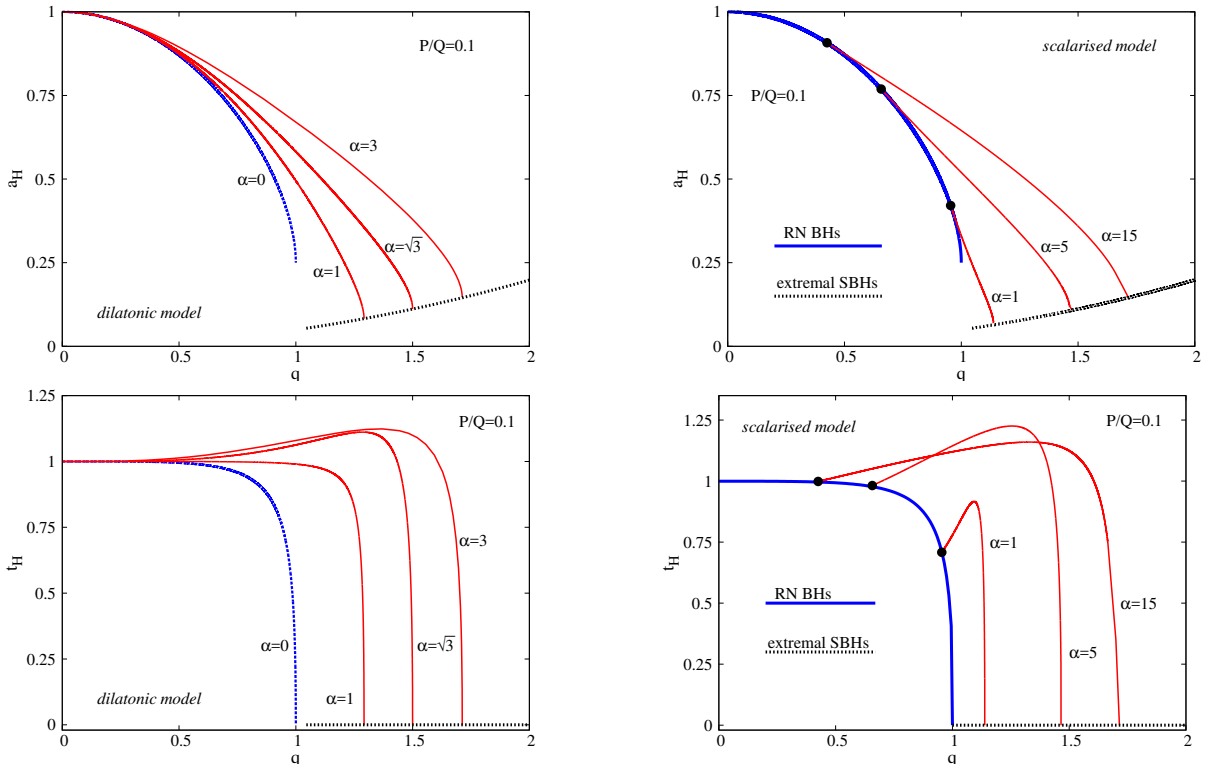

Figure 3.6: Reduced area a_H (top panels) and reduced temperature t_H (bottom panels) *vs.* reduced charge q for dilatonic (left panels) and scalarized solutions (right panels). All solutions have $P/Q = 0.1$. The blue lines are the set of RN BHs ($\phi = 0$). The red lines are sequences of BHs with a non-trivial scalar field for a given α. Different sequences are presented, for a range of values of α. The black dots indicate the RN solutions from which the scalarized BHs bifurcate. The dashed black lines represent the extremal BHs. Source: [47].

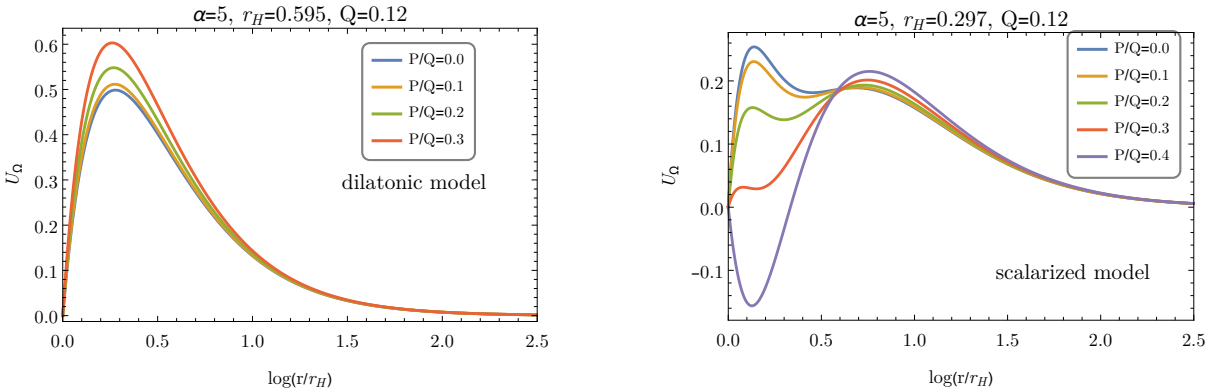

Figure 3.7: Sequence of perturbative potentials, U_Ω, for the dyonic dilaton and scalarized cases with $\alpha = 5$. The potentials are always positive definite for the dilatonic case, whereas for small enough q for a certain P/Q, the scalarized case yields a potential with a negative region.

Given a coupling function $f(\phi)$, one can express the value of the scalar field at the horizon ϕ_0 as a function of P, Q, by solving the equation $f(\phi_0) = \frac{Q}{P}$ while $r_H = \sqrt{2PQ}$. The expansion 3.38 contains two free parameters ϕ_c and δ_0, fixed by the numerics, while

$$\delta_1 = -\frac{r_H \phi_c^2 k^2}{2k-1}, \qquad v_1 = \frac{e^{-\delta_0} Q}{r_H^2 f(\phi_0)}, \qquad k = \frac{1}{2}\left(-1 + \sqrt{1 + 2\left(\frac{\dot{f}(\phi_0)}{f(\phi_0)}\right)^2}\right) > 0. \tag{3.40}$$

A non-integer k would imply that the derivative of all functions will diverge at some order as $r \to r_H$. Although everything is smooth to 2nd order (in particular, the Kretschmann and Ricci scalars should be finite everywhere), the (suitable order) derivatives of the Riemann tensor would diverge at the horizon, resulting in non-physical solutions. Thus, in order to obtain physical solutions, we arrive at the condition

$$\frac{\dot{f}(\phi_0)}{f(\phi_0)} = \pm\sqrt{2p(p+1)},\ p \in \mathbb{N}, \tag{3.41}$$

which yields for the dilatonic coupling the triangular sequence [64, 65]

$$\alpha = \sqrt{\frac{p(p+1)}{2}}. \tag{3.42}$$

Note that the first two terms of the sequence are $\alpha = 1$ and $\alpha = \sqrt{3}$. For the exponential coupling, we have

$$\alpha = \frac{p(p+1)}{4\log\left(\frac{Q}{P}\right)} = \frac{1}{2\phi_0}\sqrt{\frac{p(p+1)}{2}}. \tag{3.43}$$

The extremal solutions share the far field asymptotics with the non-extremal ones. Extremal BH solutions are constructed using a similar numerical procedure as in the generic non-extremal case through a shooting method, and as a test, we compare the maximum allowed q that was obtained for $\alpha = 1$ with the analytical result $q^{(D)}_{ext}(\alpha = 1) = \frac{\sqrt{2(1+\mathcal{Q}^2)}}{1+\mathcal{Q}}$ for the dilatonic case (*c.f.* Appendix B), with $\mathcal{Q} = P/Q$. The domain of existence of the dyonic BHs is shown in Fig. 3.8 for several values of the ratio P/Q and for both dilatonic and scalarized BHs. In particular, in both cases and for fixed α, the maximum allowed value for q decreases as the ratio P/Q increases. In other words, the domain of existence shrinks, as the magnetic charge is increased, for fixed Q, *i.e.* a stronger presence of a magnetic charge leads to smaller maximum allowed values of q. For purely electrical solutions the domain of existence is, as before, bounded by a critical line, and in the scalarized case, by an existence line as well.

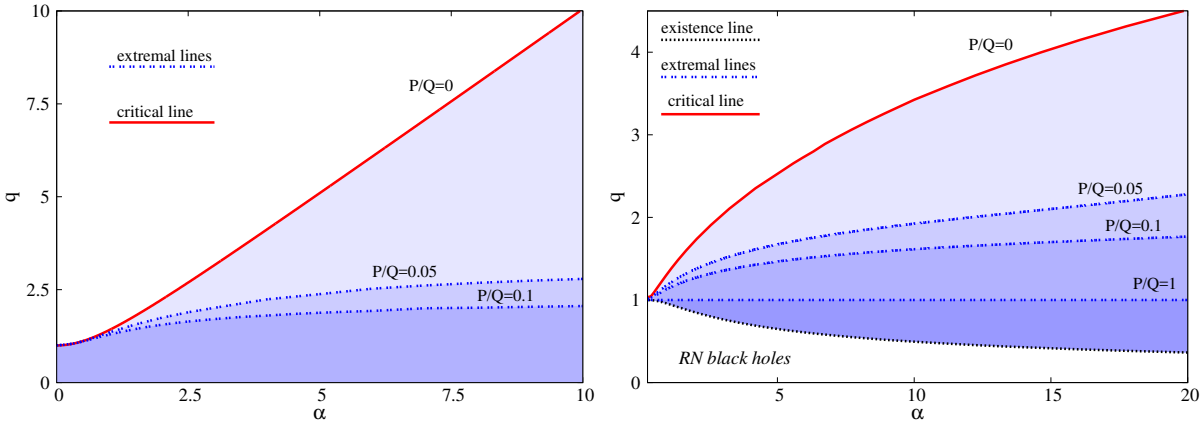

Figure 3.8: Domain of existence of dilatonic BHs (left panel) and scalarized BHs (right panel) for several values of P/Q. The existence line of the right panel is referent to the purely electrical case. Source: [47].

Chapter 4

Spontaneous scalarization of charged black holes from axion-like coupling and study of black holes with axion-hair

In order to solve the strong CP problem, Peccei and Quinn introduced a pseudoscalar known as the *axion* [66] (see also [67–69]). It was later understood that besides offering a solution to the strong CP problem, the axion could have deep implications in cosmology, being a strong candidate for both cold and non-cold dark matter [70–73]. Also, ultralight axion fields arise naturally from compactifications in string theory [74, 75]. A series of experiments are being proposed and conducted in a quest to look for axionic imprints (see *e.g.* [76] for a quick review and [77, 78] for a more detailed read). Assuming the existence of the axion ϕ, the Maxwell equations must change, forming (together with the scalar field equation of motion) the *axion electrodynamics* [79]

$$\begin{cases} \nabla\cdot(\mathbf{E}-\alpha\phi\mathbf{B}) &= 4\pi\rho_{\rm e}, \\ \nabla\cdot(\mathbf{B}+\alpha\phi\mathbf{E}) &= 4\pi\rho_{\rm m}, \\ \nabla\times(\mathbf{E}-\alpha\phi\mathbf{B}) &= -\frac{1}{c}\left[4\pi\mathbf{j}_{\rm m}+\frac{\partial}{\partial t}(\mathbf{B}+\alpha\phi\mathbf{E})\right], \\ \nabla\times(\mathbf{B}+\alpha\phi\mathbf{E}) &= \frac{1}{c}\left[4\pi\mathbf{j}_{\rm e}+\frac{\partial}{\partial t}(\mathbf{E}-\alpha\phi\mathbf{B})\right], \end{cases} \tag{4.1}$$

which are symmetric under the transformation

$$\begin{aligned} \mathbf{E}-\alpha\phi\mathbf{B}\to\mathbf{B}+\alpha\phi\mathbf{E}, \qquad \rho_e\to\rho_m, \qquad \mathbf{j}_{\rm e}\to\mathbf{j}_{\rm m}, \\ \mathbf{B}+\alpha\phi\mathbf{E}\to-(\mathbf{E}-\alpha\phi\mathbf{B}), \qquad \rho_m\to-\rho_e, \qquad \mathbf{j}_{\rm m}\to-\mathbf{j}_{\rm e}. \end{aligned} \tag{4.2}$$

BHs with axion hair have been extensively studied in the literature [80–85]. In a phenomenon associated with BH superradiance, axions can grow and "condensate" in the ergo-region of massive and

spinning BHs, causing instabilities [86, 87]. Such instabilities extract rotational energy from the BH and transfer it into the axionic cloud, leading to distinct gravitational wave imprints [88–90], that can be detected with current detectors [91, 92]. Such accumulation of ultralight bosonic particles may also lead to distinct BH shadows which can be probed via the Event Horizon Telescope [93].

In this chapter, we generalise the EMS models to include a non-minimal coupling of a scalar field to a Lorentz Chern-Simons term $F_{\mu\nu}\tilde{F}^{\mu\nu}$ (that we call "axion-like coupling"), and study the (spontaneous) scalarization related phenomena. All the notations from the last chapters are used here. In this Chapter we shall follow [2].

4.1 The model

The model in study is a generalisation of the EMS models and describes a real scalar field ϕ minimally coupled to Einstein's gravity, non-minimally coupled to Maxwell's electromagnetism and to a Lorentz Chern-Simons term. It can be described via the action

$$\mathcal{S} = \int d^4x\sqrt{-g}\left[R - 2\partial_\mu\phi\partial^\mu\phi - f(\phi)F_{\mu\nu}F^{\mu\nu} - h(\phi)F_{\mu\nu}\tilde{F}^{\mu\nu}\right], \tag{4.3}$$

where $F_{\mu\nu}$ is the usual Maxwell tensor, and $\tilde{F}^{\mu\nu} = \frac{1}{2\sqrt{-g}}\epsilon^{\mu\nu\rho\sigma}F_{\rho\sigma}$ its dual. The functions $f(\phi)$ and $h(\phi)$ are responsible for the non-minimal couplings between the scalar field and the source terms. Cases for which $h(\phi) = 0$ were extensively studied in the last chapters, and we shall focus on the new cases for which $h(\phi) \neq 0$. A generic, spherically symmetric line element to describe both the scalar free and scalarized solutions is (as before)

$$ds^2 = -N(r)e^{-2\delta(r)}dt^2 + \frac{dr^2}{N(r)} + r^2\left(d\theta^2 + \sin^2\theta d\varphi^2\right), \tag{4.4}$$

where $N(r)$ is related to the Misner-Sharp mass function $m(r)$ via $N(r) = 1 - \frac{2m(r)}{r}$. Spherical symmetry and the presence of a magnetic charge impose a 4-potential

$$A = V(r)dt - P\cos\theta d\varphi, \tag{4.5}$$

with P the magnetic charge, and a solely radial dependent scalar field $\phi(r)$. Integrating the trivial angular dependence, one can obtain an effective Lagrangian from which the equations of motion may be derived, given by

$$\mathcal{L}_{eff} = -\frac{e^{-\delta}P^2f(\phi)}{2r^2} + Ph(\phi)V' + \frac{1}{2}e^{\delta}r^2f(\phi)V'^2 + \frac{1}{2}e^{-\delta}\left(1 - N - rN' - r^2N\phi'^2\right). \tag{4.6}$$

The functions N, δ, V, ϕ are solely radial dependent, hence for simplicity this dependence shall be omitted. The prime denotes a radial derivative. Noticing the existence of a first integral

$$V' = -\frac{Q + Ph(\phi)}{r^2f(\phi)}e^{-\delta}, \tag{4.7}$$

with Q the electric charge, the equations of motion are

$$\delta' = -r\phi'^2, \tag{4.8}$$

$$\left(e^{-\delta}r^2 N\phi'\right)' = -\frac{1}{2}e^{\delta}r^2\dot{f}(\phi)V'^2 - P\dot{h}(\phi)V' + \frac{e^{-\delta}P^2\dot{f}(\phi)}{2r^2}, \tag{4.9}$$

$$N' = -\frac{(Q+Ph(\phi))^2 + P^2 f(\phi)^2 + f(\phi)r^2\left(r^2 N\phi'^2 + N - 1\right)}{f(\phi)r^3}. \tag{4.10}$$

To solve the set of ODEs we have to implement suitable boundary conditions for the desired functions and corresponding derivatives. We assume the existence of an event horizon in $r = r_H > 0$ and that the solution possesses a power series expansion in $(r - r_H)$

$$\begin{aligned} N(r) &= N_1(r-r_H) + \ldots, \qquad \delta(r) = \delta_0 + \delta_1(r-r_H) + \ldots, \\ \phi(r) &= \phi_0 + \phi_1(r-r_H) + \ldots, \qquad V(r) = v_1(r-r_H) + \ldots, \end{aligned} \tag{4.11}$$

with the lower order coefficients being

$$\begin{aligned} N_1 &= -\frac{(Q+Ph(\phi_0))^2 + P^2 f(\phi_0)^2 - r_H^2 f(\phi_0)}{r_H^3 f(\phi_0)}\,, \qquad \delta_1 = -\phi_1^2 r_H, \qquad v_1 = -\frac{Q+Ph(\phi_0)}{r_H^2 f(\phi_0)}e^{-\delta_0}\,, \\ \phi_1 &= -\frac{2P\left[Q+Ph(\phi_0)\right]f(\phi_0)\dot{h}(\phi_0) + \dot{f}(\phi_0)\left(P^2 f(\phi_0)^2 - (Q+Ph(\phi_0))^2\right)}{2r_H f(\phi_0)\left[(Q+Ph(\phi_0))^2 - r_H^2 f(\phi_0) + P^2 f(\phi_0)^2\right]}\,, \end{aligned} \tag{4.12}$$

which are fully determined via the two essential parameters ϕ_0 and δ_0. Also, of interest at the horizon we have the Hawking temperature T_H, horizon area A_H, the energy density $\rho(r_H)$ and the Kretschmann scalar $K(r_H)$ given respectively by

$$\begin{aligned} T_H &= \frac{1}{4\pi}N_1 e^{-\delta_0}\,, \qquad A_H = 4\pi r_H^2\,, \qquad \rho(r_H) = \frac{2\left(P^2 f(\phi_0)^2 + (Q+Ph(\phi_0))^2\right)}{r_H^4 f(\phi_0)}\,, \\ K(r_H) &= \frac{4}{r_H^8 f(\phi_0)^2}\Big\{5[Q+Ph(\phi_0)]^4 - 6r_H^2[Q+Ph(\phi_0)]^2 f(\phi_0) - 6P^2 r_H^2 f(\phi_0)^3 + 5P^4 f(\phi_0)^4 \\ &\qquad + f(\phi_0)^2\left(10P^2Q^2 + 3r_H^4 + 10P^3 h(\phi_0)[2Q + Ph(\phi_0)]\right)\Big\}. \end{aligned} \tag{4.13}$$

An asymptotic approximation of the solution in the far field takes the form

$$N(r) = 1 - \frac{2M}{r} + \frac{Q^2+P^2+Q_s^2}{r^2} + \ldots\,, \qquad \phi(r) = \frac{Q_s}{r} + \ldots\,, \qquad \delta(r) = \frac{Q_s^2}{2r^2} + \ldots\,, \qquad V(r) = \Phi_e + \frac{Q}{r} + \ldots\,, \tag{4.14}$$

with Q_s the scalar charge, Φ_e the electrostatic potential difference between the EH and infinity and M the ADM mass. The following results and definitions for our model will be useful later

$$F_{\mu\nu}F^{\mu\nu} = \frac{2\left[P^2 f(\phi)^2 - (Q+Ph(\phi))^2\right]}{r^4 f(\phi)^2}, \qquad F_{\mu\nu}\tilde{F}^{\mu\nu} = \frac{4P(Q+Ph(\phi))}{r^4 f(\phi)}, \tag{4.15}$$

$$q = \frac{\sqrt{Q^2+P^2}}{M}, \qquad a_H = \frac{A_H}{16\pi M^2}, \qquad t_H = 8\pi M T_H, \tag{4.16}$$

where q is defined as the reduced dyonic charge, a_H the reduced event horizon area and t_H the reduced event horizon temperature.

4.2 Conditions for the occurrence of spontaneous scalarization

As discussed in the previous chapters, in order for spontaneous scalarization to occur in a model, the coupling functions (and respective derivatives) must satisfy a set of conditions. These conditions emerge as a consequence of **i)** the far field equations of motion; **ii)** allowing the existence of a scalar free solution; **iii)** imposing a tachyonic instability in the system.

1. Maxwell's theory must be recovered near infinity, hence, for an asymptotically vanishing scalar field profile

$$f(0) = 1. \tag{4.17}$$

   There is no condition imposed on the coupling function $h(\phi)$ (this is not true for its derivatives), since the term $F_{\mu\nu}\tilde{F}^{\mu\nu}$ is a topological invariant.

2. The system must accommodate a scalar free solution. The Klein-Gordon equation of motion is

$$\Box\phi = \frac{\dot{f}(\phi)F_{\mu\nu}F^{\mu\nu} + \dot{h}(\phi)F_{\mu\nu}\tilde{F}^{\mu\nu}}{4}, \tag{4.18}$$

   from which, in order for a non-scalarized solution to exist, follows that

$$\dot{f}(0) = 0\ , \qquad \dot{h}(0) = 0 \tag{4.19}$$

3. Spontaneous scalarization occurs if the system is unstable against scalar perturbations $\delta\phi$. These obey (neglecting second order terms)

$$(\Box - \mu_{eff}^2)\delta\phi = 0, \tag{4.20}$$

   with $\mu_{eff}^2 < 0$ given by

$$\mu_{eff}^2 = \frac{\ddot{f}(0)F_{\mu\nu}F^{\mu\nu}|_{\phi=0} + \ddot{h}(0)F_{\mu\nu}\tilde{F}^{\mu\nu}|_{\phi=0}}{4} = \frac{\ddot{f}(0)(P^2 - (Q+Ph(0))^2) + 2\ddot{h}(0)P(Q+Ph(0))}{2r^4}, \tag{4.21}$$

   from which the second derivatives of the coupling functions are constrained in a way that cannot be determined *a priori*.

4.3 Bifurcating points from the scalar free solution - The existence line

Following a similar procedure as in the last chapters, the spherical symmetry allows a spherical harmonic decomposition of the scalar field to be performed

$$\delta\phi = \sum_{\ell,\mathbf{m}} Y_{\ell,\mathbf{m}}(\theta,\varphi) U_\ell(r), \tag{4.22}$$

from which the scalar field equation of motion 4.18 simplifies to

$$\frac{e^\delta}{r^2}\left(\frac{r^2 N}{e^\delta} U_\ell'\right)' - \left[\frac{\ell(\ell+1)}{r^2} + \mu_{\text{eff}}^2\right] U_\ell = 0, \tag{4.23}$$

which is an eigenvalue problem: fixing the strength of the coupling (*i.e.* fixing the coupling constant on which the coupling function depends), for a given ℓ, requiring an asymptotically vanishing, smooth scalar field, a discrete set of BHs solutions are selected, i.e. RN solutions with a certain reduced charge. These are the bifurcation points from the scalar free solution. They are labelled by an integer $n \in \mathbb{N}_0$; $n = 0$ is the fundamental mode, whereas $n > 1$ are excited states (overtones). Setting $\delta = 0$ and $N(r) = 1 - \frac{2M}{r} + \frac{Q^2+P^2}{r^2}$ allows us to recover the dyonic RN metric. Then, a scalarized solution can be dynamically induced by a scalar perturbation of the background, as long as the scalar-free RN solution is in the unstable regime. Only the spherical case ($\ell = 0$) will be studied. If $f(\phi) = 1$ and $h(\phi) = -\alpha\phi^2$ (with $\alpha > 0$), which shall be studied in greater detail later, one has $\mu_{eff}^2 = -2\alpha QP/r^4$. [1] For $\ell = 0$, one finds the following exact solution

$$U(r) = LP_u\left[-\frac{(Q^2+P^2)(r-2r_H)+r_H^2 r}{r(Q^2+P^2-r_H^2)}\right], \qquad \text{where} \qquad u \equiv \frac{1}{2}\left(\sqrt{1-\frac{8\alpha\mathcal{Q}}{1+\mathcal{Q}^2}}-1\right), \tag{4.24}$$

with $\mathcal{Q} = P/Q$ the magnetic to electric charge ratio and LP_u a Legendre function. The function $U(r)$ approaches a constant *non-zero* value as $r \to \infty$

$$U(r) \to U_\infty = LP_u\left[\frac{1+\sqrt{1-q^2}}{1+\sqrt{1-q^2}-q^2}\right] + \mathcal{O}\left(\frac{1}{r}\right), \tag{4.25}$$

thus finding the $\ell = 0$ unstable mode of the RN BH reduces to a study of the zeros of the Legendre function – *c.f.* Fig. 4.1 (left panel). Bifurcation requires α above a minimum value given by $\alpha_{min} = \frac{1+\mathcal{Q}^2}{8\mathcal{Q}}$. Some values can be found in Table 4.1.

$\mathcal{Q}$	0.01	0.1	0.2	0.3	0.4	0.5	0.6	1	2	4
α_{min}	12.5013	1.2625	0.65	0.454167	0.3625	0.3125	0.28333	0.25	0.3125	0.53125

Table 4.1: Minimum value of α for bifurcation from a dyonic RN BH for several values of $\mathcal{Q}$.

[1] In fact, this is true for any function $h(\phi)$ that respects $h(0) = 0$ and its Taylor expansion possesses a quadratic term of the form $-\alpha\phi^2$.

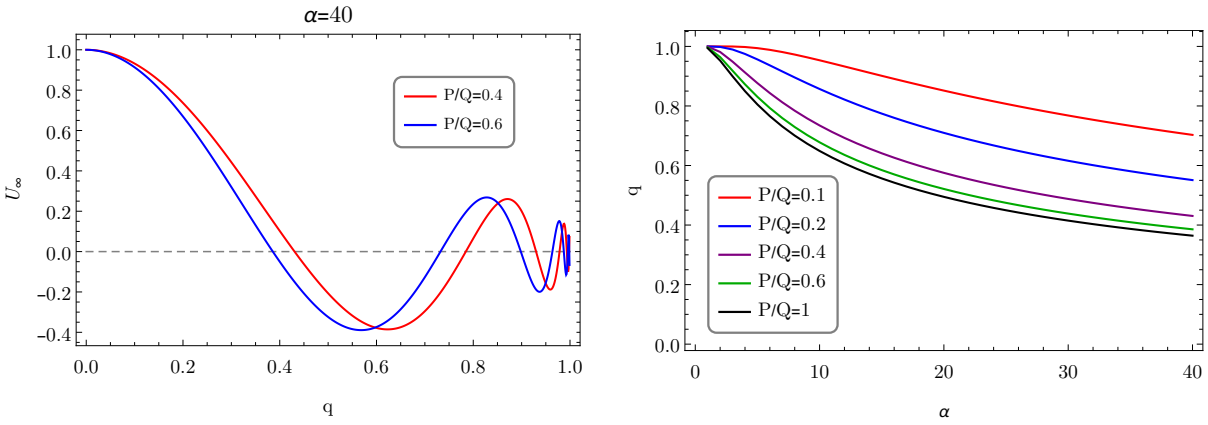

Figure 4.1: Left: U_∞ as a function of q for two values of P/Q and $\alpha = 40$. An infinite set of configurations with $U_\infty = 0$ exist, labelled by n, the number of nodes of $U(r)$. The first configuration for which $U_\infty = 0$ is labelled by $n = 0$ and so on. Right: Existence line for several values of $\mathcal{Q}$.

One can observe that for smaller $\mathcal{Q}$, a bigger α is required for bifurcation, and bifurcation occurs for a bigger q, contrarily to what was observed in Chapter 3. It is interesting to notice that for $P = 0$, the Legendre function is constant and equal to unity, for all q, and so, it possesses no zeroes. One can thus conclude that, if $P = 0$, then no scalarized BHs exist. The set of bifurcation points constitute the *existence line*, and it is shown for several $\mathcal{Q}$ in the phase space of Fig. 4.1 (right panel).

4.4 Physical relations and tests to the code

To verify that the scalarized solutions obtained when solving numerically the coupled ODE system are indeed physical we used, as before, two relations: a Smarr law and a Virial relation.

4.4.1 Smarr law

The Smarr law can be obtained via the integral mass formula, that for our model reads

$$M = \frac{1}{2} T_H A_H - \frac{1}{16\pi} \int_V (2T^b_a - T\delta^b_a) K^a d\Sigma_b, \tag{4.26}$$

where K^a is the timelike translational killing vector, and T the trace of the energy-momentum tensor. The energy-momentum tensor is

$$T_{\mu\nu} = 4\left[f(\phi)\left(F_{\mu\alpha}F^{\alpha}_{\nu} - \frac{1}{4} g_{\mu\nu} F_{\alpha\beta}F^{\alpha\beta} \right) + \partial_\mu\phi\partial_\nu\phi - \frac{1}{2} g_{\mu\nu}\partial_\alpha\phi\partial^\alpha\phi \right]. \tag{4.27}$$

as it turns out to be unnafected by the $F_{\mu\nu}\tilde{F}^{\mu\nu}$ term in the action (topological invariant). One can thus arrive at the Smarr law

$$M = \frac{1}{2} T_H A_H + \Phi_e Q + \Phi_m P + U, \tag{4.28}$$

with

$$\Phi_e = \int_{r_H}^{\infty} dr \left(\frac{Q + Ph(\phi)}{r^2 f(\phi)} e^{-\delta} \right) \equiv - \int_{r_H}^{\infty} dr V', \qquad \Phi_m = \int_{r_H}^{\infty} dr \left(e^{-\delta} f(\phi) \frac{P}{r^2} \right) \equiv - \int_{r_H}^{\infty} dr V'_m, \quad (4.29)$$

the electrostatic and magnetostatic potential differences respectively, and

$$U = - \int_{r_H}^{\infty} dr V' P h(\phi) = \frac{1}{16\pi} \int F_{\mu\nu} \tilde{F}^{\mu\nu} h(\phi) d^3x, \quad (4.30)$$

is interpreted as the axion-like related electromagnetic energy. A non-linear Smarr relation can also be established for this family of models

$$M^2 + Q_s^2 + U^2 = Q^2 + P^2 + \frac{1}{4} A_H^2 T_H^2. \quad (4.31)$$

4.4.2 Virial relation

Consider the effective action

$$\mathcal{S}_{eff} = \int_{r_H}^{\infty} dr \mathcal{L}_{eff}, \quad (4.32)$$

and assume that hairy BH solutions exist such that they are described by the functions $\phi(r), \delta(r), V(r), N(r)$ with suitable boundary conditions at the event horizon and at infinity. Next consider the 1-parameter family of configurations described by the scaled functions

$$F_\lambda(r) \equiv F(r_H + \lambda(r - r_H)), \quad (4.33)$$

with $F \in \{\phi, \delta, V, N\}$. If the initial configuration was indeed a solution, then there must be a critical point at $\lambda = 1$ such that the effective action is extremized: $\left(\frac{dS^{\lambda}_{eff}}{d\lambda} \right)_{\lambda=1} = 0$. It is then straightforward to obtain a Virial relation given by

$$\int_{r_H}^{\infty} dr \left\{ e^{-\delta} r^2 \phi'^2 \left[1 - \frac{r_H}{r} (1 + N) \right] \right\} = \Phi_e Q + \Phi_m P + U + \int_{r_H}^{\infty} dr \left\{ \frac{2 r_H}{r} \left[V' Q + V'_m P + V' P h(\phi) \right] \right\}. \quad (4.34)$$

One can show that the left hand side integrand is strictly positive. Thus, the virial identity shows that a nontrivial scalar field requires a nonzero electric/magnetic charge so that the right hand side is nonzero.

4.5 Perturbative stability analysis

For studying perturbative stability against radial perturbations, we consider spherically symmetric, linear perturbations of our equilibrium solutions, keeping the metric ansatz, but allowing the functions N, δ, ϕ, V

to depend on t as well as on r:

$$ds^2 = -\tilde{N}(r,t)e^{-2\tilde{\delta}(r,t)}dt^2 + \frac{dr^2}{\tilde{N}(r,t)} + r^2(d\theta^2 + \sin^2\theta d\varphi^2)\,, \qquad A = \tilde{V}(r,t)dt - P\cos\theta d\varphi^2\,, \qquad \phi = \tilde{\phi}(r,t)\,. \tag{4.35}$$

The time dependence enters as a periodic perturbation with frequency Ω, for each of these functions:

$$\begin{aligned} \tilde{N}(r,t) &= N(r) + \epsilon N_1(r)e^{-i\Omega t}\,, \qquad \tilde{\delta}(r,t) = \delta(r) + \epsilon\delta_1(r)e^{-i\Omega t}\,, \\ \tilde{\phi}(r,t) &= \phi(r) + \epsilon\phi_1(r)e^{-i\Omega t}\,, \qquad \tilde{V}(r,t) = V(r) + \epsilon V_1(r)e^{-i\Omega t}\,. \end{aligned} \tag{4.36}$$

From the linearised field equations around the background solution, the metric perturbations and $V_1(r)$ can be expressed in terms of the scalar field perturbation,

$$N_1 = -2rN\phi'\phi_1\,, \qquad \delta_1' = -2r\phi'\phi_1'\,, \qquad V_1' = -V'\left(\delta_1 + \frac{\dot{f}(\phi)}{f(\phi)}\phi_1\right) + \frac{e^{-\delta}P\dot{h}(\phi)}{f(\phi)r^2}\phi_1\,, \tag{4.37}$$

thus yielding a single perturbation equation for ϕ_1. Introducing a new variable $\Psi(r) = r\phi_1$, the scalar-field equation of motion may be written as

$$\left(Ne^{-\delta}\right)^2\Psi'' + Ne^{-\delta}\left(Ne^{-\delta}\right)'\Psi' + \left(\Omega^2 - U_\Omega\right)\Psi = 0, \tag{4.38}$$

which, by introducing the 'tortoise' coordinate x as $\frac{dx}{dr} = \frac{1}{e^{-\delta}N}$, can be written in the standard Schrödinger-like form:

$$-\frac{d^2}{dx^2}\Psi + U_\Omega\Psi = \Omega^2\Psi\,. \tag{4.39}$$

The perturbation potential U_Ω is defined as:

$$U_\Omega = U_0 + PU_1 + P^2U_2, \tag{4.40}$$

with

$$\begin{aligned} U_0 &= \frac{e^{-2\delta}N}{r^2}\left\{1 - N - 2r^2\phi'^2 - \frac{Q^2}{r^2f(\phi)}\mathcal{U}\right\}, \\ U_1 &= \frac{e^{-2\delta}NQ}{r^4f(\phi)}\left\{\ddot{h}(\phi) + 4r\dot{h}(\phi)\phi' - 2h(\phi)\mathcal{U}\right\}, \\ U_2 &= \frac{e^{-2\delta}N}{r^4}\left\{\frac{\ddot{f}(\phi)}{2} + 2r\phi'\dot{f}(\phi) - f(\phi)(1 - 2r^2\phi'^2) + \right. \\ &\qquad \left. \frac{1}{f(\phi)}\left[\ddot{h}(\phi)h(\phi) - \dot{h}(\phi)^2 + 4r\phi'\dot{h}(\phi)h(\phi) - h(\phi)^2\mathcal{U}\right]\right\}, \\ \mathcal{U} &= 1 - 2r^2\phi'^2 + \frac{\ddot{f}(\phi)}{2f(\phi)} + 2r\phi'\frac{\dot{f}(\phi)}{f(\phi)} - \left(\frac{\dot{f}(\phi)}{f(\phi)}\right)^2\,. \end{aligned} \tag{4.41}$$

4.6 Particular cases of the model - results

Now that the model has been shown, we will study particular cases. We shall focus on cases for which scalarization is sourced by the coupling to the Lorentz Chern-Simons term, while keeping $f(\phi) = 1$.

4.6.1 A Toy Model

We will start with a toy model that shows that spontaneous scalarization is possible in this new class of models. Consider the particular case where the background is flat ($N(r) = 1$ and $\delta = 0$). The system allows a scalar free configuration (the Coulomb configuration) given by

$$\phi = 0, \qquad A = \frac{Q}{r}dt - P\cos\theta d\varphi. \tag{4.42}$$

The scalar field equation of motion is

$$(r^2\phi')' - \frac{\dot{h}(\phi)P}{r^2}\left(Q + Ph(\phi)\right) = 0. \tag{4.43}$$

Introducing $\beta(\phi) = \left(Q + Ph(\phi)\right)^2$ and a new radial coordinate $x = 1/r$, one can arrive at

$$\frac{d^2\phi}{dx^2} - \frac{1}{2}\frac{d\beta(\phi)}{d\phi} = 0, \tag{4.44}$$

which is similar to the motion of a particle in a potential. The motion of the particle is described via the lagrangian $L = T - U$, with $T = \left(\frac{d\phi}{dx}\right)^2$ and $U = -\beta(\phi)$. We notice the existence of a first integral $E_0 = T + U = \left(\frac{d\phi}{dx}\right)^2 - \beta(\phi)$, from which analytical solutions for the radial profile of the scalar field may be obtained by solving the integral

$$x = \int \frac{d\phi}{\sqrt{E_0 + \beta(\phi)}} = \int \frac{d\phi}{\sqrt{E_0 + \left(Q + Ph(\phi)\right)^2}}, \tag{4.45}$$

and then inverting. Consider now the coupling function

$$h(\phi) = \frac{\sqrt{Q^2 - \phi^2} - Q}{P}, \tag{4.46}$$

that respects all the previously discussed conditions for the occurrence of spontaneous scalarization. It is then trivial to obtain a closed form spherically symmetric configuration

$$\phi = \frac{\sqrt{E_0 + Q^2}\tan\left(\frac{1}{r}\right)}{\sqrt{1 + \tan\left(\frac{1}{r}\right)^2}}, \qquad A = Q\,Ell\left(\frac{1}{r}, 1 + \frac{E_0^2}{Q^2}\right)dt - P\cos\theta d\varphi, \tag{4.47}$$

where Ell denotes the elliptic integral of second kind. Consider now a conducting sphere located at $r = r_0$. The energy of the configurations is

$$E = 2\pi\int_{r_0}^{\infty}\int_0^{\pi} -T_t^t\, r^2\sin\theta d\theta dr = 2\pi\int_{r_0}^{\infty}\int_0^{\pi}\rho\, r^2\sin\theta d\theta dr. \tag{4.48}$$

Denoting by $E^{\phi\neq 0}$ and by $E^{\phi=0}$ the energy of the scalarized and scalar free configurations respectively, one obtains

$$E^{\phi\neq 0} - E^{\phi=0} = 4\pi(E_0^2 + Q^2)\sin\left(\frac{2}{r_0}\right), \tag{4.49}$$

hence, the scalarized solution if energetically favoured in a set of bands given by

$$\frac{1}{r_0} \in \pi]n + 1/2, n + 1[, \tag{4.50}$$

where $n \in \mathbb{N}_0$ besides labelling the bands, also gives the number of nodes exterior to r_0 of the scalar field profile. A few conclusions about spontaneous scalarization through an axionic-type coupling may be taken/emphasised from this toy model: (i) it is not exclusive of gravitational theories; (ii) it sometimes leads to energetically favoured configurations.

4.6.2 The axionic case

Before jumping into a case where spontaneous scalarization occurs, we first study the axionic case from [80], motivated by high energy physics, that in our model corresponds to $f(\phi) = 1$ and $h(\phi) = -\alpha\phi$, with α a coupling constant and the scalar field ϕ hereby dubbed *axionic*. All BH solutions are scalarized, hence no bifurcation points from the scalar free RN solution exist. We will study the domain of existence of such axionic solutions (which is nowhere found in the literature) and verify if it is bounded by an extremal or critical set of configurations. The radial profiles of the several functions at study are also compared with known results [80] (which can in some way, constitute a third test to the code). Perturbative stability analysis of such BHs is also done.

4.6.2.1 Radial profiles

Some typical solutions of the various functions that define scalarized BHs obtained from numerical integration can be found in Fig. 4.2 for two illustrative values of the coupling constant $\alpha = 15$ and $\alpha = 35$, while keeping Q, P and r_H constant (some characteristic quantities can be found in Table 4.2).

α	P	P/Q	q	M	Q_s	Φ_e	Φ_m	U	a_H	t_H
15	0.006	0.05	0.6991237	0.171858	0.03441335	0.384395	0.0201273	-0.00204597	0.748456	0.992441
15	0.012	0.1	0.7116576	0.169461	0.061265	0.340575	0.0400918	-0.00579648	0.769778	1.02653
35	0.006	0.05	0.7138780	0.168306	0.06807724	0.324311	0.0200267	-0.00685364	0.780381	1.03639
35	0.012	0.1	0.742068	0.162517	0.094770	0.22572	0.0400274	-0.00946308	0.836965	1.0617

Table 4.2: Characteristic quantities for scalarized BH solutions for $\alpha = 15$ and $\alpha = 35$ for several values of P/Q and $r_H = 0.29736$.

A feature of these nodeless solutions is that the scalar field is a monotonically decreasing function of the radius, hence ϕ_0 is always a maximum of the scalar field. Data reveal that (as expected) for larger couplings α, there is higher scalarization as seen in Fig. 4.2 and in the values of the scalar charge (Table 4.2). As previously referred, in [80] two approximations for the scalar field radial profile are derived from

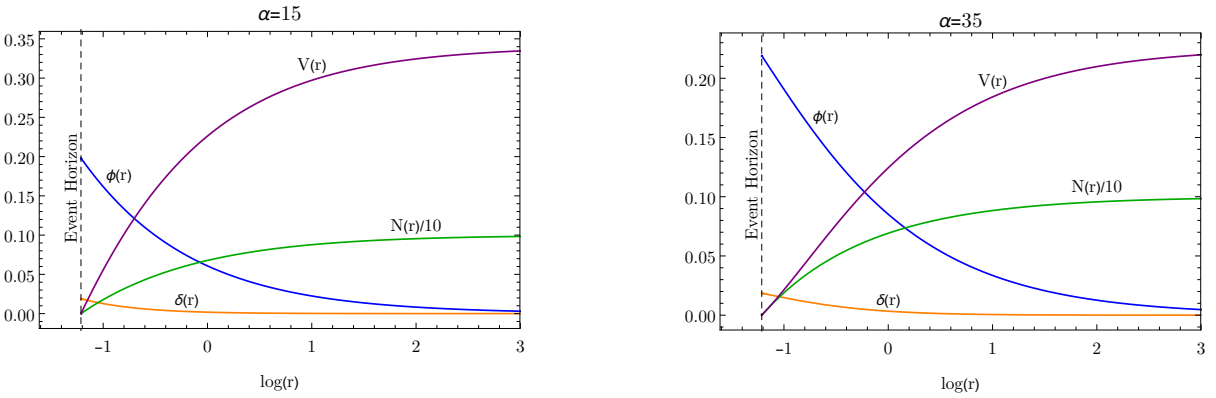

Figure 4.2: Scalarized BH radial functions for $\alpha = 15$ and $\alpha = 35$, with $Q = 0.12$, $P = 0.012$ and $r_H = 0.29736$.

eq. 4.9 as follows

$$\phi(r) \approx \alpha \frac{QP}{r_+ r_-} \ln\left(\frac{r}{r - r_-}\right) + \mathcal{O}(\alpha^2), \text{ for small } \alpha, \tag{4.51}$$

$$\phi(r) \approx \frac{Q}{\alpha P}\left(1 - \exp\left(-\frac{\alpha P}{r}\right)\right), \text{ for large } \alpha, \tag{4.52}$$

with $r_\pm = M \pm \sqrt{M^2 - Q^2 - P^2}$ the horizons of the unperturbed RN BH. A comparison between these analytical approximations and the numerical results can be seen in Fig. 4.3.

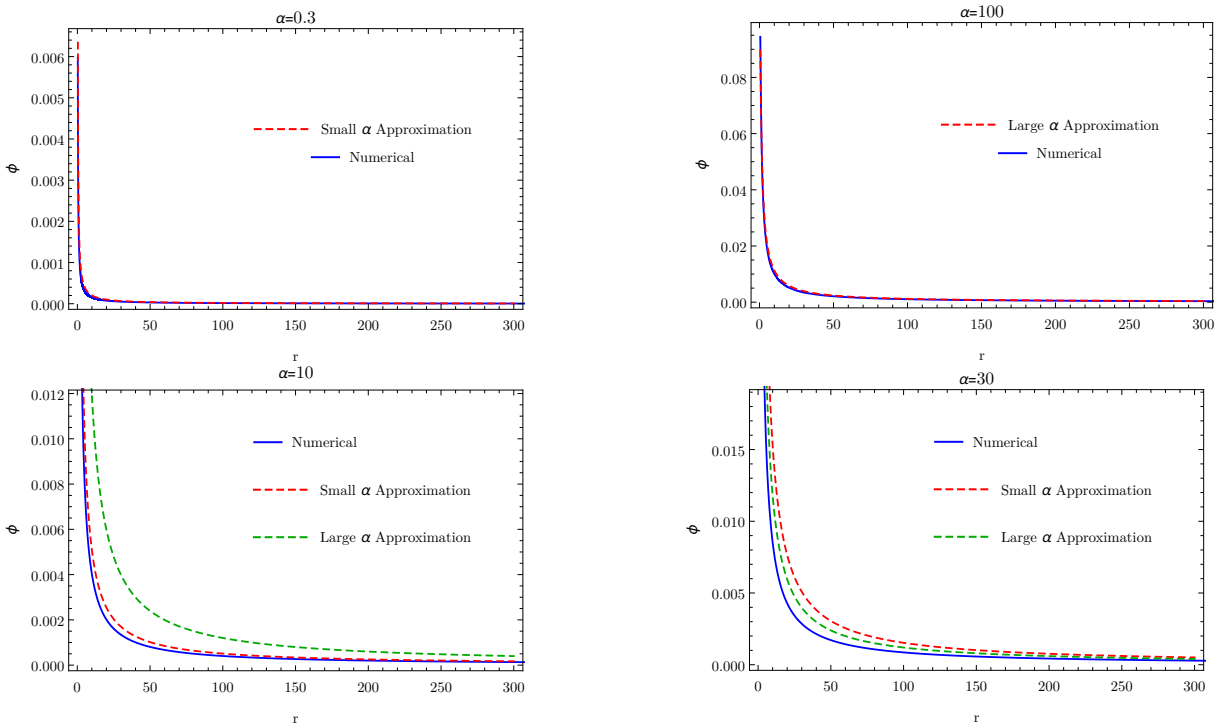

Figure 4.3: Comparison between the analytical approximations and the numerical results. Top left: $\alpha = 0.3$, $Q = 0.12$, $P = 0.012$, $r_H = 0.282474$, approximation for small α. Top right: $\alpha = 100$, $Q = 0.12$, $P = 0.012$, $r_H = 0.529659$, approximation for big α. Bottom left: $\alpha = 10$, $Q = 0.12$, $P = 0.012$, $r_H = 0.33453$. Bottom right: $\alpha = 30$, $Q = 0.12$, $P = 0.012$, $r_H = 0.33453$. The approximations hold really well for the appropriate cases. The intermediate cases show a clear deviance between the numerical solution and the analytical approximations.

We have derived two other analytical approximations for the large and small couplings (in a similar way as in [80]) that suit better our model, that besides taking into account a value ϕ_0 for the scalar field at the event horizon, in the small coupling limit does not neglect α^2 terms. These approximations are

$$\phi(r) \approx \frac{Q}{\alpha P} + A\, LP_v\left(-\frac{(Q^2+P^2)(r-2r_H)+r_H^2 r}{r(Q^2+P^2-r_H^2)}\right) + B\, LQ_v\left(-\frac{(Q^2+P^2)(r-2r_H)+r_H^2 r}{r(Q^2+P^2-r_H^2)}\right), \text{ for small } \alpha, \tag{4.53}$$

where LP and LQ are Legendre functions of first and second kind, respectively, and $v = \frac{1}{2}\left(\sqrt{\frac{4\alpha^2\mathcal{Q}^2}{1+\mathcal{Q}^2}+1}-1\right)$. A and B are integration constants chosen such that an asymptotically vanishing solution is assured and the value of the scalar field at the event horizon is ϕ_0. For large couplings we have

$$\phi(r) \approx \frac{Q}{\alpha P}\left(1 + \frac{\left(\phi_0 \frac{\alpha P}{Q} - 1\right)\sinh\left(\frac{\alpha P}{r}\right) + \sinh\left(\alpha P\left(\frac{1}{r}-\frac{1}{r_H}\right)\right)}{\sinh\left(\frac{\alpha P}{r_H}\right)}\right), \text{ for large } \alpha. \tag{4.54}$$

Plots of these approximations, and comparison with the previous ones can be found in Fig. 4.4. Data reveals that the new approximations hold indeed better than the previous ones, with the differences being more relevant in the small coupling case, where the new approximation does not neglect α^2 terms. Although it can not directly be seen from Fig. 4.4, numerics indicate that the new large coupling approximation gives an overall better approximation. Tests to the code reveal relative differences 10^{-9} for the Virial relation, 10^{-8} for the Smarr law and as seen in Figs. 4.3 and 4.4, the analytical approximations hold extremely well in the appropriate cases.

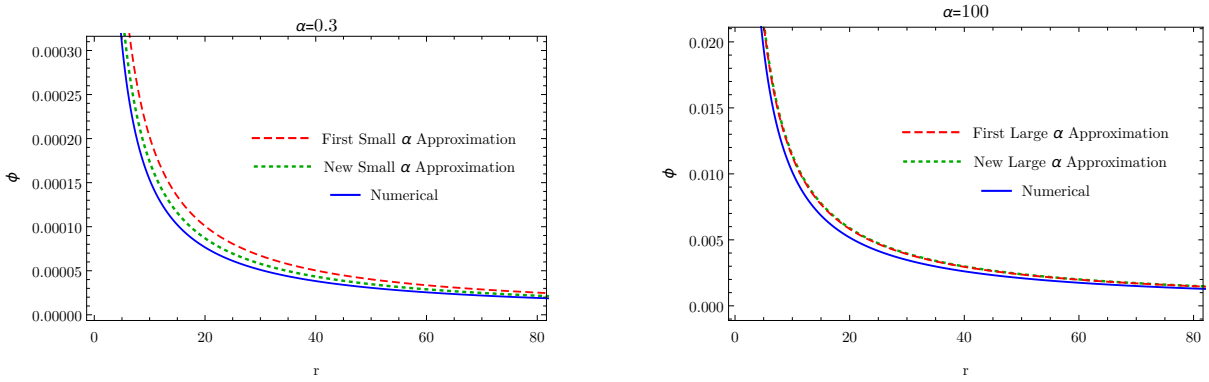

Figure 4.4: Zoomed plots for the scalar field radial profiles, in order to make a comparison between the new and first analytical approximations and the numerical results. Left: $\alpha = 0.3$, $Q = 0.12$, $P = 0.012$, $r_H = 0.282474$. Right: $\alpha = 100$, $Q = 0.12$, $P = 0.012$, $r_H = 0.529659$.

4.6.2.2 Domain of Existence

The domain of existence, in the (α, q) plane, for scalarized solutions is presented in Fig. 4.5 (left panel). The domain of existence is delimited, for sufficiently large α, by a set of critical solutions that we call the *critical line*, as in previous chapters. At the critical line numerics suggest a divergence of the Kretschmann scalar and a vanishing horizon area, whilst M and Q_s remain finite and non-zero. Exceptions occur for

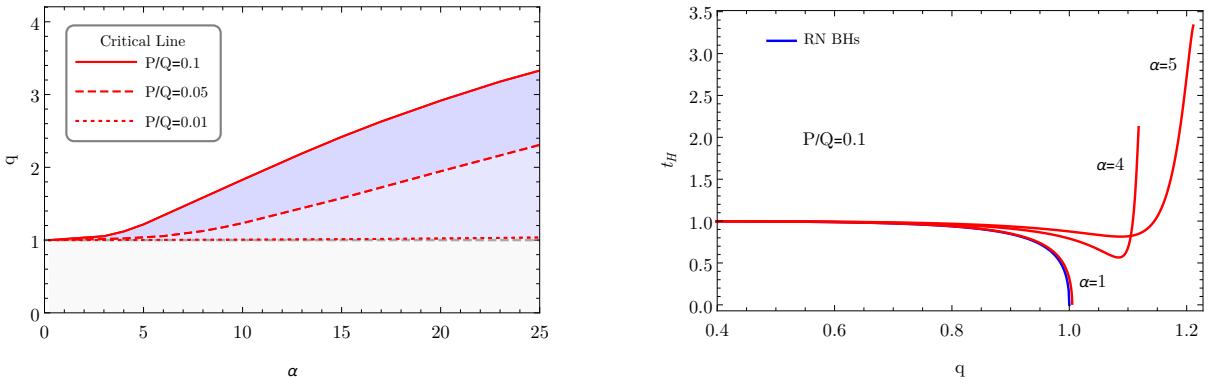

Figure 4.5: Left: Domain of existence of scalarized solutions in the (α, q) plane, in the shadowed region. The domain is bounded by a critical line at which solutions are singular, for each presented P/Q value. Right: t_H as a function of q for $P/Q = 0.1$. One observes that for small α, solutions approximate an extremal RN BH.

very small[2] values of the coupling, for which scalarization is almost negligible and solutions approximate an extremal RN BH, *c.f.* Fig. 4.5 (right panel). It is interesting to notice that, along $\alpha = constant$ branches, q increases beyond unity: therefore, scalarized BHs can be overcharged. We also remark that for a given α, as q increases, so does the scalar field's initial amplitude ϕ_0. As already mentioned, the scalar field profile is always such that the scalar field is monotonically decreasing. Thus, the global maximum of the scalar field occurs at the BH horizon, and increases, for fixed α, with q, which means one can take ϕ_0 as a measure of q and vice-versa. As another feature, for higher magnetic charges (fixing the electric charge Q) there is a wider domain of existence, which is completely opposite to the dyonic scalarized BHs case of Chapter 3 ($h(\phi) = 0$ and $P \neq 0$). In the last chapter we observed that extremal solutions are obtained for smaller values of q for higher values of P/Q along the same $\alpha = constant$ branches. This wider domain of existence, for larger P/Q, is expected since the coupling $h(\phi)F_{\mu\nu}\tilde{F}^{\mu\nu}$ is directly proportional to P: for higher values of P/Q the scalar field couples more strongly to the source term.

4.6.2.3 Perturbative stability

The potential U_Ω is plotted in Fig. 4.6. It is not positive definite in all cases but it is regular in the entire range $-\infty < x < \infty$. For other values of the coupling α, the potential always behaves in a similar way: for sufficiently small values of P/Q, the potential is always positive (and hence, free of instabilities), until P/Q reaches a value at which the potential starts to have a negative region. Moreover, the potential vanishes at the BH event horizon and at infinity.

4.6.3 Spontaneous scalarization: power law coupling

A case for which spontaneous scalarization occurs is now studied, for the coupling function $h(\phi) = -\alpha\phi^2$ (and $f(\phi) = 1$ as before), hereby dubbed "power law coupling". The coupling constant α is a dimensionless positive constant. This coupling function obeys all the necessary conditions for the occurrence of spontaneous scalarization and is the natural generalisation of the axionic case. The radial

[2] "very small" is a somewhat ambiguous term, since it highly depends on the P/Q ratio.

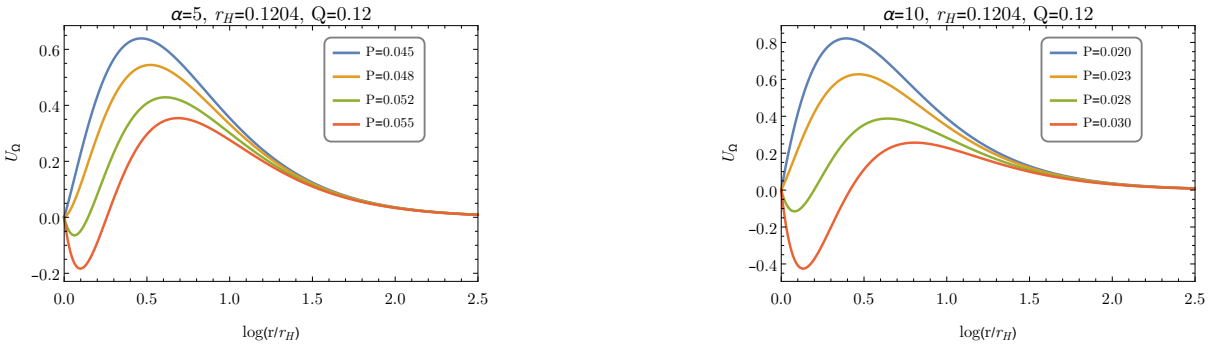

Figure 4.6: Perturbative potential, U_Ω, for $r_H = 0.1204$, $Q = 0.12$ and several values of P/Q. Left panel: $\alpha = 5$. Right panel: $\alpha = 10$. One observes that the potential is always positive until a critical P/Q value is reached, and afterwards it always has a negative region.

profiles and the domain of existence will be studied. Since the RN BH is a solution of the model (the scalar free solution), an entropic analysis will be performed. Perturbative stability analysis is also done.

4.6.3.1 Radial profiles

Some typical solutions of the various functions that define scalarized BHs in the power law coupling, obtained from numerical integration, can be found in Fig. 4.7 for two illustrative values of the coupling constant, $\alpha = 20$ and $\alpha = 35$, while keeping Q, P and r_H constant (some characteristic quantities can be found in table 4.3). Two overtone solutions (with $n = 1$ and $n = 2$) are also presented.

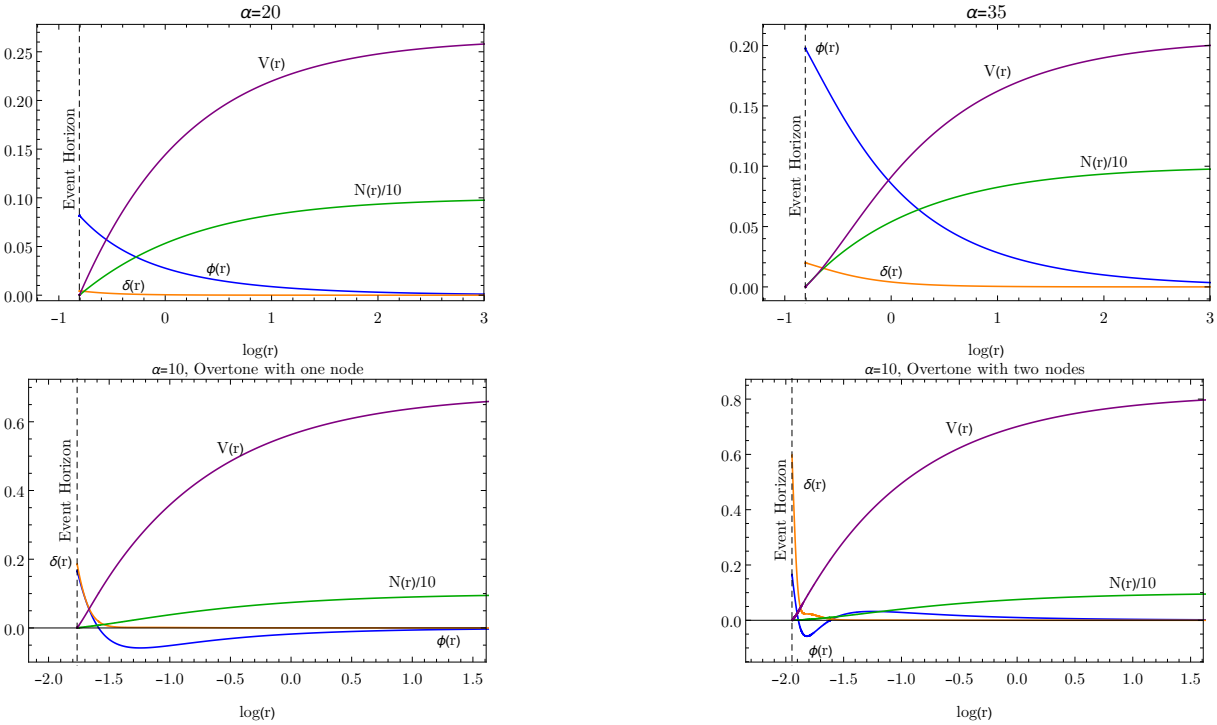

Figure 4.7: Top: scalarized BH radial functions for $\alpha = 20$ (left) and $\alpha = 35$ (right), with $Q = 0.12$, $P = 0.06$ and $r_H = 0.44604$. Bottom left: Overtone solution $n = 1$ with $\alpha = 10$, $Q = 0.12$, $P = 0.06$ and $r_H = 0.171279$. Bottom right: Overtone solution $n = 2$ with $\alpha = 10$, $Q = 0.12$, $P = 0.06$ and $r_H = 0.142733$.

α	P	P/Q	q	M	Q_s	Φ_e	Φ_m	U	a_H	t_H
20	0.06	0.5	0.5516939	0.2431857	0.02174461	0.263942	0.134363	-0.000552335	0.84103	0.997441
20	0.072	0.6	0.5719615	0.244672	0.04789236	0.242883	0.160661	-0.00242039	0.830845	1.01522
35	0.06	0.5	0.5553367	0.2415905	0.07080436	0.206099	0.133572	-0.00422197	0.852173	1.03492
35	0.072	0.6	0.5769590	0.2425525	0.07730736	0.190191	0.160293	-0.00452185	0.845427	1.0373

Table 4.3: Characteristic quantities for scalarized BH solutions for $\alpha = 20$ and $\alpha = 35$, with $Q = 0.12$, $P = 0.06$ and $r_H = 0.44604$.

Most of the features from the axionic case are shared here: for the nodeless solutions ϕ_0 is a maximum of the scalar field radial profile and for higher couplings there is bigger scalarization and smaller electrostatic potentials. The overtones of Fig. 4.7 (bottom panel) have a much greater value of δ_0 and of the electrostatic potentials when compared with the fundamental solutions. From eq. 4.9, it is also possible to derive two approximations, for small and large couplings, in a similar fashion as it was done for the axionic case:

$$\phi(r) \approx A\, LP_u\left(-\frac{(Q^2+P^2)(r-2r_H)+r_H^2 r}{r(Q^2+P^2-r_H^2)}\right)+B\, LQ_u\left(-\frac{(Q^2+P^2)(r-2r_H)+r_H^2 r}{r(Q^2+P^2-r_H^2)}\right)+\mathcal{O}(\alpha^2), \text{ for small } \alpha, \tag{4.55}$$

where LP_u and LQ_u are Legendre functions of first and second kind, respectively, and $u = \frac{1}{2}\left(\sqrt{1-\frac{8\alpha\mathcal{Q}}{1+\mathcal{Q}^2}}-1\right)$. A and B are integration constants chosen such that an asymptotically vanishing solution is assured and the value of the scalar field at the event horizon is ϕ_0. For large couplings we have

$$\phi(r) \approx \frac{Q\tanh\left(\frac{\sqrt{\alpha PQ}}{r}\right)}{\sqrt{\alpha PQ}}, \text{ for large } \alpha, \tag{4.56}$$

where the integration constants were chosen such that the solution is regular and asymptotically vanishing. A comparison between these analytical approximations and the numerical results can be found in Fig. 4.8. The approximations, although visibly good, are qualitatively worse when compared to the ones of axionic case (for an axionic profile). This happens due to the non-linearities induced by the quadratic scalar field terms. The small coupling approximation neglects α^2 terms and the large coupling one does not possess the benefit of imposing the scalar field value at the event horizon, since one of the integration constants was used to impose regularity of the approximation. We have noticed an interesting feature: the toy model scalar field radial profile from eq. 4.47 results in an approximation that is a lot similar to the one in study for large couplings, provided that the integration constant E_0 is such that the value of the scalar field at the event horizon is ϕ_0. We remark that, once again, tests to the code reveal relative differences 10^{-9} for the Virial relation, 10^{-7} for the Smarr law.

4.6.3.2 Domain of existence

Both in the previously studied axionic case and in the ones studied in Chapter 2, the domain of existence was always bounded by a critical line: a set of critical solutions for which numerics suggest a divergence

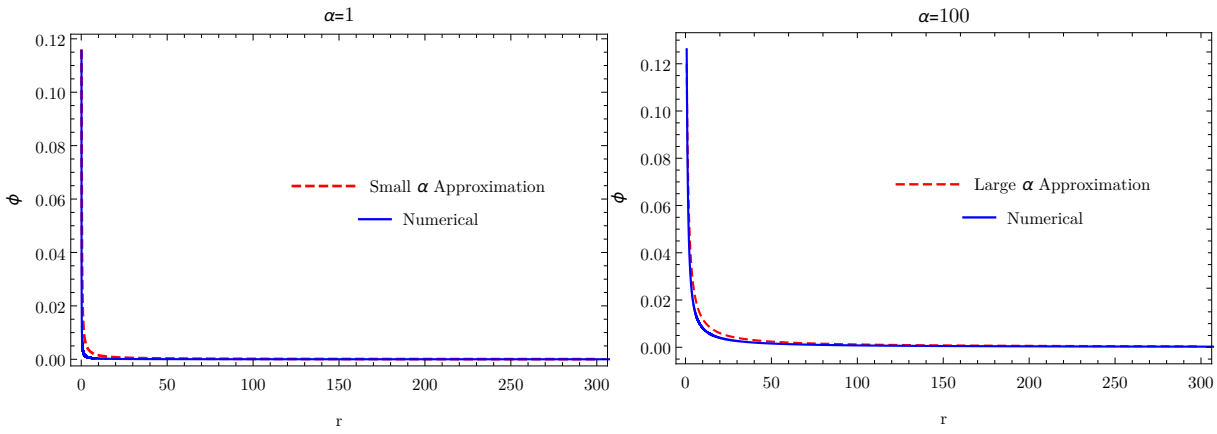

Figure 4.8: Comparison between the analytical approximations and the numerical results. Top left: $\alpha = 1$, $Q = 0.12$, $P = 0.06$, $r_H = 0.142733$, approximation for small α. Top right: $\alpha = 100$, $Q = 0.12$, $P = 0.06$, $r_H = 0.683928$, approximation for big α.

of the Kretschmann scalar and of the temperature, at the horizon, and a vanishing of the horizon area, whilst M and Q_s remain finite and non-zero. Upon evolving the $\alpha = constant$ branches with the previous near-horizon expansion, a different behaviour for the solutions was observed: numerics suggest that the temperature of the horizon tends to zero, while the Kretschmann scalar does not diverge, and the horizon area remains finite and non-zero, which is compatible with near-extremal BH solutions. As discussed in Chapter 3, a characteristic of extremal BH solutions is a vanishing horizon temperature, hence, in order to obtain the extremal BH solutions, a different near-horizon expansion which accounts for a degenerate horizon must be used (see *e.g.* [47, 64, 65]), and a double zero on the function $N(r)$ has to be imposed, with the leading order terms being

$$\begin{aligned} N(r) &= N_2 \left(r - r_H\right)^2 + \ldots, \\ \phi(r) &= \phi_0 + \phi_c \left(r - r_H\right)^k + \ldots. \end{aligned} \tag{4.57}$$

Taking ϕ_0 and r_H as the essential parameters one obtains

$$P = r_H\,, \qquad Q = \alpha \phi_0^2 r_H\,, \qquad N_2 = \frac{1}{r_H^2}\,, \qquad k = \frac{1}{2}\left(1 + \sqrt{1 + 16\phi_0^2\alpha^2}\right), \tag{4.58}$$

A non-integer k would imply that the derivative of all functions will diverge at some order as $r \to r_H$. Although everything is smooth to second order (in particular, the Kretschmann and Ricci scalars should be finite everywhere), the (suitable order) derivatives of the Riemann tensor would diverge at the horizon, resulting in non-physical solutions. Thus, in order to obtain physical solutions, we arrive at another condition

$$\alpha = \frac{\sqrt{p(p+1)}}{2\phi_0},\ p \in \mathbb{N}_0. \tag{4.59}$$

The domain of existence, in the (α, q) plane is presented in Fig. 4.9.

One can observe that there is a region of non-uniqueness where, for the same charge to mass ratio $q < 1$, RN BHs and scalarized BHs co-exist. Unlike in the domain of existence of the axionic case, one can observe that for higher P/Q values, there is a narrower domain of existence, which is unexpected

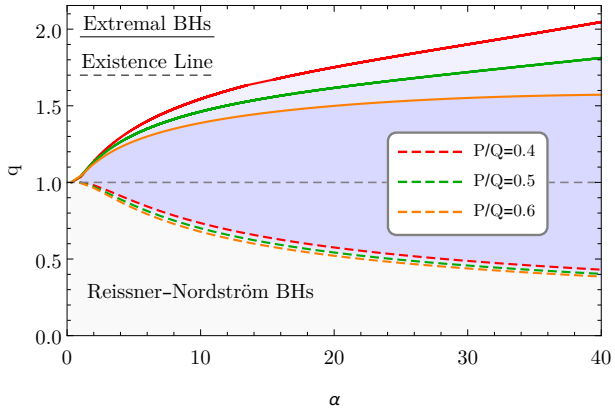

Figure 4.9: Domain of existence of scalarized solutions in the (α, q) plane. The domain is bounded by an extremal line (solid lines) at which solutions are extremal BHs and by an existence line (dashed), for each presented P/Q value.

since the coupling $h(\phi)F_{\mu\nu}\tilde{F}^{\mu\nu}$ is directly proportional to P, raising the question: is there any region for which the domain of existence is wider for a bigger P/Q ratio? There is, as presented in Fig. 4.10 (left panel). For a region where α is small enough, the domain of existence is wider for higher values of P/Q.

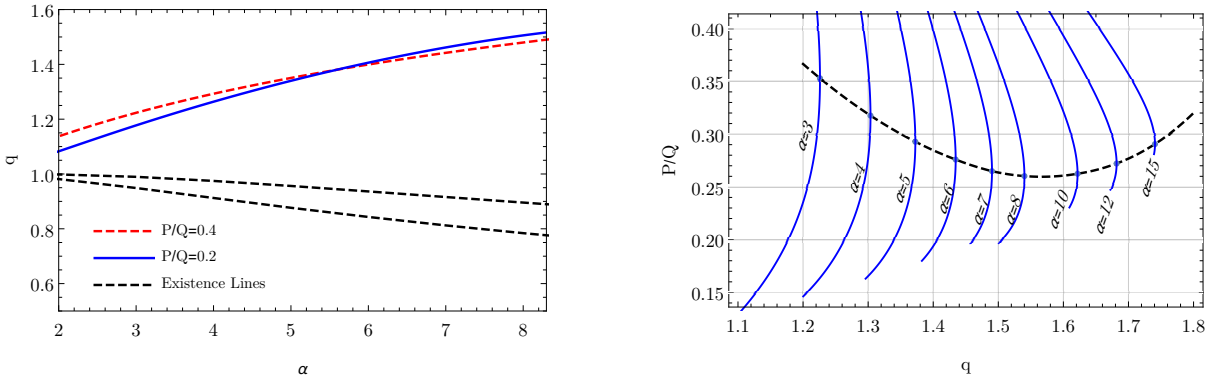

Figure 4.10: Left: Zoomed domain of existence for $P/Q = 0.2$ and $P/Q = 0.4$. One observes that there is a region at which the bigger value of P/Q allows greater overcharging. Right: $(P/Q, q)$ plane. The solid lines correspond to the extremal solution for each P/Q value, for a constant α. The black curve is the curve that interpolates the optimum values of P/Q.

Numerics suggest this effect is related to the term proportional to $P\dot{h}(\phi)$ in the scalar field equation of motion. More details can be found in Fig. 4.10 (right panel) that shows the $(P/Q, q)$ plane. The solid lines in blue correspond to the extremal solution for each value of P/Q, for a constant α. One can observe that, for each $\alpha = constant$ line, there is an optimal value of P/Q at which overcharging (and hence the domain of existence in that region) is maximum. The black curve is the curve that interpolates those optimal values of P/Q. Take the example of Fig. 4.10 (left panel): one can observe that for $\alpha = 3$ there is a bigger allowed value of q for $P/Q = 0.4$ than for $P/Q = 0.2$. Numerical integration reveals that, overall, the domain of existence is wider for smaller P/Q values.

4.6.3.3 Perturbative stability

The potential U_Ω is plotted in Fig. 4.11. It is not positive definite but is regular in the entire range $-\infty < x < \infty$. For other values of the coupling and P/Q ratios the potential always has a similar form. Also, the potential vanishes at the BH event horizon and at infinity. As discussed before, the existence of a region of negative potential does not imply instability. Thus, conclusions about stability can only be taken by computing the values of Ω by solving the perturbation equation (similarly to what was done in [43] for the purely electrical case) or with fully non-linear simulations.

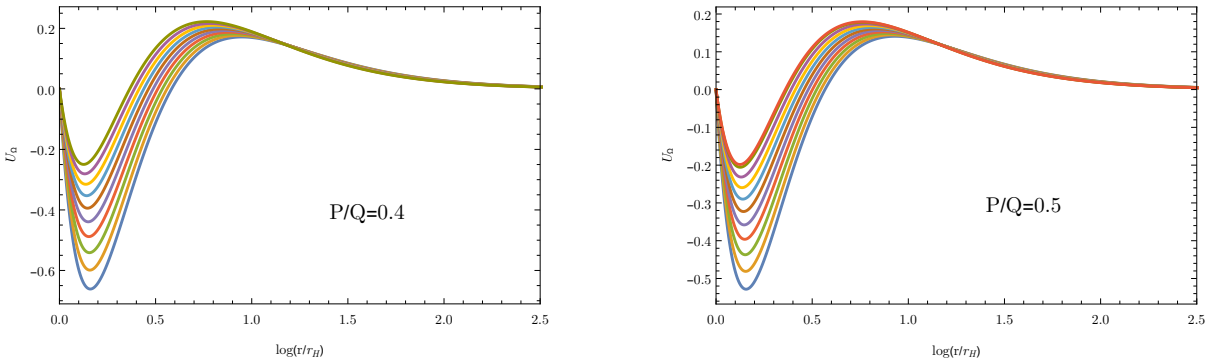

Figure 4.11: Sequence of perturbative potentials, U_Ω, for $\alpha = 10$, $P/Q = 0.4$ (left) and $P/Q = 0.5$ (right). The deeper potentials at each figure, occur for higher values of q. There is always a region where the potential is negative. Left panel: bottom curve has $q = 0.785$ and top curve has $q = 0.736$. Right panel: bottom curve has $q = 0.746$ and top curve has $q = 0.701$.

4.6.3.4 Entropic preference

In this model, the Bekenstein-Hawking BH entropy formula holds. Thus, the entropy analysis reduces to the analysis of the horizon area. It is convenient to use the already introduced reduced event horizon area a_H. Then, in the region where the Reissner-Nordström BHs and scalarized BHs co-exist - the non-uniqueness region -, for the same q, the scalarized solutions are always entropically preferred as seen in Fig. 4.12.

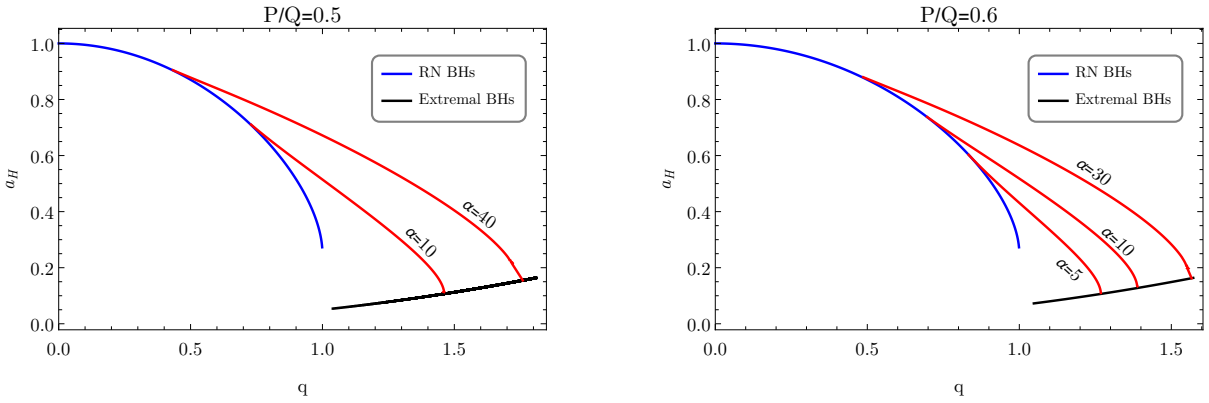

Figure 4.12: a_H vs q for $P/Q = 0.5$ and $P/Q = 0.6$. The blue lines are the sequence of non-scalarized BHs, while the red lines are sequences of (numerical data points representing) scalarized BHs for a given α. The black line represents the entropy of the extremal BH solutions for the different α values.

Chapter 5

Conclusions and Future Work

In this work we studied BH spontaneous scalarization in the framework of EMS models. We started with a study of purely electric BH for four different types of coupling functions. For all the studied couplings, the scalarized solutions are entropically favoured over a comparable RN BH in the region where non-uniqueness holds, which creates a difference with respect to eSTGB scalarized BHs, that are not entropically prefered for the same power-law coupling. The power-law, hyperbolic and exponential couplings are qualitatively very similar, although the exponential coupling maximises differences with respect to the RN case. Fundamental spherically symmetric BHs were found to be generically perturbatively stable, which is not necessarily true for eSTGB BHs (entropic non-preference and perturbative instability are probably related). The fractional coupling, on the other hand, yields qualitative differences with the existence of a different type of boundary in the domain of existence, bounding the region where physical solutions exist (solutions with positive energy density in all the extent of the radial coordinate). This boundary is associated to the divergent behaviour of the coupling for a certain value of the scalar field. In what respects dynamical evolution, results from [1, 38] show that the endpoint of unstable RN BHs in the EMS models are, for small enough q, scalarized RN BHs with the same value of q, whereas for higher values of q evolution is not conservative. Also, it was observed that the endpoint of unstable RN BHs under non-spherical perturbations are spherically symmetric scalarized BHs.

A second line of research was related to the inclusion of magnetic charge in the EMS models, yielding dyonic BHs, and the understanding of its consequences. In the well known dilatonic case, dyonic BHs have a regular extremal limit (with zero Hawking temperature), whereas purely electrical (or magnetical) ones do not; the latter becomes singular, approaching a critical solution when endowed with the maximal possible charge for a given mass. Given the special features of smooth extremal solutions, it is of interest to understand the status of these solutions in the generic EMS case, since for purely electric scalarized BHs maximal charge led to critical, rather than extremal, solutions. It was shown that the conclusions for generic EMS BHs are similar to the ones of dilatonic BHs, yielding an extremal limit. Within our framework, extremal dyonic BHs for the dilatonic case are constructed for arbitrary couplings α, whereas solutions are known in analytic closed form only for some specific values of the coupling. The entropy of scalarized BHs was computed revealing, as in the purely electric case, that scalarized solutions

are entropically favoured over a comparable RN BH in the region where non-uniqueness holds. It was shown that dilatonic BHs are always perturbatively stable, whereas, for sufficientely large magnetic charge, scalarized BHs yield a region where the perturbative potential is negative (which does not imply instability).

Lastly, the EMS model was generalised to include an axionic-like coupling. A discussion on the necessary conditions for the occurrence of spontaneous scalarization in the new model was made, and a toy model presented, which showed that the process is not exclusive of gravitational theories and that scalarized solutions can be energetically favoured provided that some conditions hold. Then the well known case of the axionic coupling was studied. The domain of existence of such solutions was obtained, being bounded by a critical line for sufficiently large α (even though magnetic charge is present), and approximating extremal RN BHs for small values of the coupling. The radial functions profiles were studied, resulting in new analytical approximations that reproduce the numerical results better than the ones previously known in the literature and a perturbative stability analisys was done, revealing that BHs with axion hair are perturbatively stable. A similar procedure was followed for a power-law coupling, for which spontaneous scalarization occurs. The domain of existence of such solutions was obtained, now being bounded by an existence line (that depends on the magnetic to electric charge ratio) and by a set of extremal solutions, as occurred in the EMS dyonic model. Once again, the radial functions profiles were studied, analytical approximations were obtained and perturbative stability analisys was done, revealing that there is always a region where the potential is negative (which does not imply instability). It was shown that in the region of non-uniqueness, scalarized solutions are entropically prefered over the comparable RN BHs. In what concerns dynamical evolution, results from [2] show, through fully non-linear simulations, that the spontaneously scalarized BHs do form dynamically.

As an avenue of further research one may include a mass term for the scalar field. As in the case of other scalar-tensor theories this is expected to suppress the effects of scalarization. Preliminary results were obtained and revealed that (i) the existence line changes; (ii) scalarization requires a larger coupling as compared to the mass-free case; (iii) the mass term quenches the dispersion of the scalar field, which becomes more concentrated in the neighbourhood of the horizon. It would be interesting to analyse such inclusion of a mass term in greater detail. Another possible extension to the EMS models would be the inclusion of rotation, similarly to what was done in ref. [40] in the context of eSTGB BHs. It would also be interesting to perform a complete study of the quasi-normal modes of scalarized BHs for both dyonic BHs of Chapter 3 and axionic(-like) BHs of Chapter 4, similarly to what was done in ref. [43].

Bibliography

[1] Pedro G. S. Fernandes, Carlos A. R. Herdeiro, Alexandre M. Pombo, Eugen Radu, and Nicolas Sanchis-Gual. Spontaneous scalarisation of charged black holes: coupling dependence and dynamical features. *Classical and Quantum Gravity*, 36(13):134002, Jun 2019.

[2] Pedro G. S. Fernandes, Carlos A. R. Herdeiro, Alexandre M. Pombo, Eugen Radu, and Nicolas Sanchis-Gual. Spontaneous scalarisation of charged black holes from axion-like coupling and study of black holes with axion-hair. TO BE RELEASED SOON.

[3] Ray D'Inverno. *Introducing Einstein's Relativity*. Clarendon Press, 1992.

[4] Carlos A. R. Herdeiro. *Notas de Teoria da Relatividade*. Universidade de Aveiro.

[5] H. Goldstein, C.P. Poole, and J.L. Safko. *Classical Mechanics*. Addison Wesley, 2002.

[6] R.M. Wald. *General Relativity*. University of Chicago Press, 1984.

[7] C. Montgomery, W. Orchiston, and I. Whittingham. Michell, Laplace and the origin of the black hole concept. *Journal of Astronomical History and Heritage*, 12:90–96, July 2009.

[8] S. Carroll, S.M. Carroll, and Addison-Wesley. *Spacetime and Geometry: An Introduction to General Relativity*. Addison Wesley, 2004.

[9] C.W. Misner, K.S. Thorne, and J.A. Wheeler. *Gravitation*. Number pt. 3 in Gravitation. W. H. Freeman, 1973.

[10] P. K. Townsend. Black Holes. *arXiv e-prints*, pages gr–qc/9707012, Jul 1997.

[11] Ibrahim Semiz. Dyonic Kerr-Newman black holes, complex scalar field and cosmic censorship. *General Relativity and Gravitation*, 43:833–846, Mar 2011.

[12] Roy P. Kerr. Gravitational field of a spinning mass as an example of algebraically special metrics. *Phys. Rev. Lett.*, 11:237–238, Sep 1963.

[13] Ramesh Narayan and Jeffrey E. McClintock. Observational Evidence for Black Holes. *arXiv e-prints*, page arXiv:1312.6698, Dec 2013.

[14] B. P. Abbott et al. GWTC-1: A Gravitational-Wave Transient Catalog of Compact Binary Mergers Observed by LIGO and Virgo during the First and Second Observing Runs. 2018.

[15] Kazunori Akiyama et al. First M87 Event Horizon Telescope Results. I. The Shadow of the Supermassive Black Hole. *Astrophys. J.*, 875(1):L1, 2019.

[16] Pedro V. P. Cunha and Carlos A. R. Herdeiro. Shadows and strong gravitational lensing: a brief review. *General Relativity and Gravitation*, 50(4):42, Apr 2018.

[17] B.W. Carroll and D.A. Ostlie. *An Introduction to Modern Astrophysics*. Pearson Addison-Wesley, 2007.

[18] Subrahmanyan Chandrasekhar. The maximum mass of ideal white dwarfs. *Astrophys. J.*, 74:81–82, 1931.

[19] Richard C. Tolman. Static solutions of Einstein's field equations for spheres of fluid. *Phys. Rev.*, 55:364–373, 1939.

[20] J. R. Oppenheimer and G. M. Volkoff. On massive neutron cores. *Phys. Rev.*, 55:374–381, Feb 1939.

[21] S. Chandrasekhar. *Truth and Beauty: Aesthetics and Motivations in Science*. Aesthetics and Motivations in Science. University of Chicago Press, 1990.

[22] D. Robinson. Four decades of black hole uniqueness theorems. *appeared in The Kerr spacetime: Rotating black holes in General Relativity, eds DL Wiltshire, M. Visser and SM Scott*, pages 115–143, 2009.

[23] Piotr T. Chruściel, João Lopes Costa, and Markus Heusler. Stationary Black Holes: Uniqueness and Beyond. *Living Reviews in Relativity*, 15:7, May 2012.

[24] R. Ruffini and J. Wheeler. Introducing the black hole. *Physics Today*, 24:30, 1971.

[25] R. O. Hansen. Multipole moments of stationary space-times. *Journal of Mathematical Physics*, 15:46–52, January 1974.

[26] Carlos A. R. Herdeiro and Eugen Radu. Asymptotically flat black holes with scalar hair: A review. *International Journal of Modern Physics D*, 24(9):1542014–219, Jun 2015.

[27] Georges Aad et al. Observation of a new particle in the search for the Standard Model Higgs boson with the ATLAS detector at the LHC. *Phys. Lett.*, B716:1–29, 2012.

[28] Serguei Chatrchyan et al. Observation of a new boson at a mass of 125 GeV with the CMS experiment at the LHC. *Phys. Lett.*, B716:30–61, 2012.

[29] B.S. Ryden. *Introduction to Cosmology*. Addison-Wesley, 2003.

[30] R. D. Peccei and Helen R. Quinn. CP Conservation in the Presence of Instantons. *Phys. Rev. Lett.*, 38:1440–1443, 1977. [,328(1977)].

[31] J Frenkel and J Dorfman. Spontaneous and induced magnetisation in ferromagnetic bodies. *Nature*, 126:274–275, 01 1930.

[32] Thibault Damour and Gilles Esposito-Farèse. Nonperturbative strong-field effects in tensor-scalar theories of gravitation. *Phys. Rev. Lett.*, 70:2220–2223, Apr 1993.

[33] Thibault Damour and Gilles Esposito-Farèse. Tensor-scalar gravity and binary-pulsar experiments. *Phys. Rev. D.*, 54:1474–1491, Jul 1996.

[34] Thibault Damour and Gilles Esposito-Farese. Tensor multiscalar theories of gravitation. *Class. Quant. Grav.*, 9:2093–2176, 1992.

[35] Daniela D. Doneva and Stoytcho S. Yazadjiev. New Gauss-Bonnet Black Holes with Curvature-Induced Scalarization in Extended Scalar-Tensor Theories. *Phys. Rev. Lett.*, 120:131103, Mar 2018.

[36] G. Antoniou, A. Bakopoulos, and P. Kanti. Evasion of No-Hair Theorems and Novel Black-Hole Solutions in Gauss-Bonnet Theories. *Phys. Rev. Lett.*, 120:131102, Mar 2018.

[37] Hector O. Silva, Jeremy Sakstein, Leonardo Gualtieri, Thomas P. Sotiriou, and Emanuele Berti. Spontaneous Scalarization of Black Holes and Compact Stars from a Gauss-Bonnet Coupling. *Phys. Rev. Lett.*, 120:131104, Mar 2018.

[38] Carlos A. R. Herdeiro, Eugen Radu, Nicolas Sanchis-Gual, and José A. Font. Spontaneous scalarisation of charged black holes. *arXiv e-prints*, page arXiv:1806.05190, Jun 2018.

[39] D. Lovelock. The Einstein tensor and its generalizations. *J. Math. Phys.*, 12:498–501, 1971.

[40] Pedro V. P. Cunha, Carlos A. R. Herdeiro, and Eugen Radu. Spontaneously scalarised Kerr black holes. *arXiv e-prints*, page arXiv:1904.09997, Apr 2019.

[41] TH. KALUZA. On the unification problem in physics. *International Journal of Modern Physics D*, 27(14):1870001, 2018.

[42] Oskar Klein. Quantum Theory and Five-Dimensional Theory of Relativity. (In German and English). *Z. Phys.*, 37:895–906, 1926. [,76(1926)].

[43] Yun Soo Myung and De-Cheng Zou. Quasinormal modes of scalarized black holes in the Einstein-Maxwell-Scalar theory. *arXiv e-prints*, page arXiv:1812.03604, Dec 2018.

[44] Yun Soo Myung and De-Cheng Zou. Instability of Reissner-Nordström black hole in Einstein-Maxwell-scalar theory. *arXiv e-prints*, page arXiv:1808.02609, Aug 2018.

[45] Yun Soo Myung and De-Cheng Zou. Stability of scalarized charged black holes in the Einstein-Maxwell-Scalar theory. *arXiv e-prints*, page arXiv:1904.09864, Apr 2019.

[46] Carlos A. R. Herdeiro and João M. S. Oliveira. On the inexistence of solitons in Einstein-Maxwell-scalar models. *arXiv e-prints*, page arXiv:1902.07721, Feb 2019.

[47] D. Astefanesei, C. Herdeiro, A. Pombo, and E. Radu. Einstein-Maxwell-scalar black holes: classes of solutions, dyons and extremality. *arXiv e-prints*, page arXiv:1905.08304, May 2019.

[48] C. Cohen-Tannoudji, B. Diu, and F. Laloë. *Quantum mechanics*. Quantum Mechanics. Wiley, 1977.

[49] Ingemar Bengtsson. Spherical symmetry and black holes.

[50] Charles W. Misner and David H. Sharp. Relativistic equations for adiabatic, spherically symmetric gravitational collapse. *Phys. Rev.*, 136:B571–B576, 1964.

[51] J. M. Bardeen, B. Carter, and S. W. Hawking. The four laws of black hole mechanics. *Comm. Math. Phys.*, 31(2):161–170, 1973.

[52] Larry Smarr. Mass formula for Kerr black holes. *Phys. Rev. Lett.*, 30:71–73, 1973. [Erratum: Phys. Rev. Lett.30,521(1973)].

[53] G. H. Derrick. Comments on nonlinear wave equations as models for elementary particles. *Journal of Mathematical Physics*, 5(9):1252–1254, 1964.

[54] J. D. Bekenstein. Transcendence of the law of baryon-number conservation in black hole physics. *Phys. Rev. Lett.*, 28:452–455, 1972.

[55] G. Antoniou, A. Bakopoulos, and P. Kanti. Black-hole solutions with scalar hair in Einstein-scalar-Gauss-Bonnet theories. *Phys. Rev. D.*, 97(8):084037, Apr 2018.

[56] Emanuele Berti, Vitor Cardoso, and Andrei O. Starinets. TOPICAL REVIEW: Quasinormal modes of black holes and black branes. *Classical and Quantum Gravity*, 26(16):163001, Aug 2009.

[57] A. Messiah. *QUANTUM MECHANICS, Chapter III2*. 1961.

[58] J.C. Maxwell. *A Treatise on Electricity and Magnetism*. Number vol. 1 in A Treatise on Electricity and Magnetism. Clarendon Press, 1873.

[59] Renato P. dos Santos. Magnetic monopoles and dyons revisited: a useful contribution to the study of classical mechanics. *European Journal of Physics*, 36(3):035022, May 2015.

[60] J. Schwinger. A Magnetic Model of Matter. *Science*, 165:757–761, August 1969.

[61] G.W. Gibbons and Kei ichi Maeda. Black holes and membranes in higher-dimensional theories with dilaton fields. *Nuclear Physics B*, 298(4):741 – 775, 1988.

[62] David Garfinkle, Gary T. Horowitz, and Andrew Strominger. Charged black holes in string theory. *Phys. Rev. D*, 43:3140–3143, May 1991.

[63] G. W. Gibbons and D. L. Wiltshire. Black Holes in Kaluza-Klein Theory. *Annals Phys.*, 167:201–223, 1986. [Erratum: Annals Phys.176,393(1987)].

[64] Dmitri Gal'tsov, Mikhail Khramtsov, and Dmitri Orlov. "Triangular" extremal dilatonic dyons. *Physics Letters B*, 743:87–92, Apr 2015.

[65] Anton Zadora, Dmitri V. Gal'tsov, and Chiang-Mei Chen. Higher-n triangular dilatonic black holes. *Physics Letters B*, 779:249–256, Apr 2018.

[66] R. D. Peccei and Helen R. Quinn. CP conservation in the presence of pseudoparticles. *Phys. Rev. Lett.*, 38:1440–1443, Jun 1977.

[67] Steven Weinberg. A new light boson? *Phys. Rev. Lett.*, 40:223–226, Jan 1978.

[68] F. Wilczek. Problem of strong p and t invariance in the presence of instantons. *Phys. Rev. Lett.*, 40:279–282, Jan 1978.

[69] Jihn E. Kim and Gianpaolo Carosi. Axions and the strong CP problem. *Reviews of Modern Physics*, 82(1):557–601, Jan 2010.

[70] L.F. Abbott and P. Sikivie. A cosmological bound on the invisible axion. *Physics Letters B*, 120(1):133 – 136, 1983.

[71] Michael Dine and Willy Fischler. The not-so-harmless axion. *Physics Letters B*, 120(1):137 – 141, 1983.

[72] John Preskill, Mark B. Wise, and Frank Wilczek. Cosmology of the invisible axion. *Physics Letters B*, 120(1):127 – 132, 1983.

[73] David J. E. Marsh. Axion cosmology. *Phys. Rep.*, 643:1–79, Jul 2016.

[74] Joseph P. Conlon. The QCD axion and moduli stabilisation. *Journal of High Energy Physics*, 2006(5):078, May 2006.

[75] Peter Svrcek and Edward Witten. Axions in string theory. *Journal of High Energy Physics*, 2006(6):051, Jun 2006.

[76] Anson Hook. TASI Lectures on the Strong CP Problem and Axions. *arXiv e-prints*, page arXiv:1812.02669, Dec 2018.

[77] Igor G. Irastorza and Javier Redondo. New experimental approaches in the search for axion-like particles. *Progress in Particle and Nuclear Physics*, 102:89–159, Sep 2018.

[78] Peter W. Graham, Igor G. Irastorza, Steven K. Lamoreaux, Axel Lindner, and Karl A. van Bibber. Experimental Searches for the Axion and Axion-Like Particles. *Annual Review of Nuclear and Particle Science*, 65:485–514, Oct 2015.

[79] Luca Visinelli. Axion-Electromagnetic Waves. *Modern Physics Letters A*, 28(35):1350162, Oct 2013.

[80] Kimyeong Lee and Erick J. Weinberg. Charged black holes with scalar hair. *Phys. Rev. D*, 44:3159–3163, Nov 1991.

[81] Mateja Boskovic, Richard Brito, Vitor Cardoso, Taishi Ikeda, and Helvi Witek. Axionic instabilities and new black hole solutions. *arXiv e-prints*, page arXiv:1811.04945, Nov 2018.

[82] Francesco Filippini and Gianmassimo Tasinato. On long range axion hairs for black holes. *arXiv e-prints*, page arXiv:1903.02950, Mar 2019.

[83] Bruce A. Campbell, Malcolm J. Duncan, Nemanja Kaloper, and Keith A. Olive. Axion hair for Kerr black holes. *Phys. Lett.*, B251:34–38, 1990.

[84] Bruce A. Campbell, Nemanja Kaloper, and Keith A. Olive. Axion hair for dyon black holes. *Phys. Lett.*, B263:364–370, 1991.

[85] M Reuter. A mechanism generating axion hair for kerr black holes. *Classical and Quantum Gravity*, 9(3):751–756, mar 1992.

[86] William H. Press and Saul A. Teukolsky. Floating Orbits, Superradiant Scattering and the Black-hole Bomb. *Nature*, 238:211–212, 1972.

[87] Vitor Cardoso, Óscar J. Dias, José P. Lemos, and Shijun Yoshida. Publisher's Note: Black-hole bomb and superradiant instabilities [Phys. Rev. D 70, 044039 (2004)]. *Phys. Rev. D.*, 70(4):049903, Aug 2004.

[88] Vitor Cardoso and Shijun Yoshida. Superradiant instabilities of rotating black branes and strings. *Journal of High Energy Physics*, 2005(7):009, Jul 2005.

[89] Sam R. Dolan. Instability of the massive Klein-Gordon field on the Kerr spacetime. *Phys. Rev. D.*, 76(8):084001, Oct 2007.

[90] Asimina Arvanitaki and Sergei Dubovsky. Exploring the string axiverse with precision black hole physics. *Phys. Rev. D.*, 83(4):044026, Feb 2011.

[91] Asimina Arvanitaki, Masha Baryakhtar, and Xinlu Huang. Discovering the QCD axion with black holes and gravitational waves. *Phys. Rev. D.*, 91(8):084011, Apr 2015.

[92] Richard Brito, Shrobana Ghosh, Enrico Barausse, Emanuele Berti, Vitor Cardoso, Irina Dvorkin, Antoine Klein, and Paolo Pani. Stochastic and resolvable gravitational waves from ultralight bosons. *Phys. Rev. Lett.*, 119:131101, Sep 2017.

[93] Yifan Chen, Jing Shu, Xiao Xue, Qiang Yuan, and Yue Zhao. Probing Axions with Event Horizon Telescope Polarimetric Measurements. *arXiv e-prints*, page arXiv:1905.02213, May 2019.

[94] Renata Kallosh, Andrei Linde, Tomás Ortín, Amanda Peet, and Antoine van Proeyen. Supersymmetry as a cosmic censor. *Phys. Rev. D.*, 46(12):5278–5302, Dec 1992.

Appendix A

Dynamical preference in the EMS model

A.1 Dynamical preference for Chapter 2 BHs (purely electric case)

Fully non-linear simulations, whose details are beyond the scope of this thesis, were performed in [1, 38] to assess the dynamical endpoint of the evolution of unstable RN BHs under a small perturbation in the EMS model.

The evolution of the process can be observed in Fig.A.1, wherein four snapshots, at times $t = 0, 100, 175, 225$, are shown for the exponential coupling with $q = 0.2$ and $\alpha = -400.979$.

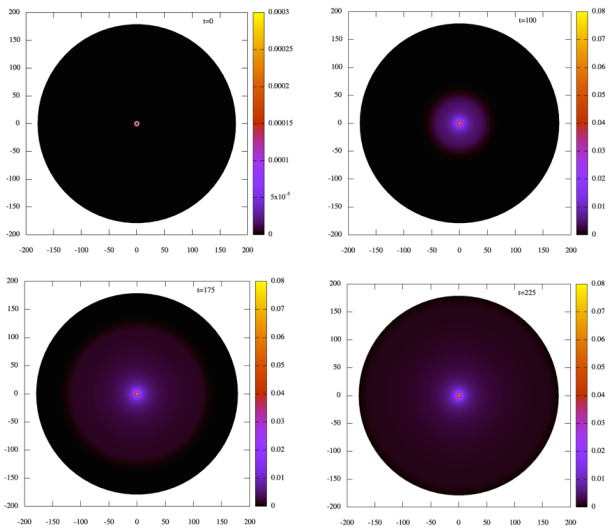

Figure A.1: Four snapshots of the time evolution of the scalar field around an unstable RN BH with $q = 0.2$ in the EMS model, with the exponential coupling and $\alpha = -400.979$.

The $\ell = 0$ small Gaussian perturbation triggered the growth of a scalar cloud in the vicinity of the

horizon that expands outwards and becomes a monotonically decreasing function of the radial coordinate. The energy transfer to the scalar field saturates by $t \sim 100$ and it reaches an equilibrium state, at least in the vicinity of the BH, around $t \sim 200$, albeit part of the more exterior scalar field distribution is still evolving outwards, settling down to the scalarized solution. The same qualitative pattern is observed for other couplings for which scalarization occurs.

The endpoint of the evolution shown in Fig. A.1 is a scalarized BH with the same value of q. This was established by comparing the value of the scalar field on the horizon obtained in the numerical evolution with the one of the previously computed static scalarized solution with the same coupling and q. As explained before, fixing α, the value of $\phi_0 \equiv \phi(r_H)$ serves as a measure of q. In Fig. A.2 (left panel) this comparison is made for various values of α, fixing $q = 0.2$ of the initial RN BH, for both the exponential coupling and the power law coupling. The crosses are from the numerical evolutions and the solid line from the static solutions. The agreement is quite good. As discussed above, the power-law coupling produces a weaker scalarization for the same coupling.

Fig. A.2 (right panel) performs a similar comparison, for the exponential coupling, but now exploring a larger range of values of q. Beyond $q \sim 0.4$, the agreement between the value of the scalar field on the horizon obtained from the evolutions and that obtained from the static solutions with the same q, ceases to hold. In other words, the endpoint of the evolution of a RN BH with a certain value of q is not a scalarized BH with the same value of q. Rather, the former matches a scalarized BH with a lower value of q. This is interpreted as a non-conservative evolution which ejects a larger fraction of electric charge than energy when forming the scalarized BH.

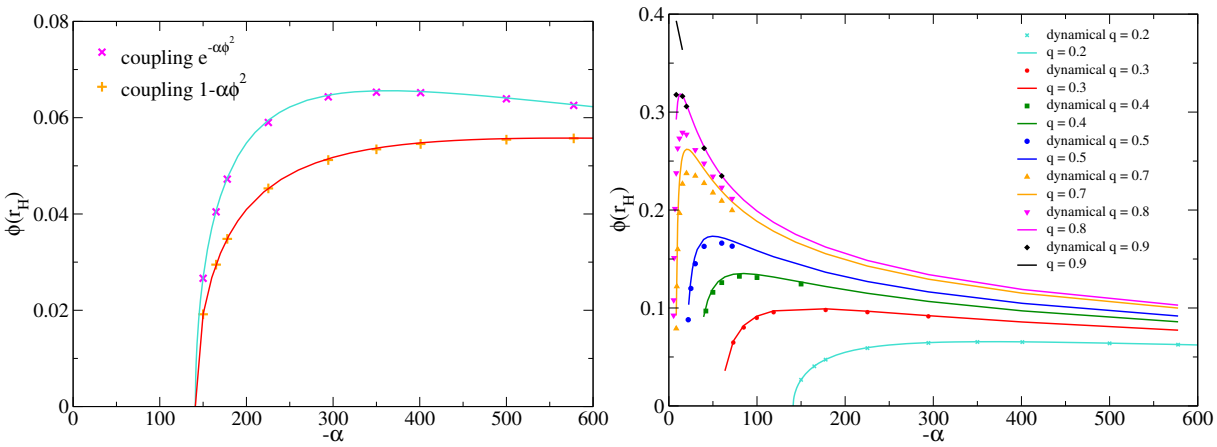

Figure A.2: (Left panel) Scalar field value at the horizon for $q = 0.2$ and a range of couplings α, for the exponential and power-law coupling. The solid line is obtained from the static solutions. The crosses are the dynamically obtained value from the numerical simulations after saturation and equilibrium has been reached. The agreement is notorious. (Right panel) A similar study, for the exponential coupling, but for various values of q. The agreement between the points and the lines with the same q is restricted to $q \lesssim 0.4$. For larger q, the evolution points match static solution lines with a smaller q.

To address the dynamical role of non-spherically symmetric scalarized BHs, evolutions of an unstable

RN BH under a non-spherical perturbations with $\ell = 1, 2$ were performed. In Fig. A.3 snapshots of such an evolution are shown for the $\ell = 2$ case. It can be observed that, initially, the non-spherical mode dissipates/is absorbed; then scalarization proceeds much as in the case of a spherical perturbation. Similar results are obtained for the $\ell = 1$ perturbation. Thus, scalarization is robust, even without imposing spherical symmetry and, moreover, no evidence of the formation of the non-spherical scalarized solutions is observed. This suggests such solutions may be unstable.

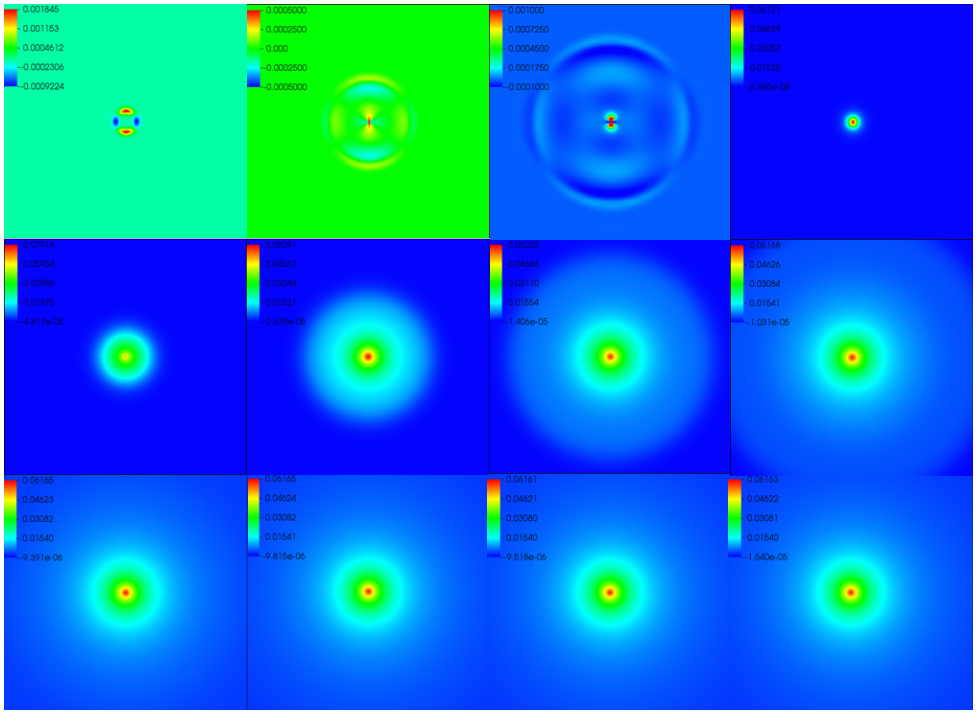

Figure A.3: Twelve snapshots in the $x - z$ ($y = 0$) plane of the time evolution of an unstable RN BH with $q = 0.2$ in the EMS system, with the exponential coupling and $\alpha = -1200$ and an $\ell = 2$, $m = 0$ perturbation. The snapshots correspond to t between 0 and 140.8. The data for negatives values of x and z are mirrored by the corresponding positive values, due to equatorial symmetry.

A.2 Dynamical preference for Chapter 4 BHs (axionic case)

Fully non-linear simulations, whose details are beyond the scope of this thesis, were performed in [2] to assess the dynamical endpoint of the evolution of unstable RN BHs under a small perturbation in the EMS-axionic model. In the dynamical scenario, the scalar perturbation triggers the spontaneous scalarization of the RN BH. The electric charge decreases as the energy of the field increases, while the magnetic charge remains unchanged, until the equilibrium is reached and a scalarized solution forms at the endpoint of the dynamical scalarization. The scalar cloud grows near the horizon and expands radially. The radial profile of the cloud decreases monotonically with increasing radii. In Fig. (A.4), the scalar field value at the horizon $\phi(r_{\rm H})$ is plotted for both the dynamical evolutions and the static solutions with the same Q and P. A notorious agreement with the static solutions is obtained. As in the last section, the dynamical solutions match better the static ones for lower values of Q.

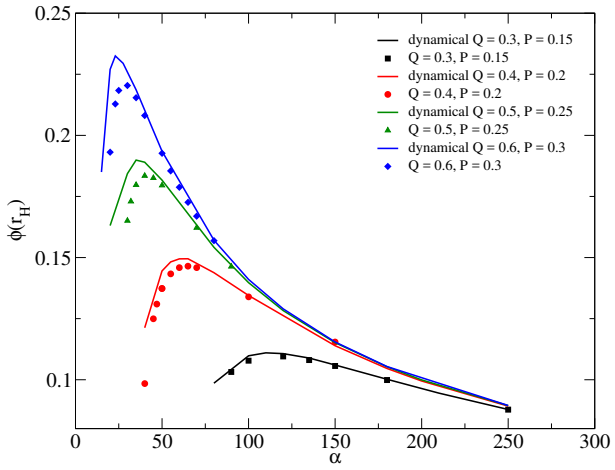

Figure A.4: Scalar field value at the horizon obtained via the dynamical simulations and the static solutions for different values of Q and P.

Appendix B

Exact solutions with a dilatonic coupling

B.1 Purely electric BHs

Purely electric dilatonic solutions of 3.3 with the dilatonic coupling (3.31) were first considered by Gibbons and Maeda [61] and Garfinkle, Horowitz and Strominger [62]. The BH solution has the line element

$$ds^2 = -a(r)^2 dt^2 + c(r)^2 dr^2 + b(r)^2 (d\theta^2 + sin^2\theta d\varphi^2), \tag{B.1}$$

with

$$a(r)^2 = \frac{1}{c(r)^2} = \left(1 - \frac{r_+}{r}\right)\left(1 - \frac{r_-}{r}\right)^{\frac{1-\alpha^2}{1+\alpha^2}} \ , \qquad b(r) = r\left(1 - \frac{r_-}{r}\right)^{\frac{\alpha^2}{1+\alpha^2}} \ , \tag{B.2}$$

together with the Maxwell potential and dilaton field[1]

$$A = \frac{Q}{r} dt \ , \qquad e^{2\phi} = \left(1 - \frac{r_-}{r}\right)^{\frac{2\alpha}{1+\alpha^2}} \ . \tag{B.3}$$

The two free parameters r_+, r_- (with $r_- < r_+$) are related to the ADM mass, M, and (total) electric charge, Q, by

$$M = \frac{1}{2}\left[r_+ + \left(\frac{1-\alpha^2}{1+\alpha^2}\right) r_-\right] \ , \qquad Q = \left(\frac{r_- r_+}{1+\alpha^2}\right)^{\frac{1}{2}} \ . \tag{B.4}$$

For all α, the surface $r = r_H = r_+$ is the location of the (outer) event horizon, with

$$A_H = 4\pi r_+^2 \left(1 - \frac{r_-}{r_+}\right)^{\frac{2\alpha^2}{1+\alpha^2}} \ , \quad T_H = \frac{1}{4\pi} \frac{1}{r_+ - r_-} \left(1 - \frac{r_-}{r_+}\right)^{\frac{2}{1+\alpha^2}} \ . \tag{B.5}$$

The extremal limit, which corresponds to the coincidence limit $r_- = r_+$, results in a singular solution (as can be seen *e.g.* by evaluating the Kretschmann scalar). In this limit, the area of the event horizon goes

[1] Following the conventions in the work, we fix $\phi(\infty) = 0$ for all solutions in the Appendix.

to zero for $\alpha \neq 0$. The Hawking temperature, however, only goes to zero in the extremal limit for $\alpha < 1$, while for $\alpha = 1$ it approaches a constant, and for $\alpha > 1$ it diverges (as was observed in Fig. 3.2).

The reduced quantities have the following exact expressions:

$$q = \frac{2\sqrt{(1+\alpha^2)x}}{1+\alpha^2(1-x)+x}, \quad a_H = \frac{(1+\alpha^2)^2(1-x)^{\frac{2\alpha^2}{1+\alpha^2}}}{(1+\alpha^2(1-x)+x)^2}, \quad t_H = \frac{(1-x)^{\frac{1-\alpha^2}{1+\alpha^2}}(1+\alpha^2(1-x)+x)}{1+\alpha^2} \ ,$$

where $0 \leqslant x \leqslant 1$ is a parameter.

B.2 Dyonic BHs

Dyonic dilatonic BH solutions are known in closed analytic form for $\alpha = \sqrt{3}$ and $\alpha = 1$ [47]. Here we address the latter as an illustrative example. A dyonic dilatonic BH solution of eq. 3.3, with the dilatonic coupling 3.31 and $\alpha = 1$, was found in [94], and extensively discussed in the literature, since it can be embedded in $\mathcal{N} = 4$ supergravity. Taking the form (B.1), it has

$$\phi = \frac{1}{2}\log\frac{(r+\Sigma)}{(r-\Sigma)}, \qquad a(r)^2 = \frac{1}{c(r)^2} = \frac{(r-r_+)(r-r_-)}{(r^2-\Sigma^2)}, \qquad b(r)^2 = r^2 - \Sigma^2 \ , \tag{B.6}$$

where

$$r_\pm = M \pm \sqrt{M^2 + \Sigma^2 - Q^2 - P^2} \ , \tag{B.7}$$

and the outer horizon is at $r_H = r_+$, while M, Q, P are the mass and electric and magnetic charges. Σ corresponds to the scalar charge, which, however, is not an independent parameter (the hair is secondary):

$$\Sigma = \frac{P^2 - Q^2}{2M} \ . \tag{B.8}$$

The extremal limit of the above solution corresponds to $r_+ = r_-$, in which case one finds two relations between the charges

$$0 = M^2 + \Sigma^2 - Q^2 - P^2 \implies (M+\Sigma)^2 - 2P^2 = 0 \qquad \text{and} \qquad (M-\Sigma)^2 - 2Q^2 = 0 \ . \tag{B.9}$$

The horizon area and Hawking temperature of the solutions are

$$A_H = 4\pi(2Mr_+ - P^2 - Q^2) \ , \qquad T_H = \frac{1}{2\pi}\frac{r_+ - M}{2Mr_+ - P^2 - Q^2} \ . \tag{B.10}$$

The expression of the reduced quantities is more involved in this case:

$$a_H = \frac{1}{4}(2x - q^2) \ , \qquad t_H = \frac{4(x-1)}{2x - q^2} \ , \tag{B.11}$$

with x a parameter expressed in terms of q as a solution of the equation (where $\mathcal{Q} = \frac{P}{Q}$)

$$q^4 - \frac{4(1+\mathcal{Q}^2)^2}{(1-\mathcal{Q}^2)^2}(q^2 + x(x-2)) = 0 \ . \tag{B.12}$$